2
10/3/77

LA-6707-P
Proposal

Special Distribution

Issued: August 1977

Fast Liner Proposal

A. R. Sherwood
B. L. Freeman
R. A. Gerwin
T. R. Jarboe
R. A. Krakowski
R. C. Malone
J. Marshall
R. L. Miller
B. Suydam

with contributions from

R. L. Hagenson
E. L. Kemp
R. W. Moses, Jr.
C. E. Swannack

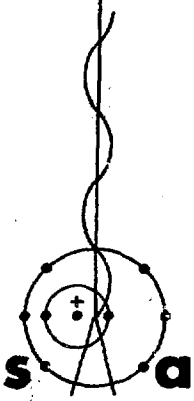

los alamos
scientific laboratory
of the University of California
LOS ALAMOS, NEW MEXICO 87545

CONTENTS

FAST LINER PROPOSAL

by

A. R. Sherwood, B. L. Freeman, R. A. Gerwin,
T. R. Jarboe, R. A. Krakowski, R. C. Malone,
J. Marshall, R. L. Miller, B. Suydam

with contributions from

R. L. Hagenson, E. L. Kemp,
R. W. Moses, Jr., C. E. Swannack

ABSTRACT

This is a proposal to study, both theoretically and experimentally, the possibility of making a fusion reactor by magnetically imploding a cylindrical metallic shell on a prepared plasma. The approach is characterized by the following features: (1) the nonrotating liner would be driven by an axial current, (2) the plasma would also carry an axial current that provides an azimuthal magnetic field for thermal insulation in both the radial and longitudinal directions, (3) solid end plugs would be utilized to prevent axial loss of particles, and (4) liner speeds would be in the 10^6 cm/s range.

Our preliminary calculations indicate (1) that the energetics are favorable (energy inputs of about 10 MJ might produce a machine in the break-even regime), (2) that radiation and heat losses could be made tolerable, (3) that alpha-particle heating could be made very effective, and (4) that Taylor instabilities in a fast liner might be harmless because of the large viscosities at high pressures.

A preliminary conceptual design of the sort of fusion reactor that might result from such an approach is discussed, as are some of the relevant reactor scaling arguments.

1. INTRODUCTION

Liner systems use the kinetic energy of a rapidly imploding shell to compress a plasma to high pressure. The external impulse accelerating the liner is applied over a relatively large area, but the impulse decelerating it against the plasma occurs over a much smaller area, and generally is applied for a shorter time at the end of the implosion. The process can be visualized as an energy compression system which produces much larger pressures on the plasma than are applied to accelerate the liner. Imploding liner fusion systems would use the high pressure obtainable with liners to compress and heat a plasma to thermonuclear temperatures at much higher density than in thermonuclear systems limited by strength of materials. The high-density (10^{18}-10^{21} cm^{-3}) short burn-time (10^{-6}-10^{-3} s) nature of this approach provides a fundamentally different alternative to the present main-line efforts being pursued within the field of magnetic confinement.

The various approaches to fusion using imploding liners can be characterized in terms of the liner velocity as follows:

(1) For a passive liner (i.e., zero liner velocity) plasma heating must be accomplished entirely by some means other than liner compression. The liner is used for inertial confinement only. A group from the Kurchatov Institute[1] has suggested the use of liners in this manner to confine high-velocity plasma streams produced by coaxial guns. Some proponents of fast high-density Z-pinches suggest passive liner containment for those systems. By its nature the passive liner tends to be an element of an approach that would be characterized primarily by the plasma production and heating scheme.

(2) For a liner velocity in the 10^4-10^5 cm/s range, the implosion time would typically be of the order of 30-3000 μs. For such times some form of magnetic containment of the plasma is required. However, the use of imploding liners allows the confining magnetic fields to reach the megagauss range, so in principle a 10-keV plasma having a density of 10^{19} could be contained.

(3) With an initial liner velocity of the order of 10^6 cm/s, the implosion time would be in the 3-30 μs range. These times are short enough that wall confinement becomes of interest. Magnetic fields are required for thermal insulation, but not for containment. This $\beta >> 1$ regime has the advantage of less magnetic field energy, and the wall-confined plasma approach could lead to a more stable plasma containment system than might be expected with magnetic

confinement. The main plasma physics considerations are associated with transport problems such as cross-field heat conduction and particle loss caused by magnetic field diffusion into the imploding liner. An important uncertainty associated with this attractive regime lies in the problem of plasma preparation. The required compressed plasma of about 10^{21} cm^{-3} and 10 keV for a 1 μs burn time implies an initial density and temperature of about 10^{18} cm^{-3} and 100 eV, for a compression ratio of 1000.

(4) Finally, if solid (or liquid) liner velocities of 10^7 cm/s could be achieved, a variety of approaches appear to be quite interesting. With such a high velocity, the plasma can be shock-heated to an appreciable temperature before final compression, and the thermal relaxation time without magnetic fields can be longer than the burn time. Although such high liner velocities appear to be very difficult to achieve, the ANGARA e-beam experiment of Rudakov[2] can be considered to be a liner implosion of this class.

In the proposal which follows, we shall primarily be concerned with regime (3), that is, with liner systems having a wall-confined plasma and liner velocities of about 10^6 cm/s. We shall be considering nonrotating thin solid liners driven by an axial current. The plasma is contained in the axial direction by solid end plugs, and it has an embedded azimuthal magnetic field for thermal insulation against heat flow in the radial and axial directions. Some advantages of this approach are:

(1) The wall confinement of the plasma with $\beta > 1$ avoids the equilibrium and stability problems that have plagued magnetic confinement schemes. This is potentially a tremendous advantage.

(2) The azimuthal insulating magnetic field provides axial as well as radial energy confinement. This leads to the possibility of short systems, that is, less than a meter long.

(3) This same azimuthal magnetic field can confine axially and radially the alpha-particles produced during thermonuclear burn, leading to greatly improved reactor energetics.

(4) The short liner implosion time, implied by the fast liner velocity, ameliorates the elastic-plastic and the Rayleigh-Taylor liner instabilities. (For the Rayleigh-Taylor instability, this statement is based upon a model for viscous damping, but there is also experimental evidence to support it. See Sec. III.E.)

(5) As opposed to a B_z drive field, a B_θ field gives increasing driving pressure as the liner collapses and gives higher efficiency of energy transfer to the liner.

(6) From the reactor viewpoint, a high-power-density, compact, and relatively simple system is conceivable.

Finally, it should be mentioned that idealized calculations, presented in Sec. III.A, which do not include plasma energy losses, indicate that very interesting experiments (Q approaching 1) could be done for a 10-cm-long liner with bank energies of a few megajoules.

There are also disadvantages to the approach:

(1) Energy losses due to line radiation and bremsstrahlung from the cold plasma near the walls and due to an associated convective flow of plasma toward the walls may be severe.

(2) The magnetic diffusion of the drive field into the liner is likely to be a serious problem. It may be necessary to drive the liner with an external current-carrying plasma rather than have the liner carry its own drive current.

(3) For a B_θ drive, with the liner carrying its own drive current, either a sliding or deformable current contact is required for at least part of the liner implosion.

(4) For a reactor, the required initial plasma ($n_i \approx 1 \times 10^{18}$ cm^{-3}, $T_i \approx 200$ eV, $B_i \approx 50$ kG) falls into an unexplored region. At present we do not know how to produce such a plasma.

(5) The reactor would involve a rapidly pulsed energy transfer system and an explosive thermonuclear energy release.

The suggestion of an imploding liner approach to fusion is certainly not new. An exhaustive history will not be attempted here, but among the earlier papers are those of Linhart[3] and Alikhanov et al.[4] It is well known that at present, the approach is being pursued in the USSR (e.g., Budker,[5] Alikhanov et al.,[6,7] and Rudakov[2]), in France (e.g., Rioux and Jablon[8]) and in the USA at NRL (e.g., Robson,[9] and Turchi and Robson[10]). The liner velocity regime of 10^6 cm/s that we propose to investigate has been considered previously[4,6,7] but it is not clear that such velocities for magnetically driven liners have yet actually been achieved. The present proposed program forms a natural complement to the NRL LINUS program,[11] which is concerned with the 10^4-10^5 cm/s liner velocity regime. The two programs involve different plasma problems and different reactor

considerations, and both approaches show promise and should be explored.

The use of imploding liners to heat and contain thermonuclear plasmas involves three physics problem areas. These are (a) liner implosion, (b) initial plasma preparation, and (c) plasma containment in the liner during implosion and burn. These are discussed in the context of the present approach in the sections which follow. The design of an imploding-liner fusion reactor would involve many further problems, and preliminary considerations of these are also discussed.

Section II contains the proposed LASL experimental program. This program divides naturally into two parts: the liner implosion and the plasma preparation. A preliminary design for a cheap capacitor bank for driving imploding liners is discussed, and the results of some calculations for circuit behavior and liner trajectories are presented. The requirements for the initial plasma are considered, assuming classical transport, and it is shown that the initial conditions $n_i = 2 \times 10^{16}$ cm^{-3}, $T_i = 200$ eV, $B_i = 20$ kG would be sufficient for quite interesting experiments. Possible ways of producing such a plasma are discussed, including gun injection and two hard-core geometries. Finally, the diagnostic requirements for liner implosions and for the plasma preparation program are considered.

Section III contains theoretical considerations of several important topics. Two models, one analytical and one numerical, are presented for the liner dynamics and plasma conditions. These models include the effects of liner compressibility but neglect plasma losses. The two models are found to be in good agreement with each other. The analytical model predicts, for optimized conditions,

$$Q\,(2\pi/\rho)^{1/2} = 7.0\,(E_L/\ell)^{1/2}\ , \qquad \text{(I-1)}$$

where Q is the output fusion energy divided by the input liner energy, E_L is the input liner energy (GJ), ℓ is the length of the system (m), and ρ is the density of the liner (gm/cm^3). For a copper liner this would imply $Q \approx 1$ for a liner input energy of only 20 MJ/m. Although the results from these models are very encouraging, a self-consistent calculation including plasma losses is required. The numerical model is also used to investigate the internal state of the liner. It is found that (1) compressibility effects do not cause the liner to melt, (2) one can expect significant viscosity inhibition of Rayleigh-Taylor instabilities,

(3) the driving magnetic field may penetrate the liner before the liner reaches its minimum radius, and (4) in a reactor the neutron flux from the burn might vaporize the liner. The predicted magnetic field diffusion into the liner, and the accompanying melting of the liner, are of serious concern. Thicker than optimum liners may be required, or it may be necessary to drive the liner with a plasma instead of having the liner carry its own driving current.

Section III also contains discussions of liner instabilities and of plasma energy losses. Initial calculations show that the radial plasma losses can be held to acceptable levels if the required plasma currents can be obtained. (These are about 1-2 MA for the reactor and about 1/4 MA for a good experiment.) A pessimistic calculation for the energy loss down the axis indicates that this loss might be significant at low input energies. The problem of bremsstrahlung and line radiation from the cold plasma near the walls, and a possible associated convective transport toward the walls, is not treated here. It is possible that these effects could cause serious energy loss. Buckling and Rayleigh-Taylor liner instabilities are not expected to be serious if the liner is driven hard enough. For the elastic buckling instability this occurs because the driving pressure exceeds the material yield stress in a time short compared to the instability growth time. An expression for this latter time is given by Velikhov et al.,[12]

$$t_{buckle} \simeq (\Delta E/c)\,(\rho/12E)^{1/2} \qquad (I\text{-}2)$$

where E is Young's modulus, σ is the material yield stress, Δ is the liner thickness, and ρ is the material density. Typical values yield t_{buckle} of the order of 10 μs, which, for the liner drives being proposed, is about a liner implosion time and is long compared to the time for the yield stress to be exceeded. The growth rate of the fastest growing Rayleigh-Taylor mode is examined in the presence of viscous damping. An empirical model for the viscosity at high pressures is presented, namely that the viscosity is proportional to the pressure. Using this model the Rayleigh-Taylor instability of the inner liner surface is not expected to grow fast enough to be serious, whereas the instability of the outer surface during liner acceleration is marginal. In this context the magnetic field diffusion into the liner is expected to be beneficial.

Section IV contains preliminary considerations of the reactor that would result from the proposed fast liner approach to fusion. Such a reactor would have the advantages of high-power-density and compactness and the disadvantages of the requirements of large fast-pulsed energy release and transfer. For the purposes of these reactor considerations, another model is introduced for the combined plasma/imploding liner system. This model assumes an incompressible liner, allows liner rotation for generality, and includes a simplified treatment of axial plasma loss. For comparable cases this third model agrees fairly well with the others. From the results of this model a feasible but unoptimized reactor operating point is chosen. A description of a possible reactor concept is presented. Basically this concept involves plunging a preformed liner into a liquid-metal bath which absorbs the thermonuclear energy release. At this very preliminary stage, of course, such a reactor concept can only be regarded as an illustration of the general type of reactor that might eventually evolve. The subjects of energy storage and transfer into the liner driving circuit and of neutron energy deposition into the liner are also briefly considered.

Section V describes the proposed experimental schedule in terms of an orderly transition from the present Implosion Heating Experiment (IHX), beginning when that experiment is completed. The level of effort would remain at the present level of the IHX during the early exploratory phases of the program.

II. PROPOSED LASL EXPERIMENTAL PROGRAM

A. General Description

We are proposing a three-element program (liner implosion, plasma preparation, and theoretical support) to explore the liner implosion approach to fusion in the 10^6-cm/s liner velocity regime. Such a program would form a natural complement to the NRL LINUS program,[11] which is concerned with the 10^4-10^5-cm/s liner velocity regime. The present approach is based on the concept of a magnetically driven, thin, nonrotating, metallic liner imploded at a velocity of about 10^6 cm/s. The geometry is roughly cylindrical. The liner is driven by a magnetic field in the theta direction. The liner would either carry its own implosion current (the "directly driven" case), or perhaps the current would be carried by a supplementary plasma just outside of the liner (the "plasma driven" case). The initial plasma would be warm and dense (~200 eV and ~10^{18} cm^{-3} ultimate goals) and would be protected against thermal losses by an embedded magnetic field in the theta direction. Material end plugs would be employed.

A modest program, at first treating liner implosion and plasma preparation separately, would lead later, assuming success, to liner compression of plasma systems. A cheap 2.4-MJ capacitor bank would be constructed, mostly from surplus parts. This bank would be used to implode small aluminum liners (e.g., 5-cm diameter, 0.8-mm thick, and 10-cm long). For the initial implosions non-plasma loads, such as a B_z field or a compressed gas, would be employed. Liner velocities, symmetry of implosion, and efficiency of energy transfer from bank to liner are examples of quantities that would be measured. The ultimate goals of this portion of the experimental program would be to understand the relevant physical processes occurring during the liner implosion and to obtain liner implosion velocities of 10^6 cm/s.

A parallel effort would be directed towards the preparation of a suitable plasma for the liner implosion. The initial goal for plasma preparation is $n = 2 \times 10^{16}$ cm^{-3} at T = 200 eV with a 20-kG embedded field, whereas the ultimate goal is $n = 1 \times 10^{18}$ cm^{-3} at 200 eV with 50-kG field. Containment and thermal insulation during implosion and burn appear to be adequate with wall-supported diffuse Z-pinch plasmas. Such plasmas can be generated with coaxial gun-type discharges, but some development will be required. In a diffuse Z-pinch containment system, end loss appears to be adequately reducible by material plugging, either by liner implosion against plugs or by end closure by faster implosion of the liner at the ends. Other possibilities for plasma preparation are: a) the

electromagnetic shock tube approach, e.g., the early MAST experiments[13] and the more recent work at Columbia University,[14] and b) the explosion of a solid D_2 thread.

The techniques and equipment required for a magnetic liner drive are very similar to those required for θ pinches or Z pinches. They include large capacitor banks or inductive energy storage systems with fast switching capable of handling millions of amperes at tens of kV. The requirements for the plasma production fall within the pulsed high-β approach. Thus LASL is well equipped to handle the liner drive problems and also problems of initial plasma preparation and containment. Many of the problems encountered in the diagnostics of the liner implosion are very similar to those handled routinely at LASL. Finally we have strong theoretical support available, including numerical codes which have been developed for other applications.

B. Liner Implosions

We plan to construct a bank to drive the liner from surplus capacitors taken from the old Zeus bank. They are 14.7-μF, 20-kV capacitors that have 60-nH inductance, and there are presently about 3000 of these available. About 800 would be used for this bank. These capacitors would be arranged with four in series and 200 in parallel to make an 80-kV, 2.35-MJ bank. This bank would have 20 modules with 40 capacitors in each module. A schematic diagram of one such module is shown in Fig. II-1. The switch could be a dielectric switch or possibly a low-pressure switch. Group CTR-5 at LASL has built and successfully tested dielectric switches which were to be used in IHX as a backup for the rail gaps. The modules can be connected to the collector plate with cables in such a manner as to give inductive isolation for each subgroup of four capacitors, as protection in case of individual capacitor failure. The 2-m-diameter collector plate is shown in Fig. II-2. The liner will be housed inside a 1.3-m-diameter steel containment vessel. Presumably everything inside the vessel will be destroyed with each shot and everything outside will be saved. The total weight of the vessel would be over 3000 lbs, and it should be capable of safely containing 6 MJ of energy.[15]

Z-pinch drive is chosen for these experiments because for a given liner it allows the use of a slower, less expensive bank to achieve the desired liner velocity. Ignoring resistive losses, about 80% of the bank energy can be transferred to a liner with either a θ-pinch or Z-pinch drive. However, to get this efficiency the bank must be much faster for a θ-pinch drive. With such a drive the work must be done on the liner early in the implosion because the area of the

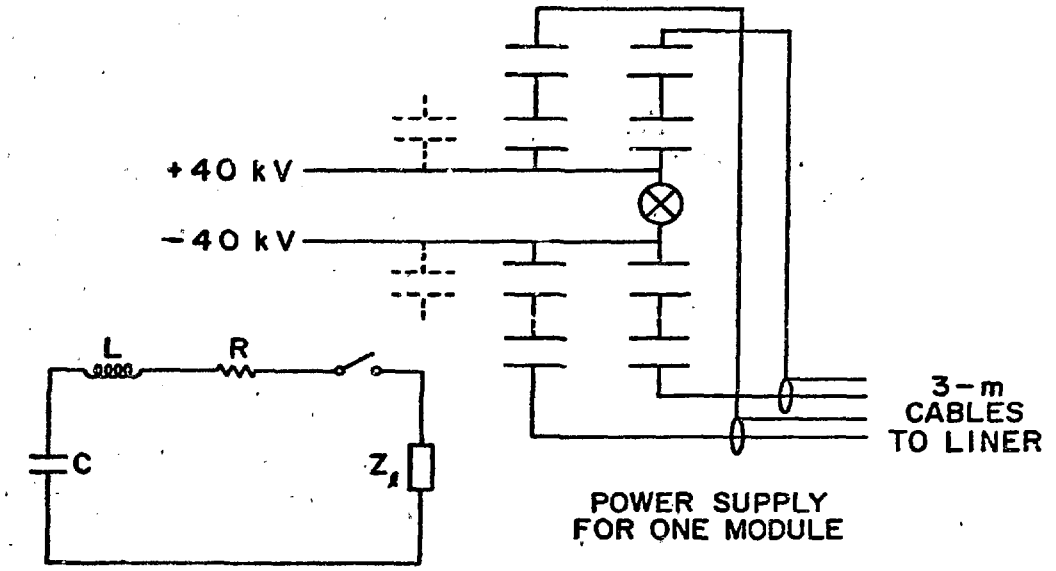

Fig. II-1.

Schematic of bank and liner imploding circuit.

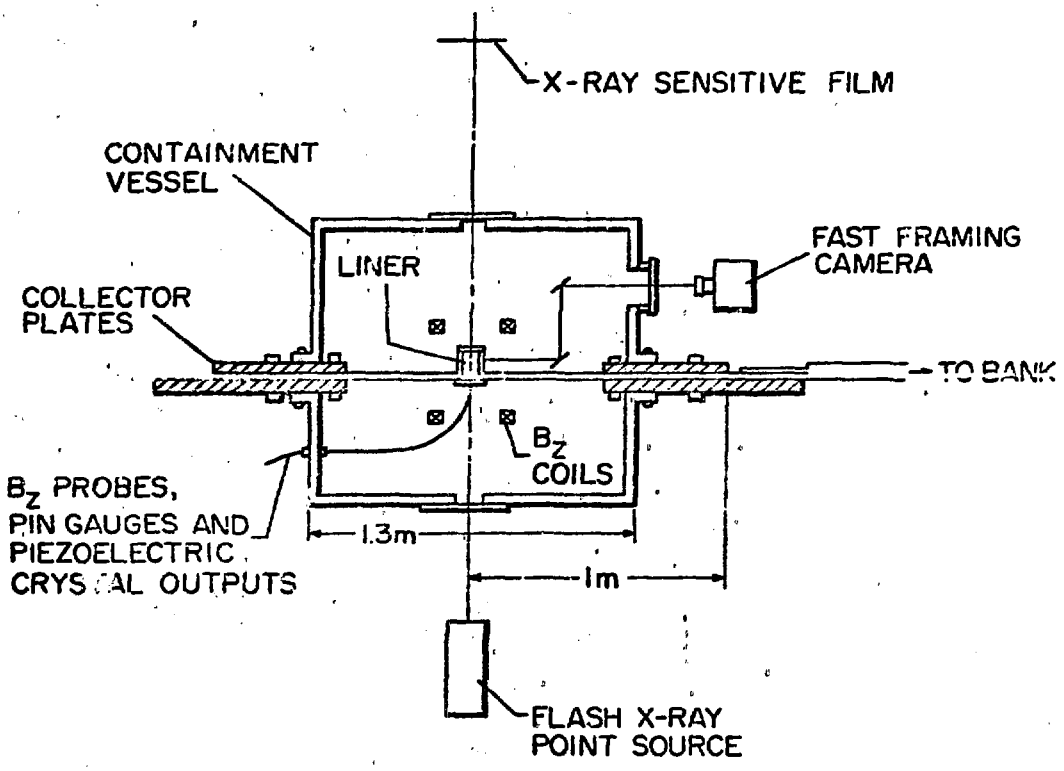

Fig. II-2.

Experimental arrangement for liner implosion studies.

liner drops later in time, causing a decrease of the force on the liner. In the Z-pinch case, the area decrease is more than compensated by the increase in magnetic field, $B_\theta \propto 1/r$. Alternatively, the $\dot{L}$ of the liner peaks early in time for the θ-pinch drive, where $\dot{L} \propto vr$, and increases monotonically in the Z-pinch case where $\dot{L} \propto v/r$. In order to get high transfer efficiency it is necessary for the current to peak well before the $\dot{L}$ maximum because the rising $\dot{L}$ is needed to transfer most of the inductive energy to the liner. Therefore, a slower and thus less expensive bank can be used with a Z-pinch drive, because the $\dot{L}$ in this case peaks later in time. Finally, θ-pinch drives may introduce an azimuthal asymmetry in the implosion because of end effects at the feed slot. The use of Z-pinch drive however, introduces the problem of maintaining dynamic electrical contact with the liner.

In designing the bank a thin liner model is used to calculate the dynamic impedance of the liner. The circuit is shown in Fig. II-1, where C, R, and L are due to the bank, transmission line, and collector plates, and Z_ℓ is due to the liner. When the switch is closed the liner moves under the influence of the magnetic pressure, producing a dL/dt effect in the driving circuit. Estimating 150 nH as the inductance per capacitor and its cable connection to the collector plate, and assuming an insulation thickness between the collector plates of 0.2 cm, one finds L = 4.5 nH and C = 735 μF. The value of R will probably be determined primarily by the switch resistance and by the current contact to the liner; thus it will not be known until we do the experiment. However, assuming that R = 0.5 mΩ, it is possible with this 2.35-MJ bank and collector plate arrangement to get 1.5 MJ into an aluminum liner of the dimensions r_i = 2.5 cm, δ = 0.8 mm, and ℓ = 10 cm. This corresponds to a liner velocity of 0.9×10^6 cm/s. The calculated circuit behavior and liner trajectory for this case are shown in Fig. II-3. For a smaller thinner liner, r_i = 1.25 cm, δ = 0.4 mm, and ℓ = 10 cm, the liner energy would be 0.6 MJ with a corresponding velocity of 1.2×10^6 cm/s. Velocities such as these are two or three times those reported by Alikhanov[6] for Z-pinch driven liners and are near the values given by Knoepfel[16] as the velocity limits for aluminum.

These velocity limits of Knoepfel are derived under the condition that the driving current is carried by the metallic liner, with the assumption of a planar geometry. In Section III.D the results of a calculation for magnetic

diffusion in a cylindrical geometry are presented. For the particular conditions treated there, a liner velocity of 5 x 10^5 cm/s was obtained. This value is consistent with the corresponding Knoepfel limiting velocity. Thus there is reason to suspect that magnetic diffusion may limit the liner velocities that can be obtained with the proposed 2.35-MJ bank to values below 10^6 cm/s. If this turns out to be the case, it might be possible to devise a plasma drive for the liner, that is to have a plasma just outside of the liner carrying most of the drive current. For example such a plasma might possibly be created by coating the outside of the liner with a low boiling point material which would be ablated, ionized, and heated during the early phases of the implosion.

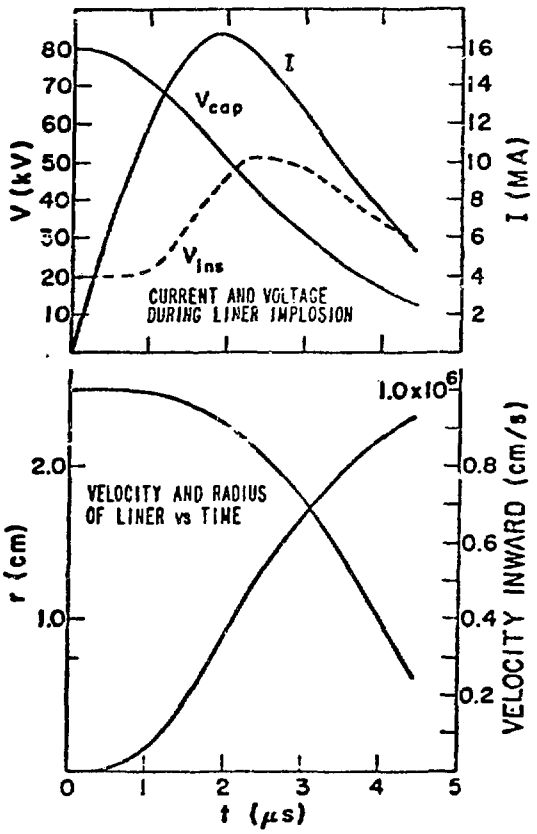

Fig. II-3.
Calculated circuit and liner parameters during an implosion of a liner onto vacuum. The initial liner has r_i = 2.5 cm, ℓ = 10 cm, δ = 0.8 mm. The series resistance is 0.5 mΩ.

In summary, an inexpensive 2.35-MJ, 80-kV bank can be built from existing capacitors. This bank is calculated to be capable of driving reasonably sized aluminum liners to velocities of about 10^6 cm/s, but magnetic diffusion may limit the attainable velocity to a lower value. In the latter case a plasma drive could be attempted.

As was mentioned previously, the initial experiments (in this liner implosion portion of the overall program) would be directed towards investigating the liner implosion itself. Undoubtedly direct drive of the liner would be tried first. The efficiency of transfer of bank energy into kinetic energy of the liner would be investigated. Hopefully high efficiency ($\sim$ 50%) can be achieved with sliding current contacts; if not, deformable contacts would be used. Naturally the liner velocity would be measured. To investigate the possibility of liner instabilities, the symmetry of the liner implosion would be studied, as would be the symmetry of deceleration on a load such as a B_z field.

Liner Diagnostics

Tc accomplish the program just described, the following things need to be determined:

a) the energy transfer from bank to kinetic energy of liner

b) the liner velocity

c) the energy transfer from liner to load

d) the symmetry of the liner drive

e) the symmetry of deceleration on a load.

Since the mass of the liner and the initial energy of the capacitor bank can be measured accurately, the first two items are closely related. The usual measurements of circuit parameters, such as the driving current and the collector plate voltage, will help determine the energy transfer from the bank to the liner. Electrical contact probes can be used to measure the liner velocity. Flash x rays can be used for this same measurement, and for investigating the symmetry of liner dynamics as well. A framing camera, in conjunction with mirrors, may also be useful for these velocity and symmetry measurements. A magnetic probe would be used for measurements of the load pressure when B_z loads are employed. In short, the standard diagnostics would be sufficient, at least at the start. The equipment and expertise are available at LASL for all of these measurements.

C. Plasma Preparation

1. Requirements. In a lossless adiabatic compression $T \alpha r^{-4/3}$, where T is the plasma temperature. Assuming a radial compression ratio of 30:1 (28:1 has been achieved[17] for solid aluminum liners by the NRL group), the initial plasma temperature must be about 100 eV if the final temperature is to be 10 keV. According to the previous subsection, as much as 1.5 MJ could be transferred from the capacitor bank to the liner. Assuming 1.0 MJ is transferred from the liner to the plasma during the lossless compression to a temperature of 10 keV, an initial plasma energy of about 10 kJ is required for energy balance. This initial energy implies an initial plasma density of about $1 \times 10^{18}/cm^3$, if the 200 cm^3 volume of the liner described in the previous subsection is used. Noting the assumption of ideal lossless compression, perhaps $n_i = 1 \times 10^{18}/cm^3$ and $T_i = 200$ eV are reasonable goals for the initial plasma. In the proposed experiment the implosion time would be about 3 μs. Using the simplest estimate for the radial heat loss from ion thermal conduction, it appears that an initial value of about 50 kG for the embedded B_θ field will provide a thermal relaxation time

long compared to the implosion time. Thus the values $n_i \approx 1 \times 10^{18}/cm^3$, $T_i \approx 200$ eV, $B_{\theta i} \approx 50$ kG are taken as ultimate goals for the initial plasma. Using these values, the classical times for electron-electron and ion-ion collisions are 1×10^{-10} s and 6×10^{-9} s, respectively, and the ion and electron cyclotron times are $\omega_{ci}^{-1} = 4 \times 10^{-9}$ s, and $\omega_{ce}^{-1} = 1 \times 10^{-12}$ s.

The following discussion supports the initial field value of 50 kG. Since the ratio of unmagnetized to cross-field thermal conduction is about $1/(\omega_c t_c)^2$, and since the unmagnetized thermal conductivity is proportional to $1/(m)^{\frac{1}{2}}$, the electron thermal conduction is only 10^{-2} of the ion thermal conduction, using the above values for collision and cyclotron times. Also, at the beginning of the implosion, the magnetic field does not greatly inhibit the ion thermal conduction. Thus one obtains a thermal relaxation time of about 6 μs for the above initial plasma conditions, using the Spitzer[18] value for the ion thermal conductivity, and using r_i for the scale length for temperature gradients and $\pi r \ell$ as the area for thermal loss. This estimate of 6 μs is long compared to the implosion time. At the end of the compression, ion cross-field thermal conduction dominates, and a similar estimate gives a thermal relaxation time of 0.8 μs, which is long compared to the dwell time (∿ 100 ns). The assumption of classical heat loss is supported somewhat by the experiment of Feinberg and Gross,[19] although the plasma conditions are not the same.

The calculations used to obtain the above "ultimate goal" values for the initial plasma conditions are admittedly very crude. The "optimized" initial conditions derived in Sec. III.A from the analytical scaling model are $n_i \approx 5 \times 10^{17}/cm^3$ and $T_i \approx 500$ eV. The estimates for thermal losses in Sec. III.C based on the same model imply a less stringent requirement of about 25 kG for the initial magnetic field.

The above two sets of conditions for the initial plasma have been derived from the viewpoint of making efficient use of the liner energy. Very interesting experiments, however, can be done with considerably relaxed conditions. Holding the liner dimensions and the initial temperature constant, conditions at lower densities and magnetic fields can be found that should also be thermally insulated. This can be seen by noting that the thermal relaxation time scales roughly as B_i^2/n_i times a function of the initial temperature and radius. Therefore, according to this method of estimating the required magnetic field, a plasma with the initial conditions $T_i = 200$ eV, $n_i = 1 \times 10^{16}/cm^3$, and $B_i = 6$ kG

should also be heated. However, this value of B_i is too small, for a B_i of around 20 kG is required in order that at the end of compression the ion gyroradius be small compared to the plasma radius. With B_i = 20 kG and T_i = 200 eV, a value $n_i = 2 \times 10^{16}$ gives $\beta_i \approx 1$. These initial conditions make a nice goal for the first liner-imploded plasma experiments. Such a plasma should allow interesting experiments of liner-driven wall-supported plasmas, although non-optimum use of the liner energy would result.

It should be emphasized that the method employed here of estimating the required insulating magnetic field is quite crude. Although reasonable agreement is obtained with the better treatment of Sec. III.C, potentially important effects like convective flow and radiation from the cold plasma at the walls are not included.

2. Possible Methods. It was shown in the previous subsection that to take good advantage of the liner energy in the experiments proposed above, the liner should be imploded on a plasma having initial conditions approximately as follows: $n_i = 1 \times 10^{18}/cm^3$, T_i = 200 eV, and $B_{\theta i}$ = 50 kG. On the other hand, the analytical scaling model of Sec. III.A suggests the following as ideal initial conditions: $n_i = 5 \times 10^{17}/cm^3$, T_i = 500 eV, and $B_{\theta i}$ = 25 kG. Both of these sets of conditions represent plasmas rather different than those commonly produced in the laboratory, especially when the required volume ($\approx$ 200 cm^3) and lifetime ($\approx$ 3 μs) are considered. Thus an experimental program, directed towards the eventual production of such plasmas, is required. Fortunately, interesting liner implosion experiments can be done with initial plasmas having parameters (e.g., $n_i = 2 \times 10^{16}/cm^3$, T_i = 200 eV, and $B_{\theta i}$ = 20 kG) much closer to those that can presently be obtained. To produce such a plasma in a geometry suitable for liner implosion, however, still requires an exploratory experimental program.

We are proposing such a program to complement the liner implosion effort. Initially the emphasis would be on a flexible approach, that is on maintaining the ability to try new ideas quickly until a particular approach proves especially promising. A small, very flexible capacitor bank facility is available for such plasma preparation experiments.

The remainder of this subsection describes several possible approaches by which the initial plasma might be produced.

a. Gun Injection. It may be possible to provide the initial plasma for liner compression by plasma gun injection. Coaxial plasma guns, such as those described by Marshall and Henins[20] and by Cheng and Wang,[21] are presently capable

of producing plasmas with energies and densities close to those required. At LASL, for example, gun plasmas having a density of $2 \times 10^{17}/cm^3$, a directed energy of about 200 eV, and total energy 300 kJ have been produced. Gun plasmas are believed to contain frozen-in B_θ field, but the magnitude is unknown.

Gun injection is the main approach of the Soviet liner program. One of the main problems with gun injection is transport of the plasma from the gun or guns to the liner. In the Soviet approach this is being done in two ways, one by transport along an axial magnetic field,[22] and the other by locating the guns directly adjacent to the liner as in the experiments of Alikhanov et al.[6] The axial magnetic guide field approach takes several forms. One is to inject plasmas from the two ends of the system, with the two gun plasmas interacting in the liner region to produce a stopped dense plasma. In general this leads to a standard linear θ-pinch situation, with particle and thermal end-loss difficulties during compression leading to the requirement of a long system. The two gun plasmas carry frozen-in B_θ fields in opposite directions. Thus it is difficult to see how a two-gun approach can lead to a simple diffuse Z-pinch plasma of the kind desired in a short system with reasonable hydromagnetic stability.

Another possibility with gun injection is to take the diffuser-compressor approach studied by Zhitlukhin et al.,[23] at the Kurchatov Institute. A gun plasma injected into an axial magnetic field, which increases gradually with axial position, can be compressed isentropically and be raised considerably in density with its translational kinetic energy converted into thermal particle energy during the compression. This process should also raise the frozen-in B_θ field and produce the desired initial plasma conditions, high density and reasonably large frozen-in B_θ. The B_z guide field would tend to be pushed outward by the plasma and would form a buffer between plasma and liner, kept at low temperature by axial heat conduction. The diffuser-compressor system would be particularly applicable to a highly ordered plasma like that produced by the deflagration gun of Cheng.[21]

It appears also to be possible to guide and compress plasma by simple conducting walls. Zhitlukhin et al.,[23] have demonstrated a tenfold compression using converging copper plates, and conical compression has been demonstrated by Dunne and Benham[24] in 1965 using a Xe plasma. Such a system would be desirable, since it would require no axial guide field. Whether it could be adapted to give the desired conditions is not known.

Finally it should be pointed out that the diffuser-compressor system might well lead to a passive liner reactor concept. Zhitlukhin et al.,[23] have observed a 60-fold plasma compression to a density of $1.5 \times 10^{18}/cm^3$, starting with a Mach 5 gun plasma with a flow speed of 2×10^7 cm/s. Presumably the compression ratio is limited by the initial plasma temperature (10 eV in this case). It would appear that a plasma from a Cheng deflagration gun, or a scale-up thereof, would be capable of much greater compression, conceivably to the $10^{20}/cm^3$ range at thermonuclear temperatures. A reactor based on such a liner system would be operationally attractive because of its simplicity.

b. Hardcore Gun Geometry. Another possible system for plasma production is shown in Fig. II-4. It can be described as a diffuse wall-supported Z pinch. This system and the following explanation of its operation are suggested by the coaxial gun experiments done in the past by John Marshall.[20] A pre-plasma is formed by a coaxial discharge between the liner and the hard core. This drives a B_θ magnetic piston away from the insulator, pushing magnetized plasma outward against the liner. When the discharge reaches the end of the center electrode, the magnetic flux in the piston flows out, allowing the magnetized plasma to collapse against the hard core. The liner would then be imploded, short-circuiting against the hard core, trapping flux and plasma and compressing them to high density. Most likely not all of these things will happen as visualized so it would probably be necessary to do a certain amount of parameter searching and diagnosis, just to prepare a reasonable pre-plasma. This hard-core geometry may not be ideal, but the system could provide a first plasma for liner implosions while other plasma preparation schemes are developed.

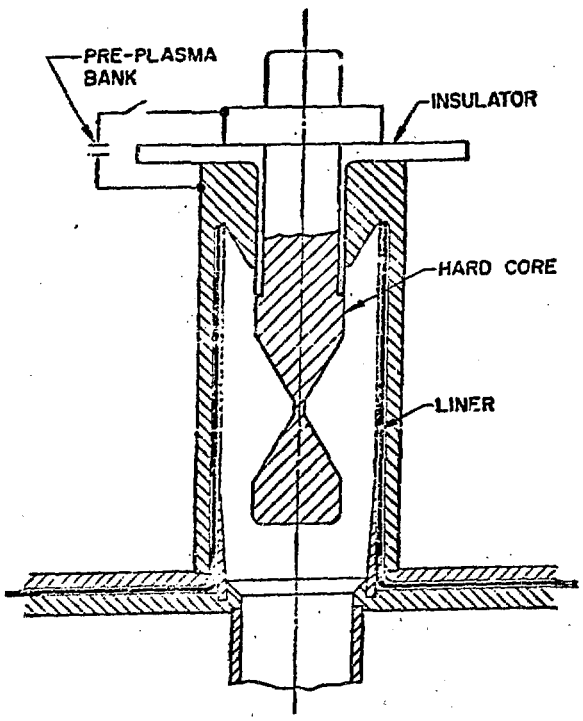

Fig. II-4.
Conceptual drawing of an inverse-pinch hard core liner implosion system.

c. Electromagnetic Shock Tube. A possibility that has the advantage of good plasma-magnetic field mixing and control over B_θ is the electromagnetic shock tube approach similar to the early

MAST experiments[13] and the experiments of Gross et al.[14,26,27] With modest voltages and currents (40 kV and 10^6 A) one should be able to get magnetic piston velocities of around 2×10^7 cm/s and densities of about $10^{17}/cm^3$. Increasing the voltage and current might produce plasmas approaching the desired initial plasmas. Plasmas of $T \approx 500$ eV and $n \approx 10^{16}/cm^3$ have been produced by this method.[21] Figure II-5 shows a geometry that could be tried; perhaps the central conductor in the liner region could be a small wire of Li or D.

d. Exploding Solid D_2 Thread. Another possible source for the initial plasma is a deuterium thread heated to the approximate temperature with a large current. See Fig. II-6. The pinch will be unstable causing a scrambling of field and plasma. It might be possible to adjust the external circuit so as to give the desired plasma and field conditions. It would require a 300-μm-diameter thread of solid D. Threads of this size can be produced in one of the modes of operation of the thermal spinner device of Jarboe and Baker.[25]

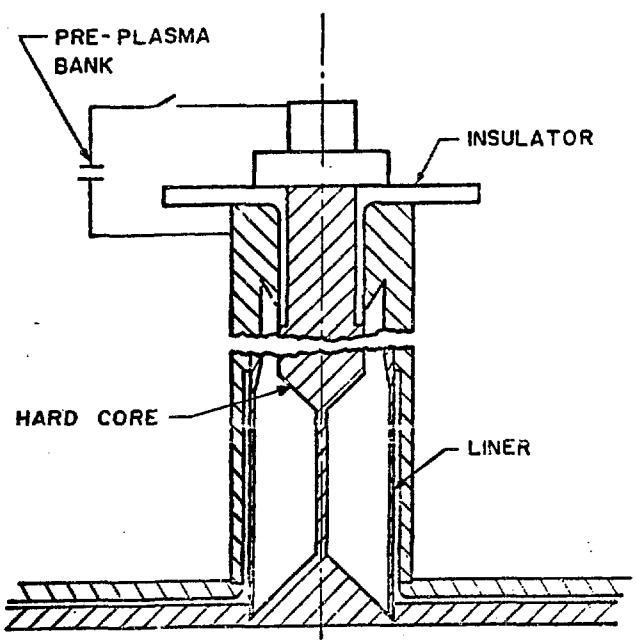

Fig. II-5.
Schematic of liner and initial plasma-producing apparatus for the shock heated initial plasma (deforming contact).

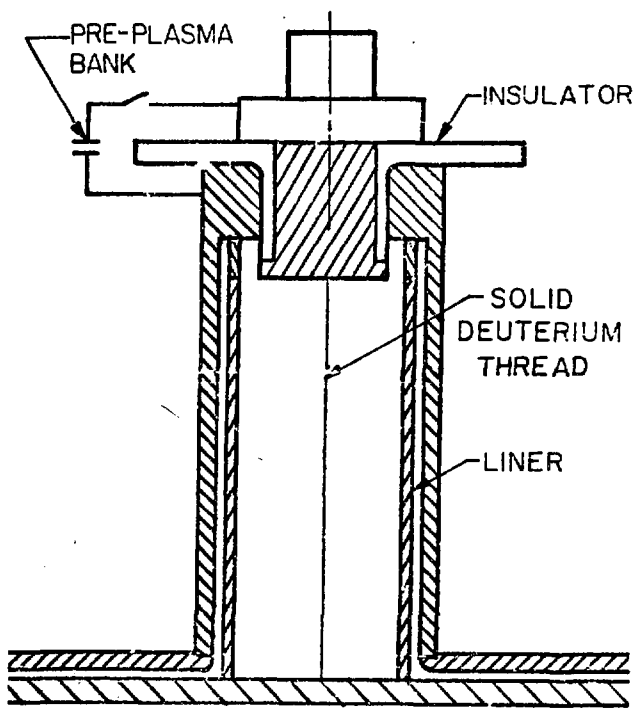

Fig. II-6.
Conceptual drawing of an inverse-pinch hard-core liner implosion system (sliding contact).

3. Plasma Diagnostics. The goals of the plasma preparation experiments have been described in terms of required values for the quantities n_i, T_i, and B_θ; therefore we need to measure all three of these quantities. During the initial phases of the plasma preparation experiments, it is desirable to have some relatively simple diagnostics to assess progress in plasma production without the diagnostics themselves requiring a great deal of effort. For example, during this development phase the density could be measured by counting fringes in a Mach-Zehnder interferometer; a ten-fringe shift of 633-nm wavelength light would be observed if the density were $3.5 \times 10^{17}/cm^3$ along 10 cm of length. Such measurements are presently made on the IHX, although they are for area densities corresponding to less than a single fringe shift. The temperature can be estimated by the technique of measuring the degree and rate of ionization of impurity carbon atoms by observing carbon ion spectral lines. Alternatively, the temperature can be measured by the double-foil transmission soft x-ray technique. The measurement of B_θ may be a difficult task if magnetic probes prove impractical. Measuring Faraday rotation is a possibility, although the geometry is not ideal because the magnetic field is azimuthal. For a 2.5-cm tangential path near the wall, a rotation of 0.029 rad would occur if $n = 2 \times 10^{16}/cm^3$, $B_\theta = 20$ kG, and $\lambda = 10.6$ μm. This amount of rotation is larger than those typically measured in IHX. For $n = 2 \times 10^{18}/cm^3$, $B = 50$ kG, and $\lambda = 0.633$ μm, the rotation is 0.026 rad, which should also be measurable. Such Faraday rotation measurements would probably be more straightforward than the present measurements in IHX because the time scale will be much longer and the desired accuracy will be less.

These diagnostics should give a good estimate of the plasma parameters. When we are confident that the plasma conditions are close to those desired, T_e, n_e, $\frac{dT_e}{dt}$ and $\frac{dn_e}{dt}$ can be measured using Thomson scattering. Accurate measurements of B_θ are not really necessary since its only function is to lower $\frac{dT}{dt}$ and $\frac{dn}{dt}$. If the energy and particle losses are to be tolerable during the ≈ 3 μs implosion time, the desired conditions for the initial plasma are: $\frac{1}{T}\frac{dT}{dt}$ and $\frac{1}{n}\frac{dn}{dt} \leq 10^6/s$.

In contrast to separate plasma preparation experiments, diagnostic access to the plasma of an imploding liner system is expected to be very poor. The

plasma would be completely surrounded by metallic walls, and all diagnostic elements located close to the liner would be destroyed on each shot. Therefore, the most promising diagnostic, assuming some degree of success, will be neutron emission from the hot deuterium plasma. The number of neutrons produced in the liner-imploded plasma experiment will depend strongly on the degree to which the requirements of both the liner and the plasma experiments are met. There could well be sufficient number to allow a measurement of the ion temperature from the broadening of the neutron velocity distribution. Then, from the total number of neutrons and the volume as measured by flash x rays, one can deduce n. If the neutron yields are too small, a small hole can be used in one of the end plates to allow particles and radiation to escape. In this case charged-particle energy analyzers can be used, and spectroscopy and soft x-ray measurements can be performed on the radiation to give further information on plasma parameters.

III. THEORY

A. Analytical Scaling Model

An approximate analytic model has been constructed for the calculation of the final plasma conditions, produced by adiabatic compression, and the resulting DT-burn effected by an imploding compressible liner. For the parameter regime of interest to us, no shocks are produced in the liner material during the implosion phase. The work differs from the fundamental work of Shearer and Condit[28] in the following respects.

1. Cylindrical convergence of a possibly thick liner is allowed.
2. A simple Gruneisen equation of state is applied to the liner.[29]
3. The parametric dependence of the final plasma temperature and the gain (Q) on the initial conditions is emphasized.

The simple liner equation of state used here is equivalent to a linear variation of the bulk modulus with pressure,

$$B(P) = B_o + B'P = \rho\, dP/d\rho \qquad \text{(III-1)}$$

where, for many metals of interest (copper, silver, gold, aluminum), $B' \simeq 5$ (Ref. 30). The final results prove to be very insensitive to the elastic modulus B_o. The equation of state derivable from Eq. (III-1) can be used to represent the compressional energy of the liner in the form shown below.

The key to the physics of the compressible liner lies in writing the liner internal energy corresponding to Eq. (III-1) in the "symmetrical" form

$$\rho w = \frac{B_o}{B'-1}\left(\frac{P}{B_o} - \frac{\rho-\rho_o}{\rho_o}\right) , \qquad \text{(III-2)}$$

where w is the specific internal energy, and observing that for moderate material compressions ($\rho/\rho_o \simeq 1.5$, say), the pressure term, P/B_o dominates the density term $(\rho-\rho_o)/\rho_o$. This approximation greatly facilitates the theory and proves accurate for those implosions that are sufficiently strong that, somewhere in the liner, $(\rho-\rho_o)/\rho_o$ is not <u>too</u> small. [For everywhere very small $(\rho-\rho_o)/\rho_o$, the

two terms of Eq. (III-2) exactly cancel, and the liner behaves as an incompressible material.] The accuracy of Eq. (III-2) is not very crucial, since only its integral over the liner cross section enters the final results.

By means of Eq. (III-2), system energy balance, pressure balance across the inner liner surface, and an approximate calculation of the pressure profile in the liner, it is possible to obtain a simple transcendental equation for a supplementary variable θ, in terms of which the energy transfer efficiency (initial liner kinetic energy, E_L, into final plasma thermal energy, E_{pf}) and final plasma temperature can be expressed.

The pressure profile is estimated in a manner similar to that employed by Shearer and Condit,[28] however, without neglecting cylindrical convergence effects. The essence of the method is to observe, from code runs, that the liner moves roughly as a whole, even for liners whose radius and thickness have become comparable. The fact that each layer of liner undergoes roughly the same acceleration implies that the force on a layer, divided by all the liner mass beyond that layer, is roughly independent of which layer is singled out. One can thereby obtain a relation between the pressure profile and an integral of the density profile. Since a further integral is performed to obtain the liner internal energy, the results will be very insensitive to the specific density enhancement profile. We have chosen the latter to be a flat profile, with $\rho \approx \rho_o$.

The equation for θ then proves to be

$$\frac{E_{pi}}{E_L}\left(10\,\frac{\pi R_{pi}^2}{A_{Li}}\right)^{2/3}(1+\tfrac{5}{2}\theta)^{2/3}\,\theta^{2/3}\,(\theta+1) = 1\,, \qquad \text{(III-3)}$$

where E_{pi} is the initial plasma energy, R_{pi} is the initial plasma radius, and A_{Li} is the initial metal cross-sectional area. Equation (III-3) is trivial to solve numerically. Then the energy transfer efficiency, $\varepsilon = E_{pf}/E_L$, can be expressed as

$$\varepsilon = 1/(1+\theta)\,. \qquad \text{(III-4)}$$

Thus, θ can be interpreted as the ratio of the liner internal energy to the plasma energy, at peak compression. The final plasma temperature T_f can be

written as

$$T_f = T_i \left[10 \left(1 + \frac{5}{2}\theta\right) \theta \frac{\pi R_{pi}^2}{A_{Li}} \right]^{2/3} . \qquad \text{(III-5)}$$

To calculate the system gain (fusion energy out relative to liner energy in), we first make a rough estimate of the burn time as the fusion energy divided by half the peak fusion power for a triangular power pulse. The energy calculation involves a time integral of the fusion power over the liner motion. Each point on the trajectory involves plasma conditions and liner conditions that are expressible in terms of the final state and the fractional distance to be traveled to reach the final radius. The "rough" estimate of the burn time made here involves setting the temperature-dependence of $\langle\sigma v\rangle_{DT} \propto T^2_{plasma}$, a good approximation between 7 keV and 20 keV (see Ref. 28 and Table III-I).

TABLE III-I. RELATIVE VALUES OF $\langle\sigma v\rangle_{DT}/T_f^2$.

T_f(keV) =	8.0	9.0	10.0	11.0	12.0	13.0	
$\langle\sigma v\rangle/T_f^2$ =	183	196	206	213	219	222	
T_f(keV) =	14.0	15.0	16.0	17.0	18.0	19.0	20.0
$\langle\sigma v\rangle/T_f^2$ =	224	225	225	224	223	221	219

Then the trajectory integral can be done practically analytically. (The velocity of the liner inner surface also enters the trajectory irtegral when converting the integration variable from time to plasma radius. This velocity is estimated from conservation of energy and approximated by its values near the final state, where most of the burn occurs.) The resulting expression for the burn time, τ, can be written as

$$\tau\sqrt{\frac{2\pi}{\rho_i}} = 2\,\frac{\pi}{4}\sqrt{\frac{2}{15}}\,A_{Li}\,\frac{\varepsilon}{5/3-\varepsilon}\,\frac{1}{\sqrt{(E_L/\ell)(1-\varepsilon)}}\;x\;\frac{.285}{.25}\;x\;G(\theta), \qquad \text{(III-6)}$$

where ℓ is the system length and ρ_i is the initial liner density in g/cm^3. The prefactor of 2 comes from dividing the energy by half the peak power. The post-factor (.285/.25) comes from a more accurate numerical evaluation of the trajectory integral which is provisionally evaluated analytically to be $(\pi/4)$. The trajectory integral, after much reduction, has the form

$$\int_0^\infty \frac{d\delta}{(1+\delta)^{14/3}\sqrt{\delta}} ,$$

where δ represents the fractional distance to the final radius. The post-factor, $G(\theta)$, is a complicated function of θ that comes from an accurate evaluation of the mass-averaged root-mean-square liner velocity $\langle u\rangle$. $G(\theta)$ is always very close to 1.0, as illustrated in Table III-II.

TABLE III-II. VALUES OF $G(\theta)$

$$G(\theta) \equiv \left[\frac{10/3 - 2\varepsilon}{7/3 - \varepsilon + (1-\varepsilon)/\sqrt{1+\alpha\theta}}\right]^{1/2}$$

$$\varepsilon(\theta) = 1/(1+\theta) \text{ and } \alpha(\theta) = 10 + 25\theta$$

θ =	.1	.2	.3	.4	.5	.6	.7	.8	.9
$G(\theta)$ =	1.010	1.025	1.041	1.054	1.065	1.075	1.084	1.091	1.098
θ =	1.0	2.0	3.0	4.0	5.0	6.0	7.0	8.0	9.0
$G(\theta)$ =	1.103	1.138	1.153	1.162	1.168	1.172	1.175	1.177	1.179

To complete the calculation of the system gain, we write the fusion energy out (peak power times $\tau/2$ for a triangular power pulse) as Q times the input liner energy, and the latter as (E_{pf}/ε). The resulting Lawson-type expression can be written as

$$\frac{\varepsilon}{Q} n_f \tau = \frac{12\ T_f(\text{ergs})}{y\langle\sigma v\rangle_{DT}} \equiv F\ (T_f) \quad , \qquad \text{(III-7-a)}$$

where y is the energy yield (17.6 MeV) per D-T reaction, in ergs.

Here, according to Glasstone and Lovberg,[31] we have taken

$$\langle\sigma v\rangle_{DT} = \frac{5.0 \times 10^{-12}}{T_f^{2/3}\ (\text{keV})} \exp\left[-\frac{19.94}{T_f^{1/3}\ (\text{keV})}\right] \ \text{cm}^3/\text{s} \quad . \qquad \text{(III-7-b)}$$

where the numerical coefficient of 3.68 has been changed to 5.0 to give better agreement with the values of J. L. Tuck[32] between 6 and 20 keV. Equations (III-6) and (III-7) and the definition, $\varepsilon \equiv (E_{pf}/E_L)$, can be folded together to give an explicit expression for the normalized gain. It reads

$$Q \sqrt{\frac{2\pi}{\rho_i}} = \frac{1}{2} \frac{y\langle\sigma v\rangle_{DT}}{12\ T_f^2(\text{ergs})} \pi \sqrt{\frac{5}{6}}\ \varepsilon \sqrt{(1-\varepsilon)(E_L/\ell)} \times \frac{.285}{.25} \times G(\theta) \quad . \qquad \text{(III-8)}$$

(The appended prefactor of (1/2) comes from the fact that in a triangular power pulse, the yield is the burn time times <u>half</u> tne peak power). Because of the approximate treatment of Eq. (III-2), Eq. (III-8) is only meaningful provided ε is not very close to 1.0, i.e., for appreciable liner compressions.

Comparison[33] of this analytic model with R. Malone's computer code, CHAMISA, is displayed in Fig. III-1 and Table III-III. This sophisticated code is described in Section III.B. It is seen that the transfer efficiencies, final temperatures, and Q values are in excellent agreement. Thus, the approximate analytic model can be used to check the code and for rapid and inexpensive exploration of the initial parameter space, $(E_L/\ell,\ N \equiv n_{pi}\pi R_{pi}^2,\ T_i,\ \pi R_{pi}^2/A_{Li})$. Note that even in the unoptimized case shown in the figure, break-even ($Q \simeq 1$) at $E_L/\ell \simeq 100$ MJ/m is predicted, or 10 MJ for a 10-cm-long liner. By optimization of density and

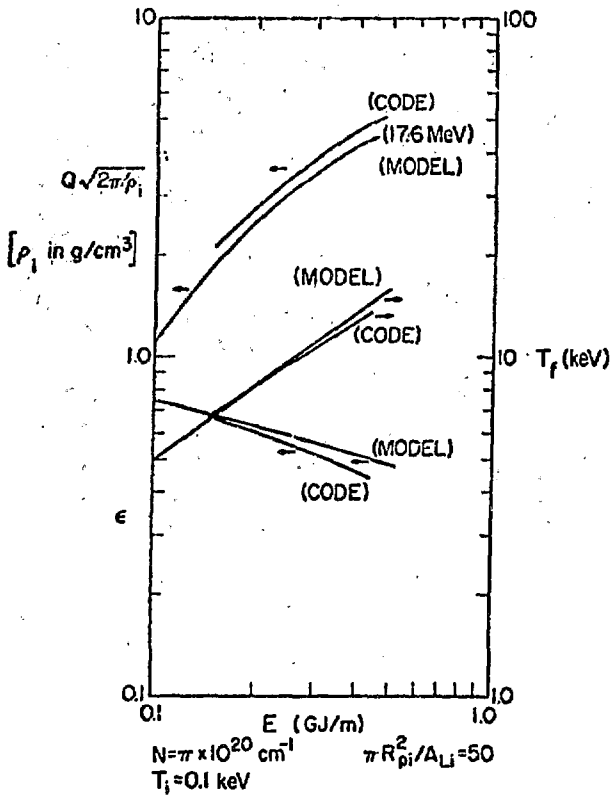

Fig. III-1. Comparison of the model and the code, CHAMISA.

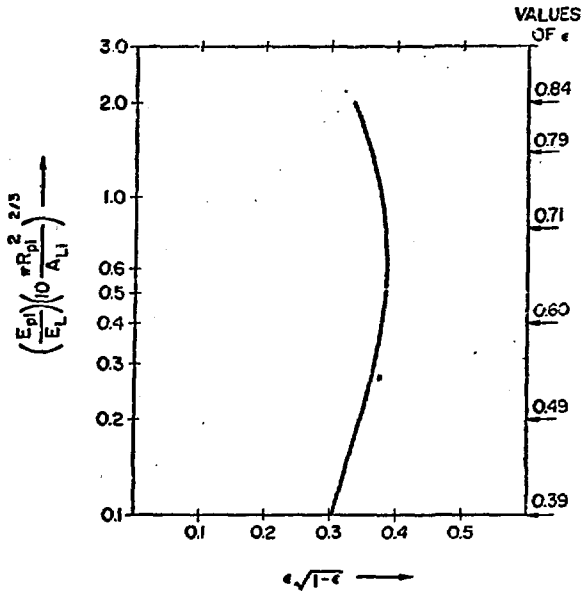

Fig. III-2. Relation between the transfer efficiency and initial parameters.

temperature of the initial plasma, the gain can be doubled at E_L/ℓ = 0.1 GJ/m, for N = 0.9 x 10^{20}cm^{-1} and T_i = 0.22 keV. The optimization procedure is described next in this section. Note also that, in spite of the liner being compressible, the energy transfer efficiencies remain quite high, $\varepsilon \simeq$ 50 to 60%.

TABLE III-III. COMPARISON OF MODEL OPTIMIZATION WITH CODE OPTIMIZATION

	Model	Code
$[Q\sqrt{2\pi/\rho_i}]_{opt.}$	2.7	3.4
$\tau_{opt.}[\mu s]$	1.6	1.9
$(T_{pi}[eV])_{opt.}$	220	270
$(P_{pf}[dynes/cm^2])_{opt.}$	1.2 x 10^{13}	1.2 x 10^{13}

Based upon the above description and results of the model, it is now possible to prescribe scaling laws that lead most directly to high-Q machines. Since Q essentially depends upon the product

$$\frac{\langle\sigma v\rangle}{T_f^2}\left(\epsilon\sqrt{1-\epsilon}\right)\sqrt{E_L/\ell}\ ,$$

the best that one can do, aside from increasing the liner energy, E_L, is to maximize the first two factors. The ϵ factor peaks at $\theta = 1/2$, $\epsilon = 2/3$. According to Eqs. (III-3) and (III-4), and the corresponding solution plotted in Fig. III-2, we must then have an optimal combination of initial parameters,

$$\frac{E_{pi}/\ell}{E_L/\ell}\left[10\,\frac{\pi R_{pi}^2}{A_{Li}}\right]^{2/3} = 0.6\ . \qquad \text{(III-9)}$$

At the same time, since $(\langle\sigma v\rangle_{DT}/T_f^2)$ has a broad maximum around $T_f = 15$ keV, we then have from Eq. (III-5)

$$T_i(\text{keV})\left[10\,\frac{\pi R_{pi}^2}{A_{Li}}\right]^{2/3} = (15\ \text{keV})(8/9)^{2/3}\ , \qquad \text{(III-10)}$$

or, also,

$$T_i(\text{keV})(\pi R_{pi}^2/A_{Li})^{2/3} = 3.0\ . \qquad \text{(III-10-a)}$$

Dividing Eq. (III-9) by Eq. (III-10) with a conversion from keV to ergs, we then find the following optimal condition

$$\frac{N}{(E_L/\ell)} = 9.0 \times 10^6\ \text{ergs}^{-1}\ , \qquad \text{(III-11)}$$

where E_L/ℓ is in ergs/cm, or, also

$$N[cm^{-1}] = 9.0 \times 10^{20} \, (E_L/\ell \; [GJ/m]), \qquad \text{(III-11-a)}$$

where $N \equiv n_{pi}\pi R_{pi}^2$ is the plasma line density in cm^{-1}. Equation (III-11) just says that, for fixed final temperature and fixed efficiency, the liner energy per particle is an invariant. Equations (III-10) and (III-11) constitute optimal relations between the initial parameters.

Under these conditions, the system gain from Eq. (III-8) will then scale exactly as

$$Q\sqrt{2\pi/\rho_i} = 6.94 \sqrt{(E_L/\ell)[GJ/m]} \quad ,$$

or, also, rounding off slightly,

$$\left[Q\sqrt{2\pi/\rho_i}\right]_{opt.} = 7.0\sqrt{E_L/\ell \; [GJ/m]} \quad . \qquad \text{(III-12)}$$

Other relations of interest under these optimal conditions are as follows. The burn time under optimal conditions proves to be

$$\tau_{opt.} = \left(0.5 \, R_{pi}[cm] \, \Delta_i[cm]/\sqrt{E_L/\ell \; [GJ/m]}\right)\sqrt{\rho_i/2\pi} \quad [\mu s] \; , \qquad \text{(III-12-a)}$$

where Δ_i is the initial liner thickness, and the final plasma pressure under optimal conditions is found to be

$$[P_{pf}]_{opt.} = 5.0 \, \frac{\tau_L/\ell}{A_{Li}} \; . \qquad \text{(III-12-b)}$$

The relations, Eqs. (III-10-a), (III-12), (III-12-a), and (III-12-b) were compared with a run of the code CHAMISA, for a copper liner, with $(\pi R_{Pi}^2/A_{Li}) = 50$ and $E_L/\ell = 0.15$ GJ/m. The comparison is tabulated below. The agreement appears to be quite satisfactory. Eq. (III-12) implies "break-even" with input energies on the order of 20 MJ/m!

Since there will probably be a practical upper limit to the initial plasma volume density that can be achieved, Eq. (III-11) implies that

$$R_{pi}/\sqrt{(E_L/\ell)} = \text{const.} \qquad \text{(III-13)}$$

Since there will also probably be a practical upper limit to the initial plasma temperature that can be achieved, Eqs. (III-10) and (III-13) imply

$$A_{Li}/(E_L/\ell) = \text{const.} \qquad \text{(III-14)}$$

But $A_{Li} = 2\pi R_{pi}\,\Delta_i$, where Δ_i is the initial liner thickness. Again noting Eq. (III-13), Eq. (III-14) becomes

$$\Delta_i\sqrt{(E_L/\ell)} = \text{const.} \qquad \text{(III-15)}$$

We conclude that, for given plasma initial density and initial temperature, the scaling, $Q \sim \sqrt{(E_L/\ell)}$, can be achieved by simultaneously increasing the liner initial radius and thickness as $\sqrt{(E_L/\ell)}$.

B. Numerical Code Capabilities

Detailed numerical calculations have been made in order to verify the analytic model discussed above and to provide information on the temporal behavior of the system.

The basic features of the code, CHAMISA, which was used are summarized below:

- One-dimensional cylindrical geometry (planar or spherical geometry available also).
- Lagrangian hydrodynamics; treats liner compressibility.
- Inviscid fluid flow; no elastic-plastic effects.
- One or two material temperatures (electrons and ions).
- Realistic material equations of state (calculated by Group T-4,

LASL). Density and temperature based, treating solid, liquid, and gas phases, ionization, crystalline phase changes, and degeneracy. Descriptions of the methods used to calculate the equations of state and results for several materials are given in Refs. 34,35,36.

- Thermal conduction (along or across a magnetic field).
- Magnetic field diffusion, including temperature, density, and phase change effects on the electrical resistivity. Ohmic heating of liner treated. Alternatively, the simple magnetic field boundary condition options (see below) can be used if field diffusion is not of interest.
- Thermonuclear burn.
- Boundary condition options for liner dynamics:
  - Constant or time-variable external pressure.
  - Adiabatic ideal gas. Can be used in conjunction with magnetic field options below. Bremsstrahlung losses and thermonuclear burn (DT plasma) monitored; no feedback to affect state of gas.
  - B_θ magnetic field generated by Z-pinch current in liner. Current can be programmed in time in an arbitrary way or to describe a driving circuit for the liner system. Field excluded from liner (perfect conductor).
  - B_z magnetic field; constant total flux assumed. Field excluded from liner (perfect conductor).
- Liner rotation.

The results of the calculations which have been made with this code appear in various sections of this proposal. In particular, numerous parameter studies of compressible liners driving adiabatic plasmas have been made to verify the analytic model and scaling laws presented in Section III.A; appropriate results are presented there. In Section III.C, simple scaling relations are used to obtain non-self-consistent estimates of plasma loss rates using the plasma parameters obtained from code calculations. In Section III.D code results are used extensively in a discussion of the thermal state of the liner as determined by adiabatic compression, shock and viscous heating, magnetic field diffusion and ohmic heating, and neutron energy deposition in the liner. Finally, in Section IV, code calculations are compared with an incompressible liner model used for

certain aspects of the reactor analysis.

It is clear from the list of code features that the numerical capability is already available to go well beyond the preliminary calculations presented in this proposal, especially in regard to the interaction of the central plasma and magnetic field with the liner. We propose to study the time-dependent problem, with a spatially inhomogeneous plasma and a nonideal solid wall, which involves magnetic field diffusion into the liner, thermal conduction to and into the liner, and radiation from both the plasma and the ablated liner material. This can also be done in the context of a liner implosion, in which the plasma energy gains and losses are calculated self-consistently.

Numerous other codes are available within the Laboratory which complement the capabilities of the code just described. In particular both one- and two-dimensional codes[37,38,39] exist which treat the elastic-plastic material state which exists during the implosion phase. The two-dimensional code[39] has previously been used for analysis of the effects of yield strength[40] and viscosity[41] on the development of Rayleigh-Taylor growth in solids.

C. State of the Plasma

1. Estimates Based on Analytical Model. In Sec. III.A, an approximate analytic model was constructed for the elucidation of the final state and burn of an adiabatically compressed plasma imploded by a compressible cylindrical liner. The notion of system optimization for a given input energy was introduced, and the scaling from one optimized system to the next with increasing input energy was displayed. In this subsection, we shall restrict our attention to these optimized systems only, and shall roughly estimate their losses due to bremsstrahlung and heat conduction, and their additional heating due to 3.5-MeV alpha-particle redeposition. Clearly, the notion of an optimized ideal system, derived by neglecting these losses and gains, is only sensible provided that these effects prove to be small perturbations on the ideal system itself.

For nonoptimized systems, we can use the more general loss expressions in conjunction with our short, fast, model code which basically involves just the numerical solution of the transcendental equation for θ. We hereby propose to carry out these more general parameter studies as part of our theoretical liner program.

a. Bremsstrahlung Losses. In calculating these losses, we distinguish two regions of time, the time during the implosion to the final state, and the burn time. The fact that these regions have some overlap is of no great importance to the following discussion.

The instantaneous power density of bremsstrahlung radiation is

$$P_{brem} = 5.35 \times 10^{-24}\, n^2\, T_p^{1/2}(\text{keV}) \ [\text{ergs cm}^{-3}\text{s}^{-1}] \ . \qquad \text{(III-16)}$$

If we multiply by the instantaneous plasma volume and integrate over time up to the final state, we get the bremsstrahlung energy lost during the implosion, $E_{brem,f}$. As earlier, it is useful to convert from an integral over time to one over plasma radius, which involves dividing the integrand by a liner velocity obtained from global energy conservation. As before, we only require the liner velocity near the final state. We then take the ratio of the lost bremsstrahlung energy to the final plasma energy, and find

$$\frac{E_{brem,f}}{E_{pf}}\sqrt{\frac{2\pi}{\rho_i}} = \frac{5.35 \times 10^{-24}}{4.8 \times 10^{-9}} \frac{N}{\left[2T_f(\text{keV})\,\frac{E_L}{\ell}\right]^{\frac{1}{2}}} \sqrt{\frac{\alpha(\theta)\theta}{\frac{5}{3} - \varepsilon(\theta)}}\, G(\theta) I_{brem} \ , \qquad \text{(III-17)}$$

where ρ_i is the initial liner density in g/cm^3, N is the plasma line density in cm^{-1}, (E_L/ℓ) is the input energy in ergs/cm, and the functions $\varepsilon(\theta)$, $\alpha(\theta)$, $G(\theta)$ are defined as follows.

$$\varepsilon(\theta) = 1/(1+\theta)$$

$$\alpha(\theta) = 10 + 25\,\theta \qquad \text{(III-18)}$$

$$G(\theta) = \left[\frac{(2)(5/3-\varepsilon)}{7/3-\varepsilon + (1-\varepsilon)/\sqrt{1+\alpha\theta}}\right]^{1/2} .$$

Also, I_{brem} is the final form of the trajectory integral,

$$I_{brem} = \int_0^\infty \frac{d\delta}{(1+\delta)^{8/3}\sqrt{\delta}} = \int_{-\infty}^{\infty} \frac{dx}{(1+x^2)^{8/3}} \approx 1.28 \ . \qquad \text{(III-19)}$$

If we now specialize Eq. (III-17) to an optimized system, wherein $\theta \approx 1/2$, $T_f \approx 15$ keV, and $N \approx [9.0 \times 10^6 \times (E_L/\ell)][cm^{-1}]$ with E_L/ℓ in ergs/cm, then Eq. (III-17) reduces to

$$\left[\frac{E_{brem,f}}{E_{pf}}\sqrt{\frac{2\pi}{\rho_i}}\right]_{opt.} = 8.4 \times 10^{-2} \sqrt{\frac{E_L}{\ell}\left[\frac{GJ}{m}\right]} \quad , \tag{III-20}$$

where ρ_i is still in g/cm^3, but now (E_L/ℓ) is the input energy expressed in gigajoules per meter.

We conclude that the input energy can become as large as 100 GJ/m before the bremsstrahlung losses during the implosion become comparable to the energy obtained by the plasma from the liner.

Next, we suppose that the plasma sits in its final state for a burn time, and we compare that time to a bremsstrahlung cooling time. The latter is estimated by dividing the final plasma energy by the total bremsstrahlung power radiated under final-state conditions. We find

$$\tau_{brem} = \frac{E_{pf}/\ell}{P_{brem}/\ell} = \frac{[3N\, T_f(ergs)]\, \pi R_{pf}^2}{5.35 \times 10^{-24}\, N^2\, T_f^{1/2}(keV)}$$

or

$$\tau_{brem} = \frac{4.8 \times 10^{-9}}{5.35 \times 10^{-24}} \frac{T_f^{1/2}(keV)}{N} \pi R_{pf}^2 \, . \tag{III-21}$$

We now divide this by the burn time estimated in Subsection III.A. The result is

$$\frac{\tau_{brem}}{\tau}\sqrt{\frac{\rho_i}{2\pi}} = \frac{4.8 \times 10^{-9}}{5.35 \times 10^{-24}} \frac{T_f^{1/2}(keV)}{N} \frac{5/3-\varepsilon}{\alpha} \sqrt{\frac{(E_L/\ell)}{1-\varepsilon}} \frac{1}{[.574 \times G(\theta) \times \frac{.285}{.25}]} \, , \tag{III-22}$$

where ρ_i is the initial liner density in g/cm^3, and (E_L/ℓ) is the input energy in ergs/cm. Finally, we specialize this expression for an optimized system and find

$$\left[\frac{\tau_{brem}}{\tau}\sqrt{\frac{\rho_i}{2\pi}}\right]_{opt.} = \frac{4.3}{\sqrt{(E_L/\ell)[GJ/m]}} \quad , \tag{III-23}$$

where (E_L/ℓ) is now in gigajoules per meter. We see that the input energy can be as large as 10 GJ/m before the bremsstrahlung cooling time becomes as short as the burn time. We conclude that for input energies of less than a few GJ/m, bremsstrahlung losses from the body of the plasma will not be a serious concern.

b. Thermal Conduction Losses

i. Introduction. We envision a B_ℓ trapped in the plasma to provide thermal insulation in the radial and axial directions. At the same time, we suppose B_θ is sufficiently small as not to influence the plasma dynamics. These two conditions can be written, respectively, as

$$\omega_{ci}\,\tau_{ii} > 1 \qquad \text{(III-24)}$$
$$2n_{pi}\,T_{pi} > B_{\theta i}^2/8\pi \ .$$

Here, ω_{ci} is the ion gyrofrequency, and τ_{ii}, later sometimes called τ_i, is an ion-ion collision time, and all quantities are evaluated at the initial time. [Hence $B_{\theta i}$ means the initial B_θ.]

If we take, for simplicity,

$$\sqrt{m_{ion}/2m_{proton}}/(\Lambda/10) \simeq 1,$$

where Λ is the Coulomb logarithm, these inequalities can be written as

$$2.7 \times 10^{-15}\,\frac{n_{pi}[cm^{-3}]}{(T_{pi}[keV])^{3/2}} < B_{\theta i}[Gauss] < 2.8 \times 10^{-4}\,(n_{pi}[cm^{-3}])^{1/2}(T_{pi}[keV])^{1/2} \ , \qquad \text{(III-25)}$$

where we have set[42] $\tau_{ii} = 3 \times 10^{10}\sqrt{10}\ T_{pi}^{3/2}(keV)/n(cm^{-3})$.

Here $B_{\theta i}$ is a representative value of the initial azimuthal magnetic field, and n_{pi}, and T_{pi} are respectively the initial plasma volume density and temperature. The inequalities of Eq. (III-25) become more and more strongly satisfied as the adiabatic compression of the plasma proceeds. These inequalities have been mapped in Fig. III-3. We see that for $T_{pi} \simeq 100$ eV and $n_{pi} \simeq 3 \times 10^{17} cm^{-3}$, trapped fields of about 40 kgauss are required. For higher initial temperatures, the allowed range of fields becomes broader.

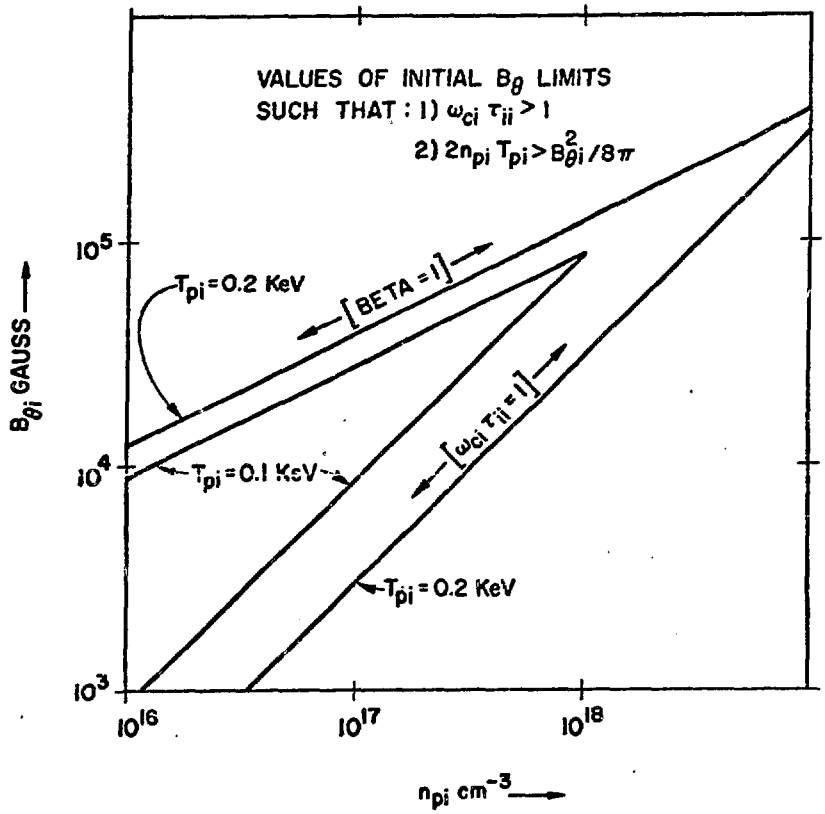

Fig. III-3. Values of B_θ such that i) the ions are magnetized, ii) magnetic pressure is small.

In this proposal, we do not present self-consistent calculations of the losses. Such complicated and detailed calculations are proposed for future work. Here, we provisionally assume that the radial gradient length is on the order of the instantaneous plasma radius. Thus, we neglect the short transient time required for the initial thin thermal boundary layer to relax to gross plasma dimensions. One might expect the initial thermal boundary layer to be only a few ion gyro-radii thick, and for initial densities like 10^{17} cm^{-3}, temperatures like 100 eV, and magnetic fields like 50 kGauss, the relaxation time of such a boundary layer is found to be only a few hundredths of a microsecond. This transient phenomenon differs from the analogous one discussed by Jensen[43] in that the initial plasma here has a high density (10^{17} to 10^{18} cm^{-3}) and a low temperature (100 to 200 eV), whereas the one discussed by Ref. 43 has a density of 10^{16} cm^{-3} and kilovolt temperatures.

ii. Radial Ion Heat Conduction. The instantaneous radial ion heat flux near the wall is approximated here by

$$q_{ion,r} \simeq \kappa_{\perp}^{ion} T_p/R_p \quad ; \tag{III-26}$$

where T_p is the central temperature, so that the total ion radial heat loss per second per cm is

$$\frac{Q_{ion,r}}{\ell} = 2\pi \kappa_{\perp}^{ion} T_p \quad . \tag{III-27}$$

Here the cross-field ion thermal conductivity for $\omega_{ci} \tau_{ii} > 1$ is given near the wall by

$$\kappa_{\perp}^{ion} = 2 \frac{n_p \Phi T_p}{m_{ion} \Phi^{3/2} \tau_{ii} \omega_{ci}^2} = \frac{2}{m_{ion} \tau_{ii}(initial) \Phi^{1/2}} \frac{N T_p}{\left[\pi R_p^2 \omega_{ci}^2\right]_{initial}} , \tag{III-28}$$

with τ_{ii} the ion-ion collision time referred to the central temperature, N the line density, and both are constants of the motion. Also, we have noted that $(R_p^2 \omega_{ci}^2)$ is a constant of the motion which we set to its initial value. Finally, we have represented the temperature near the wall by some fraction, Φ, times the central temperature.

The energy lost due to radial ion heat conduction during the implosion to the final state, $E_{ion,r,f}$, can now be evaluated by the same methods used for bremsstrahlung. We find, after normalization to the final plasma energy,

$$\frac{E_{ion,r,f}}{E_{p,f}} \sqrt{\frac{2\pi}{\rho_i}} = \tag{III-29}$$

$$\frac{4}{3}\pi \frac{T_f(ergs) G(\theta) I_{brem}}{(\omega_{ci}\tau_{ii})_{in.} \Phi^{1/2} (\pi R_{pi}^2 / A_{Li}) (m_{ion} \omega_{ci}(in.)) \sqrt{(E_L/\ell)(ergs/cm)} \sqrt{2\alpha\theta(5/3-\varepsilon)}} ,$$

where ρ_i is the liner initial density in [g/cm^3], and "in." stands for "initial value."

Upon specialization to an optimized system [$G(\theta) = 1.07$, $\theta = 1/2$, $\varepsilon = 2/3$, $\alpha = 22.5$, $T_f(ergs) = 1.6 \times 10^{-9} T_f(keV) = 1.6 \times 10^{-9} \times 15$ keV] and noting that $I_{brem} = 1.28$, this becomes

$$\left[\frac{E_{ion,r,f}}{E_{p,f}}\sqrt{\frac{2\pi}{\rho_i}}\right]_{opt.}$$

$$= \frac{2.90 \times 10^{-15}}{(\omega_{ci}\tau_{ii})_{in.}\Phi^{1/2}(\pi R_{pi}^2/A_{Li})(m_{ion}\omega_{ci}(in.))\sqrt{(E_L/\ell)[GJ/m]}} \quad . \qquad \text{(III-30)}$$

Because τ_{ii} is proportional to $[T_{pi}^{3/2}/n_{pi}]$, this result can be further reduced by means of the two optimization conditions derived earlier, namely

$$T_i^{3/2}(keV) \times (\pi R_{pi}^2/A_{Li}) = \frac{[15(keV)]^{3/2} \times (8/9)}{10} = 5.16 \qquad \text{(III-31)}$$

and

$$N = \{9.0 \times 10^{20} \times (E_L/\ell)[GJ/m]\}cm^{-1} \quad . \qquad \text{(III-32)}$$

In the further reduction of Eq. (III-30), we take $m_i = 4500\ m_e$, which constitutes an average D,T mass.

If we also recall that

$$R_p(cm)B_\theta(Gauss) = 2 \times 10^5 \times I_z(MA) \quad , \qquad \text{(III-33)}$$

where I_z is the trapped axial plasma current (a constant of the motion), then Eq. (III-30) can finally be reduced to

$$\left[\frac{E_{ion,r,f}}{E_{p,f}}\sqrt{\frac{2\pi}{\rho_i}}\right]_{opt.} = \frac{0.67}{\Phi^{1/2}} \frac{\sqrt{E_L/\ell\ [GJ/m]}}{(I_z[MA])^2} \quad . \qquad \text{(III-34)}$$

We conclude that, if the instantaneous plasma radius is a relevant scale length, then the energy loss due to cross-field radial ion thermal conduction during the liner implosion will not be a serious problem provided

$$I_z[MA] > (E_L/\ell\ [GJ/m])^{1/4}/\Phi^{1/4} \quad , \qquad \text{(III-35)}$$

which means that I_z must be at least one or two megamperes for input energies from .01 to 1 GJ/m, and, furthermore, this required plasma current scaling is predicted to be rather insensitive to the input energy to the liner. These values of plasma current are not inconsistent with those allowed values of B referred to in Fig. III-3 and in the introduction to this section. The initial trapped magnetic energies involved amount to only a few tenths of MJ per meter.

Next, we consider the cooling time of this loss mechanism, during the final state, compared to the burn time.

Dividing the final plasma energy by the radial ion heat conduction loss rate, we find a cooling time,

$$\tau_{ion,r} = \frac{3NT_f(ergs)}{2\pi K_1^{ion} T_f(ergs)} = \frac{3}{4\pi}\,\Phi^{1/2}\,\frac{m_{ion}\tau_{ii}(in.)\pi R_{pi}^2\omega_{ci}^2(in.)}{T_f(ergs)}\,, \qquad \text{(III-36)}$$

where T_f is the central temperature, and (ΦT_f) again represents an outer temperature. The ratio of this time to the previously estimated burn time is

$$\frac{\tau_{ion,r}}{\tau}\sqrt{\frac{\rho_i}{2\pi}} = \frac{3}{4\pi}\,\frac{(5/3-\varepsilon)\sqrt{1-\varepsilon}}{\varepsilon}\,\frac{\Phi^{1/2}}{\left(.574\ G(\theta)\frac{.285}{.25}\right)}\,\frac{m_{ion}\tau_{ii}(in.)}{T_f(ergs)}\,\frac{\pi R_{pi}^2}{A_{Li}}\,\omega_{ci}^2(in.)\sqrt{\frac{E_L}{\ell}}\,,$$

(III-37)

where ρ_i is the liner initial density in (g/cm^3), and (E_L/ℓ) is the input energy in (ergs/cm). We specialize to an optimized system by writing $\theta = 1/2$, $\varepsilon = 2/3$, $G(\theta) = 1.07$, $T_f(ergs) = 1.6 \times 10^{-9}\ T_f(keV)$, with $T_f(keV) = 15$ keV. Then Eq. (III-37) becomes

$$\left[\frac{\tau_{ion,r}}{\tau}\sqrt{\frac{\rho_i}{2\pi}}\right]_{opt.} = .0078\ \Phi^{1/2}\ B_\theta^2(in.)\ \tau_{ii}(in.)\ \frac{\pi R_{pi}^2}{A_{Li}}\sqrt{\frac{E_L}{\ell}\left[\frac{GJ}{m}\right]}\,, \qquad \text{(III-38)}$$

where the input energy is now in (GJ/m), and B (in.) is the edge value of the initial trapped magnetic field in gauss. Then, noting the dependence $\tau_{ii}(in.) \propto (T_{pi}^{3/2}/n_{pi})$ and again making use of Eqs. (III-31), (III-32), and (III-33), we find that Eq. (III-38) reduces to

$$\left[\frac{\tau_{ion,r}}{\tau}\sqrt{\frac{\rho_i}{2\pi}}\right]_{opt.} = 0.53\,\Phi^{1/2}[I_z(MA)]^2/\sqrt{(E_L/\ell)[GJ/m]}\ . \qquad \text{(III-39)}$$

We again conclude that essentially condition (III-35) is required in order that the radial heat-conduction cooling time exceeds the burn time.

iii. Axial Heat Conduction Driven by Radial Gradients. Axial heat flux driven across B_θ by axial temperature gradients should be relatively unimportant compared to radial heat conduction driven by radial temperature gradients, because the area at the end-plugs is generally much smaller than the lateral surface of the liner. However, according to Braginskii,[42] there also exists an axial heat flux driven by radial gradients, which we now discuss. For each species, with $\omega_{cj}\tau_{jj} >> 1$, this cross-effect heat flux has the form

$$q_{cross,z} = \frac{5}{2}\frac{n_p T_p}{m_{ion}\omega_{ci}}\frac{T_p}{R_p}\ , \qquad \text{(III-40)}$$

where T_p and R_p are instantaneous values of plasma temperature and radius, and $\omega_{ci} = eB_\theta/m_{ion}c$, with B_θ being a representative azimuthal magnetic field. The heat flux represented by Eq. (III-40) flows only along isotherms, producing neither cooling of the plasma nor changes in its entropy. Also, this heat flux is equal but oppositely directed for ions and electrons. However, it is not at all clear what becomes of this benign situation near the end plugs, where the heat flux (of the j^{th} species, say) turns the corner and flows (along isotherms) towards the axis with $\omega_{cj}\tau_j \to 0$. The region where the axis intersects the end plug presents a complicated two-dimensional problem, exacerbated by the wide range of values covered by $\omega_{cj}\tau_j$ as well as by species coupling through equipartition. We propose to study this problem further. For now, nothing more can be said as to whether the heat flux represented by Eq. (III-40) indeed remains a benign phenomenon.

iv. Axial Heat Conduction Near the Axis. We consider now the heat conduction to the end plugs in regions so near the axis that $\omega_{cj}\tau_j < 1$, for

either species. Thus, we exclude from the present discussion those hard-core systems mentioned elsewhere in this proposal. Such systems cannot have axial loss of the type we now consider, but instead might suffer the usual problems of a wall in a hot plasma environment. Within the context of a very pessimistic over-estimate derived later in this section, the total heat conduction out of these near-axis "holes" proves to be dominated by the ions, and can be obtained, to within a numerical coefficient C, by just multiplying Eq. (III-40) by the total area of an end-face! Thus, we write this power loss as

$$Q_{hole,ion} \approx C \frac{n_p T_p^2(ergs)}{m_{ion}(\omega_{ci} R_p)} \pi R_p^2 \approx C \frac{c}{e} \frac{N\ T_p^2}{(B_\theta R_p)_{in.}} , \qquad \text{(III-41)}$$

where N is the plasma line density, and C is the numerical coefficient. Here we have taken the representative value of B_θ to be near the wall, as will be justified by the derivation that is presented later in this section. Then, we have noted that $[B_\theta(R_p) \times R_p]$ is a constant of the motion and have used its initial value.

Upon integration of this power over time up to the final state, we obtain the energy lost to the plasma by this means during the implosion. The result, relative to the final plasma energy, can be written

$$\frac{E_{hole,ion,f}}{E_{pf}} \sqrt{\frac{2\pi}{\rho_i}} = \frac{C}{3} \frac{c}{e} \frac{T_f(ergs)}{[B_\theta R_p]_{in.}} \frac{A_{Li}}{\ell} \frac{1}{\sqrt{(E_L/\ell)[ergs/cm]}} \frac{G(\theta) I_{brem}}{\sqrt{2\alpha\theta(5/3-\varepsilon)}} . \qquad \text{(III-42)}$$

where B_θ is in Gauss, ρ_i is in g/cm^3, and R_p, ℓ, and $A_{Li}^{1/2}$ are in cm. Upon specialization to an optimized system, this becomes

$$\left[\frac{E_{hole,ion,f}}{E_{pf}}\right]_{opt.} \sqrt{\frac{2\pi}{\rho_i}} = 0.46 \times C \left(\frac{R_{pi}\Delta_i}{\ell}\ [cm]\right) \frac{1}{I_z[MA]\sqrt{E_L/\ell\ [GJ/m]}} . \qquad \text{(III-43)}$$

One can also estimate the cooling time, $\tau_{hole,ion}$ during the final state, as the final plasma energy divided by the loss rate given by Eq. (III-41). Here, and also in Eq. (III-43), we pessimistically assume full thermal contact between

the entire plasma and the near-axis "pipe." One thus has

$$\tau_{hole,ion} = 3N\, T_f\, \ell \cdot \frac{1}{C}\frac{e}{c}\frac{(B_\theta R_p)in}{N\, T_f^2} \quad . \tag{III-44}$$

For an optimized system, this can be written

$$\left[\tau_{hole,ion}\right]_{opt.} = \{(40/C) \times 10^{-8}\, \ell[cm]\, I_z[MA]\}\ [sec] \quad . \tag{III-45}$$

Upon division of Eq. (III-45) by the burn time of an optimized system, namely,

$$\tau_{opt.} = \sqrt{\frac{\rho_i}{2\pi}} \times 0.51 \times \frac{R_{pi}\Delta_i[cm^2]}{\sqrt{E_L/\ell\ [GJ/m]}} \times 10^{-6}\ [sec] \quad ,$$

one finds

$$\left[\frac{\tau_{hole,ion}}{\tau}\sqrt{\frac{\rho_i}{2\pi}}\right]_{opt.} = \frac{0.80}{C}\ \frac{\ell}{R_{pi}\Delta_i}\ [cm^{-1}]\ \ I_z[MA]\sqrt{E_L/\ell\ [GJ/m]} \quad , \tag{III-46}$$

where Δ_i is the initial thickness of the liner. Later in this section, we roughly estimate that the numerical factor is $C \lesssim 7$. However, we believe that this value of C is probably orders of magnitude too large.

According to either Eq. (III-43) or Eq. (III-46), we then conclude that, if $R_{pi} \sim \ell$ and $\Delta_i \sim 0.1$ cm, the heat loss due to this mechanism will not dominate the input energy provided

$$I_z[MA] > 14\sqrt{E_L/\ell\ [GJ/m]} \quad . \tag{III-47}$$

More generally, the condition that this near-axis heat loss be small can be written as,

$$I_z[MA] > \frac{\{(10\ R_{pi}\Delta_i/\ell)\ [cm]\}}{\sqrt{(E_L/\ell)[GJ/m]}} \quad . \tag{III-48-a}$$

We also recall Eq. (III-35) s the condition that the radial heat conduction be small,

$$I\ [MA] > \frac{\{(E_L/\ell)[GJ/m]\}^{1/4}}{\Phi^{1/4}} \quad . \qquad \text{(III-48-b)}$$

These conditions can be conveniently combined as

$$I_z[MA] > \frac{\{(E_L/\ell)[GJ/m]\}^{1/4}}{\Phi^{1/4}} + \frac{\{(10\ R_{pi}\Delta_i/\ell)[cm]\}}{\sqrt{(E_L/\ell)[GJ/m]}} \quad . \qquad \text{(III-48-c)}$$

This combined condition reduces to Eq. (III-48-a) at low input energies, to Eq. (III-48-b) at high input energies, and provides a reasonable transition at intermediate input energies. It is plotted in Fig. III-4, with $\Phi = 1/16$, and $(10\ R_{pi}\Delta_i/\ell\ [cm])$ as a parameter. [Recall that Φ is the plasma temperature near the radial wall, divided by the central plasma temperature.] We see that the plasma current needs to be several megamperes in order to keep the thermal losses to an acceptably small level, but we believe that the axial losses that appear to dominate at low input energies constitute a great over-estimate. This is discussed later.

We now present a derivation of the loss rate, Eq. (III-41). Since B_θ must vanish at $r = 0$, we suppose it is proportional to r throughout the plasma. We over-estimate the heat loss in this axis region by supposing that $B_\theta = 0$ up to a radius where $\omega_{ci}\tau_i = 1$ for the ions, and $\omega_{ce}\tau_e = 1$ for the electrons. We call such a radius the "hole" radius, one for each species, r_{hion} and r_{he}. Within this hole, each species is assumed to lose heat axially as if there were no magnetic field. The hole radius for the j^{th} species is calculated as follows,

$$\omega_{cj}\tau_j = 1 = \frac{B_\theta(r_{hj})}{B_\theta(R_p)}\,\omega_{cj}(R_p)\tau_j = \frac{r_{hj}}{R_p}\,\frac{B(R_p)}{B(R_{pi})}\,\omega_{cj}(R_{pi})\tau_j$$

$$= \frac{r_{hj}}{R_p}\,\frac{R_{pi}}{R_p}\,[\omega_{cj}(R_p)\tau_j]_{in.} \quad , \qquad \text{(III-49)}$$

where R_p is the instantaneous plasma radius and R_{pi} is the initial plasma radius. Here we have made the approximation that τ_j is independent of position within the plasma and have used the properties that $R_pB_\theta(R_p)$ and τ_j are constants of the

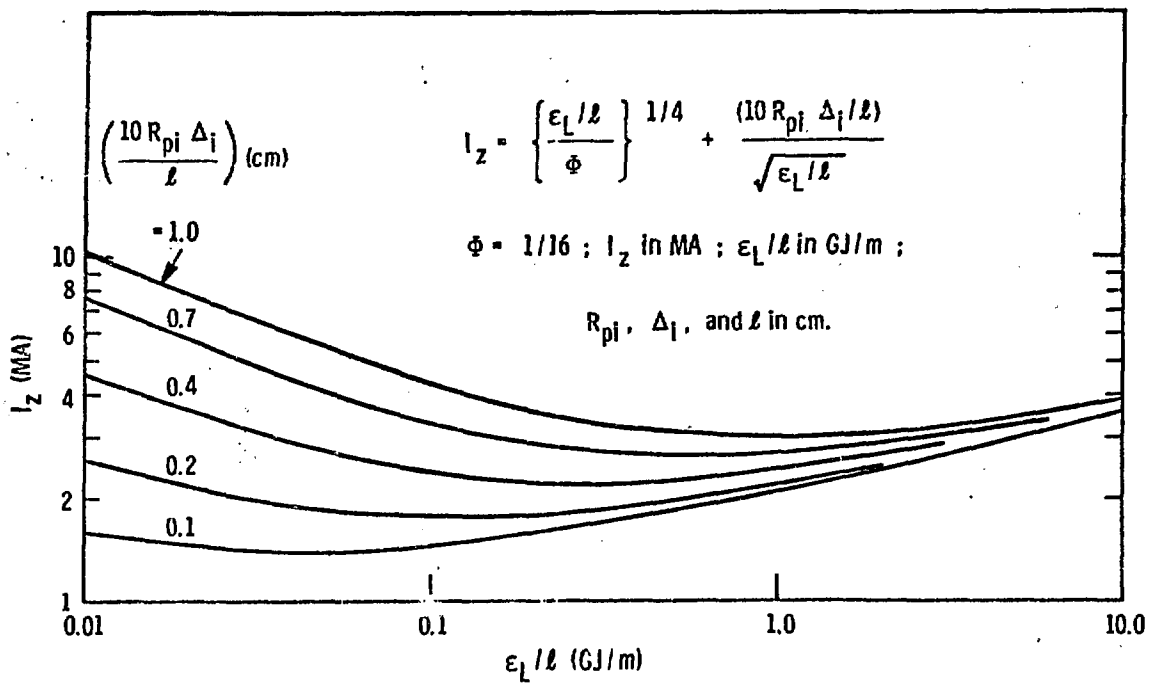

Fig. III-4. An estimate of axial plasma current required to keep thermal losses below the input energy.

motion. We then find that the ratio of the electron hole-radius to the ion hole-radius is.

$$\frac{r_{he}}{r_{hion}} = \sqrt{\frac{2m_e}{m_{ion}}} \quad . \tag{III-50}$$

The heat flux of the j^{th} species, in the absence of a magnetic field, is approximated by

$$q_{jz} = \kappa_{j_{||}}\, T_p/\ell_z \quad , \tag{III-51}$$

where ℓ_z is an axial gradient length for the temperature profile, and T_p is the central plasma temperature. Note that, as in (ii), the heat flux (and hence the thermal conductivity) is calculated near the wall, where the temperature gradient is well established, but not at the wall where complex interactions are occurring.

We now make a very pessimistic assumption. We suppose that the unknown axial gradient length, ℓ_z, is very short, on the order of the smallest macroscopic radial dimension of this model system, namely,

$$\ell_z \approx r_{he} , \tag{III-52}$$

and we furthermore suppose (pessimistically) that this holds for both the electrons and the ions because of equipartition. For $n_{in.} = 10^{18}$ cm^{-3}, $T_{in.} = 100$ eV, $B_{\theta i} = 50$ kG, $R_{pi} = 9$ cm, and a compression ratio of 30 to $R_{pf} = 0.3$ cm, we find $r_{he} \approx 3 \times 10^{-4}$ cm!

Then, the respective electron and ion power losses out of one end are given by

$$Q_{he} = \kappa_{e\parallel} T_p \pi r_{he} \tag{III-53-a}$$

$$Q_{hion} = \kappa_{i\parallel} T_p \frac{\pi r^2_{hion}}{r_{he}} . \tag{III-53-b}$$

Noting Braginskii's expressions[42] for the parallel thermal conductivities, the ratio of these two power losses is then

$$\frac{Q_{he}}{Q_{hion}} = \frac{\kappa_{e\parallel}}{\kappa_{i\parallel}} \frac{r^2_{he}}{r^2_{hion}} = \left[\frac{3}{4} \frac{\tau_e/m_e}{\tau_i/m_{ion}}\right] \frac{2m_e}{m_{ion}} = \frac{3}{2} \frac{\tau_e}{\tau_i} = \frac{3}{\sqrt{8}} \sqrt{\frac{m_e}{m_i}} . \tag{III-54}$$

Thus, the ion heat loss dominates the electron heat loss near the axis in this model, because the cross-section of the ion "pipe" is so much larger than that of the electron "pipe" that it wins over the larger electron thermal conductivity.

From Eq. (III-53-b), and the expression for the ion thermal conductivity near the end plug, namely

$$\kappa_{i\parallel} \approx \frac{4 n_p T_p \tau_i}{m_{ion}} \psi^{5/2} , \tag{III-55}$$

where T_p and τ_i are central values and (ψT_p) is the temperature near the end

plug, one can estimate the ion power loss out of one end as

$$Q_{hion} \approx \pi K_{i\parallel} T_p \frac{r_{hion}}{r_{he}} r_{hion} \quad .$$

With the help of Eqs. (III-49), (III-50), and (III-51), this can be reduced to

$$Q_{hion} \approx \left[\sqrt{\frac{m_{ion}}{2m_e}}\, \psi^{5/2}\right] 4 \frac{N\, T_p^2(\text{ergs})}{[R_p B_\theta(R_p)]_{in.}} \frac{c}{e} \quad . \tag{III-56}$$

It is reasonable to assume a temperature drop by at least a factor 5 from the body of the plasma to a point near the end plug, $\Psi \approx 0.2$. Then, with $m_{ion} = 4500\, m_e$, the square bracket becomes $[\cdots] \sim 0.85$. If we substitute this into Eq. (III-56), and double the result to allow for loss from the other end, we finally have

$$Q_{hion} \approx 6.8 \frac{N\, T_p^2}{[R_p B_\theta(R_p)]_{in.}} \frac{c}{e} \quad . \tag{III-57}$$

This completes the derivation of Eq. (III-41) where the numerical factor, C, is now seen to be about 7. It should be noted that the derivation leading to Eq. (III-57) and the further results of Eq. (III-43) and Eq. (III-46) invoked either moderate or very pessimistic assumptions, namely:

i) Perfect thermal contact between the ion "hole" and the rest of the plasma;

ii) The axial temperature-gradient length scale was set equal to the smallest relevant radial dimension;

iii) The temperature near the end plug was taken to be down only a factor 5 from the central temperature.

We particularly call attention to the small size of $\ell_z = r_{he}$, earlier estimated to be $\sim 3 \times 10^{-4}$ cm. A more relevant length for the near-axis axial heat loss problem might be a mean free path. For the initial conditions assumed earlier in order to estimate r_{he}, we find $\lambda_{ee} \sim 0.1$ cm and $\lambda_{ii} \approx 0.3$ cm. Therefore, we believe that the near-axis axial heat loss is probably several orders of

magnitude smaller than our estimate. In Fig. III-4, we have shown only the huge over-estimate! Even so, we see that only a few megamperes of plasma current suffice to keep the losses below the input energy.

c. Alpha-particle Heating. In this section, we shall see that if the initial plasma can be properly prepared ($10^{17}cm^{-3} \lesssim n_{pi} \lesssim 10^{18}cm^{-3}$; $T_{pi} \gtrsim 100$ eV), also with sufficient axial current to mitigate thermal losses as discussed in the preceding sections, then we should expect significant plasma heating by alpha-particles during the burn. We shall begin the heating estimate by writing down the expression for the energy loss of a test particle to a background of field particles,[44]

$$\frac{d\epsilon_{test}}{dt} = - \frac{4\pi n_{field}\, e^2_{field}\, e^2_{test} \Lambda}{m_{red.}\, v_{test}} F(x), \qquad \text{(III-58)}$$

where $m_{red.}$ is the reduced mass, Λ is the Coulomb logarithm,

$$F(x) = \frac{m_{test}}{m_{field} + m_{test}} \operatorname{erf}(x) - (2/\sqrt{\pi})\, x\, e^{-x^2} ,$$

and

$$X \equiv v_{test}/v_{field}, \text{ with } v_{field} = \sqrt{2T_{field}/m_{field}} .$$

Because of their small mass field, electrons see a much bigger Coulomb cross-section of the test alpha-particle than do field ions. Hence, the alpha test particle will be slowed down primarily because of Coulomb scattering of electrons. When Eq. (III-58) is specialized to an alpha test particle, and electron field particles, and a characteristic energy-loss time is defined by

$$t_A = \left| \frac{1}{E_A} \frac{dE_A}{dt} \right|^{-1} , \qquad \text{(III-59)}$$

where E_A is the 3.5 MeV alpha energy, one finds

$$nt_A = \frac{m_e m_A v_e^3}{32\pi e^4 \Lambda} \left[\frac{F(x)}{x^3} \right]^{-1} . \qquad \text{(III-60)}$$

For 2 keV $\lesssim T_e < \infty$, the function, $F(x)/x^3$, ranges from 0.65 to 0.75. Therefore, in the remainder of this section, we shall replace $F(x)/x^3$ by 0.70. Then Eq. (III-60) gives Table III-IV.

TABLE III-IV. VALUES OF nt_A SUCH THAT ALPHA PARTICLES LOSE MOST OF THEIR ENERGY TO PLASMA ELECTRONS

T_e = 2 keV	$nt_A = 2.8 \times 10^{12}$ s/cm^3
5	1.1×10^{13}
10	3.2×10^{13}
15	6.2×10^{13}
20	9.2×10^{13}

An alpha particle will have a chance to heat the plasma if its gyroradius is less than the plasma radius. Suppose an "average" alpha is born at $r = (1/2)R_p$ with $v_\perp = v_\parallel = v_A/\sqrt{2}$ and $v_A = \sqrt{2E_A/m_A} = 1.3 \times 10^9$ cm/s. Also, suppose the plasma axial current density is uniform. Then one can easily show that the gyro-radius, R_A, of this "average" alpha is related to the plasma radius, R_p by

$$\frac{R_A}{R_p} = \frac{I_A}{I_z} \quad , \tag{III-61}$$

where I_z is the total plasma current, and the characteristic current, I_A, is given by

$$I_A = \left[\frac{\pi\sqrt{2}\, m_A v_A}{\mu_o e}\right]_{\text{mks units}} = 1.9 \text{ MA} \, . \tag{III-62}$$

Thus, if the plasma current exceeds about 2 megamperes, a large fraction of the alpha particles that are born will not hit the wall at $r = R_p$. Their gyro-orbits will then lie in (r,z) planes and will drift axially to the end plugs with guiding-center drifts composed of the sum of ∇B and curvature drifts. These

drifts are in opposite directions, and one has the following drift velocity formula, in MKS units.

$$v_{dr} = \frac{1}{2}\frac{m_A}{e}\frac{R_p^2}{r^2}\frac{2\pi}{\mu_o I_z}\left(v_{\parallel}^2 - \frac{1}{2}v_{\perp}^2\right) . \qquad \text{(III-63)}$$

Again, for an "average" alpha, we take $r = (1/2)R_p$, $v_{\parallel}^2 = (1/2)v_A^2$, $v_{\perp}^2 = (1/2)v_A^2$, and thereby obtain

$$v_{dr} = \frac{1}{\sqrt{2}}\frac{I_A}{I_z}v_A . \qquad \text{(III-64)}$$

Thus, if I_z much exceeds 2 MA, the alpha particles will drift to the end plugs much more slowly than their energy-velocity would indicate.

For an "average" alpha born roughly in the center, the nt_{dr} product can then be written as

$$nt_{dr} \simeq \frac{1}{2}n\frac{\ell}{v_{dr}} = \frac{1}{\sqrt{2}}n\frac{\ell}{v_A}\frac{I_z}{I_A} . \qquad \text{(III-65)}$$

Here, we have defined a representative alpha particle dwell time as $t_{dr} = (1/2)\ell/v_{dr}$. But, the final plasma density can be written as

$$n \equiv n_{pf} = \frac{N}{\pi R_{pf}^2} = \frac{N}{A_{Li}}\frac{1}{(\pi R_{pf}^2/A_{Li})} = \frac{N}{A_{Li}}\alpha(\theta)\theta , \qquad \text{(III-66)}$$

in which θ and $\alpha(\theta)$ have been defined in III-A. If our initial parameters are nearly optimal, as we assume, then $\alpha\theta = 11.25$, $N[cm^{-1}] = 9.0 \times 10^{20}\, E_L/\ell\ [GJ/m]$, so Eq. (III-66) gives

$$n \simeq \left\{10^{22}\ \frac{E_L/\ell\ [GJ/m]}{A_{Li}[cm^2]}\right\} cm^{-3} . \qquad \text{(III-67)}$$

Substitution of Eq. (III-67) into Eq. (III-65) provides

$$nt_{dr} \simeq \left\{0.7 \times 10^{22} \frac{E_L/\ell\ [GJ/m]}{A_{Li}\ [cm^2]} \frac{\ell[cm]}{v_A[cm/s]} \frac{I_z}{I_A}\right\} \text{sec/cm}^3 \ . \qquad \text{(III-68)}$$

Now, suppose in a machine with Q ~ 2, the following parameters:

$$E_L/\ell \simeq 0.1 \text{ GJ/m}$$
$$A_{Li} \simeq 10 \text{ cm}^2$$
$$\ell \simeq 30 \text{ cm}$$
$$I_z \simeq 5 \text{ MA}$$

Then, Eq. (III-68) yields

$$nt_{dr} \simeq 4 \times 10^{12} \text{ s/cm}^3 \ . \qquad \text{(III-69)}$$

Comparing with Table III-IV, we see that the above parameters are such that most of the alpha particles that are produced ought to lose about one-tenth of their energy to the 10-or 15-keV plasma.

To calculate the temperature increment produced by the alpha particles, we need the burn fraction, f_{burn}. This is written as follows.

$$f_{burn} = \frac{\text{Total Yield}}{(\text{Yield per reaction})(\text{Total no. of ions})} = \frac{Q \times (E_L/\ell\ [ergs/cm])}{(y[ergs])(N[cm^{-1}])} \ . \qquad \text{(III-70)}$$

For an optimized system, $Q \simeq 7\sqrt{(E_L/\ell)[GJ/m]}\sqrt{\rho_i/2\pi}$, and $N = \{9.0 \times 10^{20} \ (E_L/\ell)\ [GJ/m]\}\ cm^{-1}$, and Eq. (III-70) becomes

$$\left[f_{burn}\right]_{opt} \simeq 0.028\sqrt{(E_L/\ell)[GJ/m]}\ \sqrt{\rho_i/2\pi} \ , \qquad \text{(III-71)}$$

where, as always, ρ_i is the initial liner density in g/cm^3. Then, the temperature increment, T_A, can be found from the following equation,

$$3N\ell T_A = (f_A E_A) f_{burn}\ N\ell \ ,$$

or,

$$T_A = \frac{1}{3}(f_A E_A) f_{burn} \ . \qquad \text{(III-72)}$$

Here, $(f_A E_A)$, with $0 < f_A < 1$, is the representative amount of energy lost by an alpha particle. The fraction f_A, is a function of plasma temperature defined by $f_A(T_p) = nt_{dr}/(nt_A)$ with nt_A given in Table III-IV. From Eq. (III-71), with E_L/ℓ [GJ/m] = 0.1, we have $f_{burn} \approx 0.01$. Then from Eq. (III-72) with $f_A \approx 0.1$ and $E_A = 3.5 \times 10^3$ keV, we find

$$T_A \approx 1.2 \text{ keV} \quad (E_L/\ell = 0.1 \text{ GJ/m}) \tag{III-73}$$

We conclude that, with rather modest assumptions as to the input energy, liner dimensions, and plasma current, the alpha particles will make a noticeable contribution to the plasma temperature.

The scaling of the temperature increment, T_A, with input energy is interesting. For a given final plasma temperature, $f_A \propto (E_L/\ell)/A_{Li}$, from Eq. (III-68). From Eq. (III-71), $f_{burn} \propto \sqrt{E_L/\ell}$. Then, Eq. (III-72) implies

$$T_A \propto (E_L/\ell)^{3/2}/A_{Li} \tag{III-74}$$

for nearly optimal systems. If we scale up with $A_{Li} \propto E_L/\ell$ as discussed earlier, then

$$T_A \propto \sqrt{E_L/\ell} \quad . \tag{III-74-a}$$

Thus, at $E_L/\ell \approx 1$ GJ/m, we would have $T_A = 3.8$ keV.

These modest, but noticeable temperature increments will help to maintain the plasma near the optimal DT reaction temperature (peak of $\langle\sigma v\rangle_{DT}/T_{pf}^2$) and will mitigate the thermal losses. Also, the axial plasma currents required to keep the alpha particles around are not inconsistent with those plasma currents needed to keep thermal losses under control.

To the extent that the initial liner cross section can be scaled up more slowly than the input energy, the alpha heating will scale up more favorably than is indicated by Eq. (III-74-a).

d. Other Minor Thermal Effects. The following mechanisms of thermal transfer and cooling or heating were also considered in detail and were found to be completely negligible for the parameter regime of interest for our contemplated liner implosions.

1. Axial convection of heat by the electrons due to the presence of the plasma current. [Cold electrons enter one end and hot electrons leave the other end.]
2. Radial heat flux caused by axial current flow in the presence of B_θ. [See Ref. 42]
3. Work done by the thermal force. [See Ref. 42]
4. Ohmic Heating. [Although ohmic heating is negligible within the context of the final energy given to the plasma by the liner, it might be a very important mechanism for attaining the 100 eV or so required of the initial plasma.]

e. Summary and Conclusions. We have here made estimates of plasma thermal losses based on classical plasma transport theory,[42] and an estimate of alpha-particle heating based on Coulomb collisions with electrons.[44] Admittedly, these estimates were so primitive as to amount to little more than dimensional arguments. As part of our liner program, we hereby propose an intensive theoretical and numerical effort, which would re-examine the losses and gains with suitable detail and rigor. Moreover, this would entail an extensive parameter study, not just limited to optimized systems only. Also, nonclassical transport (turbulence), and plasma-wall interactions[7] would be seriously considered.

Reference 7 has considered the phenomenon of radiation from a magnetoplasma near a cold boundary. This type of calculation is very important and has possibly serious consequences for our concept of a wall-supported plasma, called "gas-kinetic confinement" by the Russians. We feel that this kind of work needs to be re-done before it can be of use to us, for the following reasons:

i) The time-scales obtainable from Ref. 7 are of the same order as our contemplated implosion and burn time scales, so their assumption of a steady state is not valid for our situation.
ii) The presence of wall impurities was neglected.
iii) The bootstrap heating by alpha particles, which we feel could be quite contributory in a liner reactor system, was neglected.

Thus, we propose, as part of our liner program, to re-think and re-do the problem of radiation from the cold boundary layer of our wall-supported plasma.

Although the primitive state of our present calculations precludes the attachment of literal significance to the detailed numerical results, these

results probably are qualitatively meaningful. They suggest that:

1. Axial thermal losses near the axis of a nonhard-core system must be guarded against, particularly at low input energies (~ .01 GJ/m); However, we believe that we may have greatly over-estimated these losses, for the several reasons already mentioned.
2. Radial thermal losses must be guarded against, particularly at large input energies (~ 1 GJ/m);
3. Several megamperes of plasma current, probably less than 10 MA, are required to keep these losses at an acceptable level;
4. Such plasma currents should be adequate to insure at least a modest and possibly a very considerable amount of heating by the alpha particles, in systems of break-even or better capability.
5. Bremsstrahlung from the bulk plasma is unimportant compared to other losses; however, impurity radiation and cold, dense plasma radiation at the plasma-wall interface could be important[4] and needs to be studied in a self-consistent manner.

We repeat our intention to re-examine all of these questions theoretically, in a detailed and self-consistent manner. We believe that our personnel and our computing facilities are equal to the task.

2. Temporal Variation of Plasma Heating and Cooling Rates. In this subsection we examine some of the rates for plasma energy gain or loss from a different point of view. Using the time history of the plasma density and temperature given by numerical calculations with the code CHAMISA, we display the temporal variation of the loss rates. The calculations of the plasma state are not self-consistent in that the plasma densities and temperatures from the code are based on the simple scaling relations for an adiabatically compressed ideal gas. The loss rates are calculated in the sense of perturbation theory: the losses do not feed back to influence the plasma state. The code calculations do include the effects of liner compressibility. In future work it will be possible to numerically model the plasma-liner interaction so that the plasma losses are treated in a self-consistent way. The present discussion is intended only to illustrate some of the basic phenomena.

The treatment is approximate in two respects: (1) simple approximations are used to estimate the relative magnitude of the various effects; and (2) no effort is made here to calculate the interplay among the mechanisms.

The following notation will be used; units in square brackets apply in numerical expressions:

n = plasma ion (or electron) number density (DT plasma) [cm^{-3}]
T = plasma temperature [eV]
R = plasma radius [cm]
A = average ion atomic weight (= 2.5 for DT)
$N = \pi R^2 n$ = line density [cm^{-1}]
Z = ionic charge (= 1 for DT)
$\ell n\Lambda$ = Coulomb logarithm
B = magnetic field imbedded in DT plasma [Gauss]
K = coefficient of thermal conductivity [erg/cm/s/eV]
$\dot{Q}$ = rate of energy loss or gain [erg/s/cm]
ω_e, ω_i = electron or ion gyrofrequencies [rad/s]
τ_e, τ_i = electron or ion collision times [s]

Quantities with a subscript "o" refer to the initial value, while "f" refers to the final value at peak compression of the plasma. We define the radial compression ratio

$$X = R_o/R \quad . \tag{III-75-a}$$

The basic model for the plasma is that of an ionized $\gamma = 5/3$ perfect gas. The plasma is compressed adiabatically. Losses or gains, other than PdV work, are not used to modify the plasma energy. Their magnitude is calculated from the adiabatic plasma conditions; the self-consistent treatment of the various effects will be done in more elaborate computer calculations in the future. For an adiabatic plasma in cylindrical geometry, we have the scaling relations

$$n/n_o = (R_o/R)^2 = X^2 \tag{III-75-b}$$

$$T/T_o = (n/n_o)^{2/3} = X^{4/3} \quad . \tag{III-75-c}$$

Note that $N = \pi R^2 n = N_o$ is independent of the compression ratio due to our assumption that the liner is end-plugged. Most numerical examples will assume

the initial values T_o = 100 eV, $n_o = 1 \times 10^{18}$ cm^{-3}, R_o = 10 cm, $B_o = B_{\theta o}$ = 30 kG, and a compression ratio $X_f = 10^{3/2}$ required to bring the plasma to a peak temperature (no losses) of T_f = 10 keV. Figure III-5 illustrates the variation in time near peak plasma compression of the inner liner radius, the liner kinetic and internal energies, and the adiabatic plasma energy for a system with these parameters. The initial liner kinetic energy is 280 MJ/m. These values are not optimal values in any sense, but are used only to illustrate "typical" orders of magnitude of the various rates and energies.

We will use a single temperature description of the DT plasma. This is valid if the electron-ion energy equilibration time[18]

$$\tau_{ei} = 3.14 \times 10^8 \, A \, T_e^{3/2}/(Z^2 \, n \, \ell n\Lambda) \quad s \qquad \text{(III-76)}$$

is short compared to the other time scales in the problem. With the specified initial conditions, and taking[18] $\ell n\Lambda = 9$

$$\tau_{ei} = 0.08 \ \mu s$$

independent of X (except for a weak dependence in $\ell n\Lambda$). For $n_o = 10^{17}$ and T_o = 100 eV, τ_{ei} = 0.8 μs. Adiabatic compression keeps the ratio T_e/T_i fixed; but near peak compression bremsstrahlung, ion thermal conduction, and α-particle energy deposition tend to cool or heat electrons or ions relative to the other species. These processes act on a timescale ≲ 1 μs (see Fig. III-6), and might give $T_e \neq T_i$ for a short period but $T_e = T_i$ is generally a good approximation. The proposed full numerical calculations will allow $T_e \neq T_i$.

The fundamental energy input to the plasma is just the adiabatic work done on it by the incoming liner. The plasma energy per unit length is

$$E_p = 3Nk_BT \ , \qquad \text{(III-77-a)}$$

which scales as $X^{4/3}$; for our usual parameters

$$W_p = 1.5 \times 10^{11} \, X^{4/3} \text{erg/cm} \ . \qquad \text{(III-77-b)}$$

Figure III.6 shows the rate of adiabatic work, $-P\dot{V}$, as a function of time near

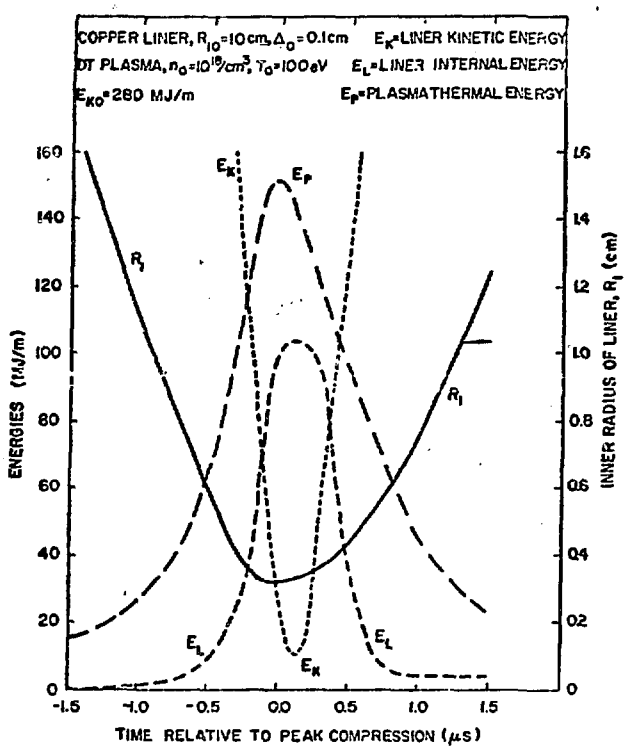

Fig. III-5. Energies and linear radius near peak plasma compression. The initial linear kinetic energy is 280 MJ/m.

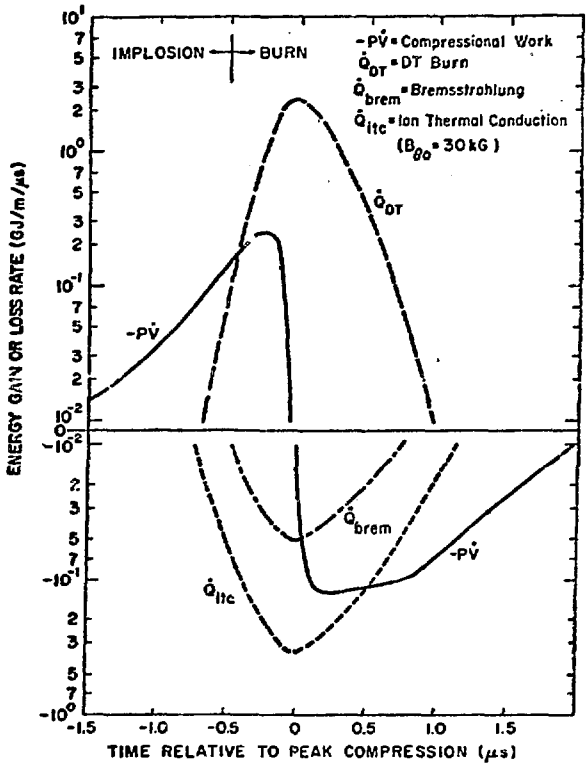

Fig. III-6. Plasmas energy gain and loss rates near peak compression.

peak compression:

$$-P\dot{V} = \dot{W}_p = -(4/3)(v/R)W_p \ , \qquad \text{(III-78)}$$

where $v = \dot{R}$ is the velocity of the inner surface of the liner.

The other potential energy source for the plasma is α-particle heating during the burn phase. The total thermonuclear power, $\dot{Q}_{DT}$, is also illustrated in Fig. III-6. It is defined by

$$\dot{Q}_{DT} = \pi R^2 n^2 \langle \sigma v \rangle \ , \qquad \text{(III-79)}$$

where $\langle\sigma v\rangle$ is defined in Eq. (III-7-b). For $T < 10$ keV, $\langle\sigma v\rangle$ scales as T^s, $s \sim 2$-3, so that $\dot{Q}_{DT}$ scales roughly as X^5. Note that the peak of $\dot{Q}_{DT}$ is nearly coincident with the peak loss rates.

The bremsstrahlung loss rate[18] in the DT plasma, when integrated over the plasma cross section, is

$$\dot{Q}_{brem} = 4.8 \times 10^{-25} R_o^2 n_o^2 T_o^{1/2} X^{8/3} \text{ erg/s/cm} . \qquad \text{(III-80-a)}$$

Figure III-6 shows the loss rate versus time near peak compression for a compressible copper liner, with total energy 280 MJ/m, $R_o = 10$ cm and plasma parameters $n_o = 10^{18}/\text{cm}^3$ and $T_o = 100$ eV, for which

$$\dot{Q}_{brem} = 4.8 \times 10^{14} X^{8/3} \text{ erg/s/cm}. \qquad \text{(III-80-b)}$$

It should be noted that the liner dynamics respond only to the plasma pressure

$$P = 2nk_BT = 2 k_B(n_oT_o)X^{10/3} , \qquad \text{(III-81)}$$

so that in the adiabatic approximation used here, the liner dynamics, the energies and radius curves in Fig. III-5, and the $-P\dot{V}$ curve in Fig. III-6 are all unchanged by variations of n_o and T_o which keep n_oT_o fixed. Figure III-6 shows that $\dot{Q}_{brems}$ is less than the compressional work rate $-P\dot{V}$ during the implosion and dominated by adiabatic expansion after peak compression. Furthermore, holding n_oT_o constant, $\dot{Q}_{brem} \propto n_o^2T_o^{1/2}$ can be decreased like $T_o^{-3/2}$ by going to lower n_o and higher T_o. The thermonuclear burn calculation also indicates that some improvement in the burn rate, $\dot{Q}_{DT}$, also occurs in going to $T_o = 200$-300 eV while decreasing n_o correspondingly. This improvement occurs because $\langle\sigma v\rangle$ for DT reactions[31] rises faster than T^2 as the temperature increases, for $T \lesssim 10$ keV. So the burn rate, proportional to $n^2\langle\sigma v\rangle \propto (nT)^2[\langle\sigma v\rangle/T^2]$ is still an increasing function of T for given nT.

For the conditions considered here, cross-field ion thermal conduction to the liner appears to be the most serious loss. Work is in progress to make detailed numerical calculations of the thermal conduction losses, which involves the self-consistent treatment of the thermal boundary layer of a wall-confined

plasma with an embedded B_θ. But for illustrative purposes we will use a simple dimensional analysis method. We take the heat loss at the liner-plasma interface to be

$$\dot{Q}_{ion} = 2\pi R \cdot K_i \nabla T \quad , \tag{III-82-a}$$

where K_i is the cross-field ion thermal conductivity[42]

$$K_i = 2nk_B^2 T \, \tau_i G(\omega_i \tau_i)/M_i \tag{III-82-b}$$

$$G(y) = (y^2 + 1.32)/(y^4 + 14.8\, y^2 + 3.8) \quad . \tag{III-82-c}$$

M_i is the ion mass, and k_B is Boltzmann's constant. In the limit $y \gg 1$, $G(y) = y^{-2}$, which gives the usual $1/B^2$ scaling of K_i. K_i is evaluated at the "central" temperature T, rather than at some intermediate temperature ΦT, where $0 < \Phi < 1$. In the strong field limit ($y \gg 1$), $K_i \propto \Phi^{-1/2}$, so taking $\Phi = 1$ is no worse than the other simplifications made here. We approximate the gradient by $-T/R$, so that with the usual values of n_o and T_o and with[42]

$$\tau_i = 2.1 \times 10^7 \, T^{3/2} \, A^{1/2}/(n \, \ell n \Lambda) \quad s \quad , \tag{III-83}$$

we get

$$K_i = 4.5 \times 10^{11} \, X^{10/3} \, G(y) \tag{III-84-a}$$

$$y = \omega_i \tau_i = 0.27 \, X \quad , \tag{III-84-b}$$

and

$$\dot{Q}_{ion} \simeq -2.8 \times 10^{14} \, X^{14/3} \, G(y) \text{ erg/s/cm}. \tag{III-85}$$

Values of $\dot{Q}_{ion}$ have been plotted in Fig. III-6 for an initial B_θ field of 30 kG. It is assumed that this field will be produced with the initial plasma, either by plasma gun injection or as the result of a Z-current used to heat the initial plasma (see Section II). B_θ is also preferable to B_z in that it reduces axial

thermal conduction losses to material plugs at the ends and inhibits axial α-particle loss during the burn phase; B_z does neither. If the internal plasma current can be maintained during the final stages of the implosion, B_θ scales as

$$B_\theta = B_{\theta o} X \ , \qquad \text{(III-86)}$$

which gives $B_{\theta f}$ = 1 MG for X_f = 30 and $B_{\theta o}$ = 30 kG.

Now consider the scaling of $\dot{Q}_{ion}$ with the same liner dynamics ($n_o T_o$ fixed) but increasing T_o and decreasing n_o. In the high field limit where $G(y) = y^{-2}$, we have $K_i \propto nT\,\tau_i/(\omega_i\tau_i)^2 \propto nT/\tau_i$ and $\dot{Q}_{ion} \propto nT^2/\tau_i \propto (nT)^2\,T^{-3/2}$, the same scaling as for bremsstrahlung losses. Going to higher T_o and lower n_o will reduce $\dot{Q}_{ion}$ as $T_o^{-3/2}$. Also, $\dot{Q}_{ion} \propto B^{-2}$ so a larger initial field is desirable. With $B_{\theta o}$ = 60 kG and $B_{\theta f}$ = 2 MG, $\dot{Q}_{ion}$ would be another factor of 4 smaller; the liner dynamics are unchanged since even with these fields, the peak magnetic pressure is less than 1% of the plasma pressure.

The results obtained here are consistent with those obtained above with the analytic model: (1) the dominant loss mechanism is radial ion thermal conduction. (2) Initial B_θ fields on the order of or greater than 30 kG will be required to keep the radial thermal loss to a tolerable level. (3) Bremsstrahlung losses from the bulk plasma are relatively unimportant. (4) The coincidence in time of the thermonuclear burn with the dominant losses implies that the deposition of a significant fraction of the α-particle energy in the plasma (see Section III.C.1 above) can play an important role in canceling the losses. (5) The adiabatic work ($-P\dot{V}$) dominates the losses considered here until very near peak compression.

The results presented above are based on highly simplified models, and more quantitative results will be needed, both for comparison with experiments and for more accurate predictions of reactor feasibility. It was pointed out in Section III.B that, to a great extent, computer codes are presently available at LASL which are capable of treating these problems.

D. Thermal State of the Liner

The thermal state of the liner during the implosion phase is of particular importance in considerations of the Rayleigh-Taylor instability of a magnetically driven liner. As shown in Section III.E, viscosity in the compressed liner material has a significant stabilizing influence for the Rayleigh-Taylor

instability. There is experimental and theoretical evidence[38] that compressed solids have a viscosity near 2 kilopoise, a value capable of preventing serious Rayleigh-Taylor growth for the liner implosion conditions considered in this proposal. In fact, Russian experiments[45] have found viscosities in aluminum of 20 to 100 kilopoise.

Two distinct modes of operation will be considered here: the "ideal" case (hereafter called A) in which the driving magnetic field does not penetrate the liner, and the case (called B) in which the magnetic field completely penetrates the liner. As will be shown, significant diffusion of the driving magnetic field into the liner can be expected to occur during the implosion phase if the applied current is carried by the liner itself. Field penetration reduces the efficiency with which electrical energy is converted to liner kinetic energy, but not by a large factor. However, the ohmic heating will cause all or a large portion of the liner to melt. It is expected that melting will significantly reduce the material viscosity and the associated stabilizing effect of that viscosity. On the other hand, as the field penetrates the liner, the conditions for Rayleigh-Taylor growth change in two ways which tend to reduce the growth: (1) the driving force, grad(B^2), is distributed over a slowly varying density gradient within the liner and (2) the maximum acceleration spends a relatively short time near any particular mass element of the liner as the field moves through the liner. The first effect reduces the local growth rate compared to that for a sharp interface with a large density mismatch, while the second reduces the growth time for a particular mass element.

It may be possible to approach the ideal limit of case A by causing the driving current to be carried by a plasma layer adjacent to the liner.[6] In this case, the driving force remains at the plasma layer-liner density discontinuity during the entire acceleration time. However, because the magnetic field does not penetrate the liner, the temperature of the liner is increased only a little by adiabatic compression. The temperature remains well below melting, so that the viscosity should be large, reducing the growth of the Rayleigh-Taylor instability.

The following discussion has three parts. We first consider heating mechanisms other than ohmic heating; these determine the liner state for case A. Next we examine magnetic field diffusion and ohmic heating. Finally we consider several processes which are important near peak compression; these do not

influence the implosion phase but may affect the dynamics of the liner-plasma interface and the liner reexpansion.

1. No Magnetic Field Diffusion (Case A). The adiabatic compressional work done on the liner is considerable, but only a small fraction of that energy goes into an increase in the material temperature. Writing the temperature, T, as a function of specific volume, $V=1/\rho$, and entropy, S, we have

$$dT = (\partial T/\partial S)_V dS + (\partial T/\partial V)_S dV \ . \qquad \text{(III-87)}$$

For an adiabatic change, dS=0; then dT can be rewritten as

$$dT = (\partial S/\partial V)_T dV/(\partial S/\partial T)_V$$

$$= - (\partial P/\partial T)_V dV/(\partial S/\partial T)_V \ .$$

The specific heat at constant volume, C_V, is

$$C_V = T(\partial S/\partial T)_V \ ,$$

so the adiabatic temperature change satisfies

$$C_V dT = - T(\partial P/\partial T)_V dV \quad (dS = 0) \ , \qquad \text{(III-88)}$$

whereas the internal energy satisfies

$$dU = - PdV \quad (dS = 0) \ . \qquad \text{(III-89)}$$

For low - temperature solids compressed somewhat above normal density ($\Delta\rho/\rho_o \gtrsim 0.1$), the pressure is a weak function of temperature. If we write

$$C_V dT = (\partial \ell nP/\partial \ell nT)_V dU \quad (dS = 0) \ , \qquad \text{(III-90)}$$

the logarithmic derivative gives the fraction of the energy increase which goes into increasing the temperature. This derivative ranges from near unity at

normal conditions (room temperature, normal density ρ_o) to 10^{-2} at ρ/ρ_o=1.3 and P=10^{12} dyne/cm^2 (=1 Mbar), to 10^{-4} at ρ/ρ_o=3.1 and P=32 Mbar (Ref. 46). The remainder of dU goes into work done against the repulsive forces between atoms in the solid lattice. The temperature increase when copper is compressed to a density of about 11.5 gm/cm^3 (ρ/ρ_o=1.3) at a final pressure of 10^{12} dyne/cm^2 is approximately

$$\Delta T = + (\partial \ell nP/\partial \ell nT)_V (P/\rho)(\Delta\rho/\rho)/C_V \qquad \text{(III-91)}$$

$$\simeq 10^{-2}\ [(10^{12}\ \text{dyne/cm}^2)/11.5\ \text{gm/cm}^3](0.3)/(5 \times 10^{10}\ \text{erg/gm/eV})$$

$$\simeq 0.005\ \text{eV} \simeq 60\ \text{K}\ ,$$

which hardly changes the temperature from its initial room-temperature value. Numerical calculations with the code described in Section III.B give an integrated $\Delta T \simeq 0.016$ eV. The essential point here is the presence of the derivative $(\partial \ell nP/\partial \ell nT)_V$ in the temperature equation; were it not considered, one would erroneously predict a temperature increase ~ 1 eV ≃ 12 000 K, far above the normal density melting temperature for copper of 1360 K = 0.117 eV (Ref. 47).

Comparison of the final temperature calculated above (0.04 eV) with the normal density melting temperature would suggest that there is little margin for error in the crude calculation following Eq. (III-91). However, the melting temperature is an increasing function of density. Kennedy[48,49] has shown that the melting temperature of many metals follows the relation

$$T_m = T_{mo}\ [1 + C_m(1-\rho_o/\rho)]\ , \qquad \text{(III-92)}$$

where T_{mo} is the melting temperature at normal density, ρ_o, and C_m is constant for a given metal. For aluminum, T_{mo} = 933 K (Ref. 47) and $C_m \simeq 5.14$ (Ref. 49), while for copper $C_m \simeq 4.00$ (Ref. 50). At a compression ρ/ρ_o=1.3, the melting temperature of copper is increased by a factor of ≃ 1.92 to about 0.22 eV = 2610 K. In fact, the melting temperature rises more rapidly with compression than does the adiabatic temperature change:

$$dT/dT_m = (\partial \ell nP/\partial \ell nT)_V\ P/(\rho_o C_V C_m T_{mo}) \simeq 0.05\ . \qquad \text{(III-93)}$$

The conclusion is that adiabatic compression is unlikely to melt the liner.

Furthermore, the adiabatic temperature change is reversible, so the temperature will drop back to room temperature when the pressure is removed.

Two other mechanisms which might heat the liner in case A are shock heating and viscous heating. These are not reversible, although if heating occurs while the material is compressed, a subsequent expansion will lower the temperature accordingly. Shock heating does not occur because the liner motion tends to be near sonic or subsonic. Also the risetime for the applied field will be of the order of several microseconds and is larger than the time for a sound wave to move through the liner, Δ/c_s where Δ is the liner thickness and c_s is the sound speed. With $\Delta \leq 0.5$ cm and $c_s \geq 5 \times 10^5$ cm/s, $\Delta/c_s \leq 1$ μs. Viscous heating is unimportant because the liner compression rate is small except near turnaround. During the implosion phase $\mathrm{div}(v) \leq 10^5\ s^{-1}$; with viscosity ~ 2×10^3 poise, the viscous heating rate is $\leq 2 \times 10^{13}$ erg/cm^3/s. The rate of change of the temperature is ~ 40 eV/s, so that for a 25-μs implosion the temperature rise is only about 10^{-3} eV ≈ 12 K. Even with larger viscosities the viscous heating is not serious.

The conclusion for case A is that in the absence of magnetic field penetration of the liner, compressibility effects do not cause the liner to melt. One can expect significant viscosity inhibition of Rayleigh-Taylor growth.

2. Magnetic Field Diffusion (Case B). As mentioned above, if the liner itself carries the driving current, one must expect significant magnetic field diffusion and ohmic heating even in a good conductor like copper. This will cause all or a large part of the liner to melt during the implosion phase. However, the field penetration time is comparable to the implosion time, so that it is possible to make either time shorter than the other by changing the initial liner radius or thickness or the driving circuit characteristics. Work is in progress to investigate the effects of changing the ratio of these times. Because the liner melts and because the acceleration takes place in a nearly uniform medium, considerations for the Rayleigh-Taylor instability are quite different than in case A. This topic is discussed in Section III.E. The present discussion is concerned only with the phenomena of magnetic field diffusion and ohmic heating during the implosion phase.

Nonlinear magnetic field diffusion is treated in great detail by Knoepfel.[51] The equations for field diffusion in cylindrical geometry with a Z-current are

$$dB_\theta/dt + B_\theta(\partial v/\partial r) = (c^2/4\pi)(\partial/\partial r)[(\eta/r)(\partial/\partial r)(rB_\theta)] \qquad \text{(III-94)}$$

$$J_z = (c/4\pi)(1/r)(\partial/\partial r)(rB_\theta) \ , \qquad \text{(III-95)}$$

where B_θ is the magnetic field, v is the radial velocity, η is the resistivity, and J_z is the current density. The time derivative is the comoving derivative: $d/dt = \partial/\partial t + v(\partial/\partial r)$. The ohmic heating rate per unit volume is ηJ^2. The diffusion process is "nonlinear" because the resistivity is a strong function of temperature: as an element of mass is heated, the resistivity increases, which in turn increases both the local heating rate and diffusion coefficient.

In the code, CHAMISA, described in Section III.B, these equations are solved simultaneously with the equations for the liner motion. The temperature and density dependence of η used in the code are based on the empirical data given in Tables 10.IV and 10.V of Reference 51. For copper this gives a resistivity in the solid phase of the form

$$\eta = \eta_o[1+\beta'(T-T_o)](\rho_o/\rho)^{2.7} \ , \qquad \text{(III-96)}$$

with $\eta_o = 1.58 \times 10^{-18}$s, $\beta' = 59.7/\text{eV}$, $T_o = 0.0235$ eV, and $\rho_o = 8.94$ gm/cm^3. This is used for temperatures less than the melting temperature given by the Kennedy melt law discussed previously (Eq. III-92). At $T = T_{melt}$, η has a discontinuity, and for $T > T_{melt}$, η is taken to have the same form as in Eq. (III-96) but with coefficients appropriate to the liquid phase. Figure III-7 shows a snapshot in time at 6.4 μs after the beginning of the implosion of a copper liner by a constant current of 40 MA. The initial inner radius of the liner was 10 cm and the thickness was 0.1 cm. The liner has moved only 0.6 cm but has a velocity of 1.8×10^5 cm/s. The outer part of the liner (to the right of r = 9.48 cm) has melted while the inner part is still solid. This transition is indicated by the sharp changes in the resistivity and current density. The high resistivity in the melted layer forces the current to be carried by the solid layer. The arrow on the vertical axis labelled η_o is the resistivity of room-temperature copper. Melting occurs slightly below the normal melting temperature of copper, $T_{mo} = 1360$ K, because the density near the solid-liquid

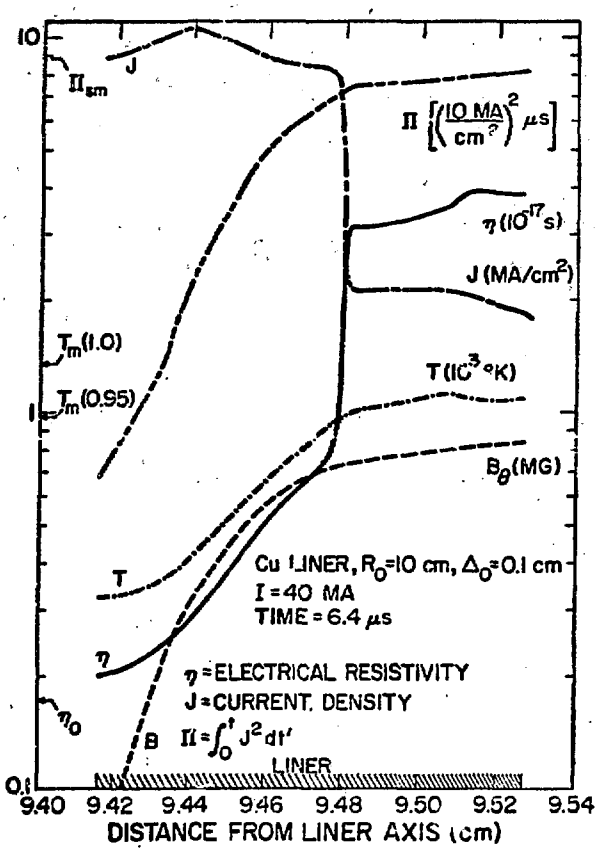

Fig. III-7. Magnetic field variables within the liner at 6.4 μs following the beginning of an implosion with a constant 40-MA current. B_θ is the magnetic field, T is the material temperature, η is the electrical resistivity, J is the current density, and Π is the current integral described in the text.

interface is slightly below normal density. The melting temperatures at relative compressions ρ/ρ_0 of 1.0 and 0.95 are indicated on the vertical axis. The quantity Π is called the current integral and is defined as

$$\Pi(m,t) = \int_0^t [J(m,t')]^2 dt' \ , \qquad \text{(III-97)}$$

where m denotes a Lagrangian mass element. The significance of Π is as follows. The local ohmic heating rate is

$$\rho C_v (dT/dt) = \eta J^2 \ . \qquad \text{(III-98)}$$

If we neglect the density dependence of η (take $\rho = \rho_0$) then from Eq. (III-96), η is a known function of T and we can integrate Eq. (III-98):

$$\Pi(m,t) = \int_0^t J^2 dt' = \int_{T_o}^{T} dT\ \rho_o C_v(T)/\eta(T) \ . \qquad \text{(III-99)}$$

The rightmost expression depends only on the initial temperature T_o, the final temperature T, and the properties ρ_o, $C_v(T)$, and $\eta(T)$ of the material being considered. The value of Π required to raise the temperature of a solid from room temperature (300 K) to the normal density melting temperature is denoted by Π_{sm}. For copper, $\Pi_{sm} = 8.9 \times 10^8$ A^2 s/cm^4, while for aluminum, $\Pi_{sm} = 3.2 \times 10^8$ A^2 s/cm^4 (Ref. 51). Π_{sm} is also indicated on the vertical axis of Fig. III-7. The time for the field to completely penetrate the liner, t_{pen}, can be estimated roughly using Π_{sm}: if we assume that $J \simeq I/(2\pi R_o \Delta_o)$ and take I to be constant (as it is in the numerical calculation considered here), then

$$\Pi_{sm} \simeq (I/2\pi R_o \Delta_o)^2\ t_{pen} \ .$$

Plugging in $I = 4 \times 10^7$ A, $R_o = 10$ cm, $\Delta_o = 0.1$ cm, and the value of Π_{sm} for copper, we get $t_{pen} \simeq 22$ μs. The numerical calculation gives $t_{pen} \simeq 12$ μs.

Despite the fact that the field penetrates the liner well before the liner reaches peak compression at 23 μs, the liner still attains a peak implosion velocity of 5×10^5 cm/s and produces a plasma volume compression of 10^3, with an initial plasma of 10^{18} cm^{-3} ion density and 100-eV temperature. The assumption of a constant current is somewhat optimistic, but most of the liner kinetic energy is acquired before the entire liner becomes resistive. The conclusion is that magnetic field diffusion per se does not eliminate from consideration configurations in which the liner itself carries the driving current.

3. Heating Near Peak Compression. Finally, we consider various mechanisms which heat the liner near peak compression. The inner surface of the liner will be heated by thermal conduction and bremsstrahlung x rays from the hot plasma and by some fraction of the α-particle energy released during the burn. The concern for liner fusion schemes is that the ablated liner material will move across the magnetic field lines and contaminate the fuel plasma. The problem of a wall-confined plasma with an imbedded magnetic field is a very difficult one, and most work to date has considered only the problem of plasma energy loss to a cold, nonablating wall,[7] with plasma densities considerably below those of

interest for liners.[19,43,52] The work most relevant to the question of ablated liner material contaminating the plasma are recent Russian liner experiments[6] which showed no impurities within the plasma. These experiments were done with liners having a length of 11 cm, initial radius of 6 cm, and initial thickness of 0.1 cm; the initial plasma parameters were a density of 3×10^{17} cm^{-3} and a temperature of 10 eV, and containing a magnetic field $B_z = 10^4$ G. Stable, symmetric implosions giving volume compression ratios of more than 100 were obtained. These results are very encouraging, not only for the question of plasma contamination, but because they indicate that magnetically driven thin-walled liners can be imploded stably and symmetrically.

The thermal state of the liner material during the post-implosion expansion is largely determined by the energy deposited by neutrons penetrating the liner during the burn phase. The thermonuclear neutrons have a mean free path which is longer than the thickness of the compressed liner, but not by a large factor. As a result, for an implosion which produces a large neutron yield ($Q \geq 1$), one can expect a non-negligible fraction of the neutron energy to be deposited in the liner. We give here approximate results for the liner which has been used as an example at other places in this proposal: a copper liner with $R_o = 10$ cm, $\Delta_o = 0.1$ cm, $\rho_o = 8.9$ gm/cm^3; maximum liner kinetic energy = 280 MJ/m; and plasma parameters $n_o = 10^{18}$ cm^{-3} and $T_o = 100$ eV. A peak volume compression of 10^3 was reached, with inner radius $R_f = 0.31$ cm, thickness $\Delta_f = 0.75$ cm, and an integrated line density

$$\bar{\rho}_f \Delta_f = \int_{R_f}^{R_f+\Delta_f} \rho \, dr \qquad \text{(III-100)}$$

of 14.4 gm/cm^2. The mean density is $\bar{\rho}_f \simeq 19$ gm/cm^3, twice normal density. The nuclear yield, Y, is 1.23 GJ/m (assuming 17.6 MeV/reaction), and the peak neutron production rate is 8.4×10^{20} neutrons/m/μs or 1.9 GJ/m/μs.

Detailed neutron transport calculations including elastic and inelastic neutron scattering and gamma-ray transport have been made for 14.1-MeV neutrons incident on the inner surface of aluminum and copper cylinders at normal density.[53] Figure 12 in Section IV shows the fraction of the neutron energy deposited in cylinders of varying thickness. Because the fundamental neutron-nucleus reaction scales with the number density of nuclei, the transmission through a thickness Δ_1 of material compressed to density ρ_1 is

roughly the same as a thickness $\Delta_o = \rho_1\Delta_1/\rho_o$ of normal density material. At a value of $\rho\Delta$ = 19 gm/cm, the energy absorbed in the liner is about 12% of the incident neutron energy. If we define a characteristic value $(\rho\Delta)^*$ for transmission by

$$T = \exp[-(\rho\Delta)/(\rho\Delta)^*] \quad , \tag{III-101}$$

where T is the fraction of incident energy transmitted, then a fit to the calculated values of T shows that for copper, $(\rho\Delta)^*$ is in fact nearly independent of $\rho\Delta$. At $\rho\Delta$ = 9 gm/cm^2, $(\rho\Delta)^*$ = 160 gm/cm^2 while for $\rho\Delta$ greater than 30 gm/cm^2, $(\rho\Delta)^*$ rapidly approaches an asymptotic value of 113 gm/cm^2. Because $\bar{\rho}_f\Delta_f$ for the liner is much smaller than the characteristic e-folding value, the deposited neutron energy density is simply proportional to 1/r in the liner. Thus the inner edge of the liner will be heated more than the outer edge; we neglect this variation in the discussion below. The energy deposited in the liner causes the temperature to reach a final value T_ℓ given by

$$M(U_F+U_V + \int_{T_V}^{T_\ell} C_V dT) = A_n\ (0.8\ Y) \quad , \tag{III-102}$$

where M is the mass per unit length of the liner, A_n is the fraction of the neutron energy deposited in the liner, and Y is the thermonuclear yield per unit length; only 80% of the yield is in neutron energy. The heat of fusion, U_F, for copper is U_F = 3.1 kcal/mole = 2.05 x 10^9 erg/gm, and the heat of vaporization is U_V = 72.8 kcal/mole = 4.79 x 10^{10} erg/gm (Ref.54). The vaporization temperature is T_V = 2855 K = 0.246 eV (Ref. 54). The specific heat, C_V, is a slowly varying function of temperature up to melting and even into the liquid phase,[54] so we can simply write

$$U_F + U_V + C_V(T_\ell - T_V) = A_n\ (0.8Y)/M \quad . \tag{III-103}$$

With A_n = 12%, Y = 1.23 x 10^{14} erg/cm and M = 56 gm/cm, the right-hand side of Eq. (III-103) equals 2.1 x 10^{11} erg/gm, which is significantly larger than U_F + U_V, so the liner will be heated above its vaporization temperature. Using $C_V \approx 6$ x 10^{10} erg/gm/eV appropriate to the vapor state,[54] we get $T_\ell \approx 3$ ev $\approx$ 34 000 K; note that $T_\ell > 10\ T_V$, a large margin for error. Such a liner will not rebound as

shrapnel, but as a hot gas. This should significantly reduce the damage within the reactor vessel.

Some qualitative aspects of Eq. (III-103) are worth pointing out. First of all, $Y/M = Q(E_L/M) = QV_*^2/2$, where $E_L = MV_*^2/2$ is the liner energy per unit length and V_* is a characteristic velocity. A minimum condition for vaporization is

$$0.4\ A_n Q V_*^2 = U_V + U_F = 5.0 \times 10^{10}\ \text{erg/g} \quad . \tag{III-104}$$

Reactor considerations require Q to be at least 5, so if we take $Q \gtrsim 5$ and $A_n \approx 0.1$, we find that a velocity $V_* \sim 5 \times 10^5$ cm/s is sufficient to ensure vaporization of the liner by neutron heating.

The value of A_n depends, as discussed above, on the integrated mass density at peak compression, $\rho_f\Delta_f$. A simple scaling argument shows that $\rho_f\Delta_f$ must be $\gtrsim$ 10 gm/cm^2 for "interesting" liner implosions. As shown in Section III.A, the optimal Q satisfies the relation (Eq. III-12)

$$Q_{opt} = 7.0\ [E_L\rho_i/2\pi]^{1/2} \quad , \tag{III-105}$$

where the liner energy per unit length, E_L, is in GJ/m and the initial liner density, ρ_i, is in gm/cm^3. (Note change of notation: the energy per unit length, denoted by E_L/ℓ in Sections III.A and III.C, is denoted simply by E_L here.) Writing E_L as $MV_*^2/2$, and using cgs units

$$Q = 3.5 \times 10^{-7}\ [\rho_i M/\pi]^{1/2} V_* \quad , \tag{III-106}$$

with M in gm/cm and V_* in cm/s. At peak compression of a strongly imploded liner, the inner liner radius is small compared to the thickness, so $M \approx \rho_f\pi\Delta_f^2$. Also, many numerical calculations have shown that $\rho_f/\rho_i \sim$ 2-3 is typical in a strong implosion. Taking $\rho_f/\rho_i = 3$, we get

$$\rho_f\Delta_f \approx Q\ \frac{5 \times 10^6\ \text{cm/s}}{V_*}\ \text{gm/cm}^2 \quad . \tag{III-107}$$

With $Q \gtrsim 2$ and $V_* \lesssim 10^6$ cm/s, $\rho_f\Delta_f \gtrsim 10$ gm/cm^2. This, in turn, ensures that the fraction of neutron energy absorbed, A_n, is $\gtrsim 10\%$.

In conclusion, the implosion of a fast, thin liner to conditions giving a thermonuclear yield ratio $Q > 1$ will produce a neutron flux sufficiently intense that the neutron energy deposited in the compressed and thickened (due to cylindrical convergence) liner will raise the temperature of the liner above the vaporization temperature. The detailed calculation above gave a liner temperature, T_ℓ, more than ten times the vaporization temperature; while the scaling arguments which followed indicated the general applicability of the parameters used in the detailed calculation.

E. Liner Instabilities

The high driving B field we contemplate will very quickly drive the outer layers of the liner beyond the yield point of the metal and into the range of plastic behavior. For a directly driven liner (i.e., a liner carrying its own driving current), the current carried in the liner will melt the outer layers through ohmic heating. Thus at some intermediate stage there will be an outer layer of melted metal, beneath this will be a layer of normal material, and finally, the innermost layer will have yielded. At this stage the Rayleigh-Taylor instability can develop in the outer layers and the inside layer may be prone to buckling. Later on, even the innermost layers become plastic. When the liner collapse is finally stopped by the compressed plasma, Rayleigh-Taylor instabilities can develop on the inner surface. In this section we examine these instabilities and conclude that they will probably do no serious harm.

A unique feature of our proposed drive with a B_θ field is the stiffening effect which this field has. For example, the driving field will strongly stabilize flute modes, so that the only possible Rayleigh-Taylor modes will be of the sausage type. Thus these modes can be studied by side-on X-ray flash photography. If such instabilities are not observed, then we can safely ignore this problem. If they are observed, we could in principle measure wavelengths and growth rates; these should lead to new experimental measurements of the viscosity of the metal or metals used.

1. The Bucklin Instability. In an earlier section of this report (Sec. I) a formula was given for the growth rate of the buckling instability in the form[12]

$$t_{buckle} = (E\Delta/\sigma)(\rho/12E)^{1/2}. \qquad \text{(III-108)}$$

In this expression E is Young's modulus and σ is the yield stress for the material in question, ρ is its density and Δ is the liner thickness. In deducing this formula, one supposes that the liner is driven by a perturbation to the point of plastic yield of the inner surface in a negligible time. Thereafter the load which produces buckling is equal to the yield stress, and Young's modulus of the unyielding remainder of the shell supplies the restoring force. The growth

rate of any perturbation depends on the mode number m; Eq. (III-108) is the reciprocal growth rate for the fastest growing mode.

In our case we are loading the liner quickly, therefore the correct value for σ should be the dynamic yield stress, not the static. Dynamic yield strengths[55,40] for metals of interest to us range from about 3.5 kbar for aluminum to 10 kbar for steel. We have supposed that the first figure also applies to copper and have prepared the following table of buckling times, calculated under the assumption that $\Delta = 0.1$ cm and $\rho = \rho(\text{normal})$. Static yield strengths of metals tend to be three to four times less than those given in Refs. 55 and 40 and their use would have given correspondingly longer buckling times. The yield strengths quoted in Refs. 55 and 40 are, if anything, too high, so our buckling times are probably pessimistic.

TABLE III-V

BUCKLING TIMES OF SEVERAL METALS TOGETHER WITH THE PARAMETER VALUES ASSUMED. ALL ASSUME $\Delta = 0.1$ CM

Metal	E (kbar)	σ (kbar)	ρ (g/cm^3)	t_{buckle} (μs)
Aluminum	700	3.5	2.699	11.3
Copper	1000	3.5	8.89	24.6
Steel	2000	10.0	7.8	11.4

According to Table III-V, the e-folding time of the buckling instability is about the same as the collapse time, so the instability would only e-fold once or twice. The actual situation is probably better than this, however, because as the shell collapses, the thickness Δ increases with time, approximately linearly over the major part of the collapse. Thus if the initial Δ were 0.1 cm, the effective value (i.e., the time average over the initial acceleration period) would be more like 0.2 cm, doubling the growth times given in Table III-V. One should also point out that the dynamic yield strengths used in Table III-V are probably upper limits rather than accurate numbers, although Refs. 40 and 55 seem to agree reasonably well.

From the above considerations we would expect the buckling instability to grow <u>at most</u> two or three generations, provided the liner is driven hard enough. This expectation is in full agreement with the experience of Fowler and co-workers.[56,57,58] They employed explosively driven liners to compress an axial

magnetic field. Their published data show implosions free of buckling; Fowler has, however, stated in a private communication that buckling was observed on occasions when the liner was sufficiently gently driven. The drive velocities in the published experiments were of the order of magnitude of those we contemplate, but numerically somewhat smaller than what we hope to achieve. Alikhanov et al.[6] also report symmetric implosions for magnetically driven metallic liners. It would appear that buckling will probably not develop if our implosions go more or less as expected.

2. Rayleigh-Taylor Instability. As we have seen, ohmic heating is very likely to melt the outer layers of the liner for the case where the liner is driven directly. This has two consequences unfavorable to the implosion, namely, energy dissipation through irreversible heating, and ultimate loss of driving owing to the field fully penetrating the shell. From the limited point of view of the Rayleigh-Taylor instability, however, the consequences of field penetration are favorable, as we shall now explain.

The electrical resistance of metals rises as the temperature rises. When the melting point is reached, the resistivity commonly undergoes an upward jump by a significant factor. Thus the magnetic field penetrates the metal liner more or less as a radiation front advances into cold material. The front encounters cold material which is relatively opaque (low resistance). Behind the front is the heated, relatively transparent (high-resistance) material. In the magnetic case, there is, furthermore, behind the front, a melted zone in which the transparency (i.e., the electrical resistivity) is even greater. To maintain the flow of the magnetic field, the gradient must be large in the cold (low-resistance) region, smaller in the heated region, and quite small indeed in the liquid region. This means that most of the current flow and hence the $\bar{J}x\bar{B}$ driving force, is developed in the unmelted region. Thus, once melting starts, the principal driving force is developed in the neighborhood of the liquid-solid boundary. As the density gradient here is very small, the Rayleigh-Taylor growth rate will be very small also. Furthermore, because this current-carrying layer advances through the liner the growth time at any particular layer is severely limited.

We consider now the problems of Rayleigh-Taylor instabilities at the outer and inner surfaces, respectively, during the acceleration and during the bounce

periods. Theoretical considerations suggest, and experimental evidence seems to support the idea that at high pressure both liquids and solids stressed beyond yield exhibit rather high viscosities. This is discussed in more detail below in subsection 4, where it is suggested that the viscosity may depend on pressure roughly as

$$\eta = \varepsilon p \ , \tag{III-109}$$

η being in poise, p is in bars, and $\varepsilon \simeq 0.06$. If this be true, then viscosity will quasi-stabilize the liner implosion very nicely; that is, it will not truly stabilize it, but will reduce the maximum growth rate to a point where the instability will not manifest itself in the short time available.

To see how this comes about we refer Chandrasekhar's monumental treatise;[59] the relevant formulas are given on page 447, Table XLVI. The formulas for k_M, the wave number of maximum growth rate, and ν_M, the maximum growth rate are given as

$$k_M = a(\rho^2 g/\eta^2)^{1/3}, \tag{III-110}$$

and

$$\nu_M = b(\rho g^2/\eta)^{1/3}, \tag{III-111}$$

where ρ is in g/cm^3, g is in cm/s^2, and η is the viscosity in poise. The constants a and b depend in a complicated fashion on the ratio $(\rho_2-\rho_1)/(\rho_2+\rho_1)$, and are tabulated as functions of this parameter. Medium 1 (density ρ_1) is driving medium 2 (density ρ_2) and $\rho_2 > \rho_1$. It is assumed in Chandrasekhar's calculation that $\eta_1/\rho_1 = \eta_2/\rho_2$, therefore the ρ's and η's on the right-hand sides of Eqs. (III-110) and (III-111) above need no subscripts. The pressure p, in bars, driving the liner is

$$p = 10^{-6} \ \rho \Delta g, \tag{III-112}$$

where Δ is the effective liner thickness. Let τ denote the total acceleration period and s denote the distance over which the acceleration takes place. Then

the instability growth in generations can be writ en as

$$\nu_M \tau = 100\, b\, (4s^2/\Delta\epsilon v)^{1/3} \qquad \text{(III-113)}$$

if we accept Eq. (III-109) for the viscosity. Here v denotes the peak velocity to which the liner is accelerated, or from which it is decelerated. Consider first the instability at the outer surface during the acceleration. If the driving medium is a nondiffusing magnetic field or a plasma drive, $\rho_1 = 0$ and b has its maximum value b = 0.46. Setting $\epsilon = 0.06$, s = 2.5 cm, $v = 10^6$ cm/s, and $\Delta \approx 0.1$ cm, one finds $\nu_M \tau = 7.4$.

For a plasma-driven liner this figure is marginal since $\exp(\nu_M \tau) \approx 1600$. On one hand for a directly driven liner it is too pessimistic, for the layer where the principal drive is applied becomes buried in the metal [due to field diffusion] where the density discontinuity at the liquid-solid interface is small. A density jump of 10%, for example, reduces the value of b to 0.061. This has a very strong effect on the value of $\nu_M \tau$. On the other hand, the reduction of the viscosity by the heating caused by the magnetic diffusion may be important. Equation (III-109), with $\epsilon = 0.06$, was obtained by fitting shock data in aluminum, and the shock pressures and irreversible heating were not enough to melt the metal. Some of the data[45] indicate that at melting temperature, ϵ might well drop by a factor of about 10, which would raise $\nu_M \tau$ by a factor 2.2. Presumably the first of these two effects can dominate the latter; for the work of Alikhanov et al.[6] furnishes experimental evidence that direct drive can indeed be quasistable. Furthermore the estimate $\Delta = 0.1$ cm is pessimistic. For as the liner collapses, Δ increases. A more reasonable estimate might be to set $\Delta_{effective} = 2\,\Delta_{initial}$, which buys a factor of 1.3. Finally, from Eq. (III-113) it is apparent that the instability can be ameliorated by making s shorter, v larger, or Δ thicker. This suggests using a more energetic and more impulsive drive.

The fact that our figures are marginal is not in itself a good reason to rule out this approach. They are based on viscosities which are not very well known and are more likely to be too low than too high, for all the experiments measured viscosity versus pressure in shocked materials. On the average, shocked material will be at reduced density and an elevated temperature, as compared with adiabatically compressed material at the same pressure, and both these effects

reduce the viscosity. Finally we should mention that there are experimental data which indicate that Rayleigh-Taylor instabilities may not cause trouble. We quote the experiments of Fowler et al.[57,58] Their liners were imploded at velocities close to what we contemplate. They were driven by explosives; thus the liner material was shocked and, according to our above argument, should be less stable than our adiabatic drive.

The Rayleigh-Taylor instability of the inner liner surface can be treated in a similar manner, if our model of the viscosity is not too far off at the high pressures involved. The effective thickness, Δ in Eq. (III-113) stands for $A_L/2\pi R_p$, where A_L is the metallic cross-sectional area and R_p is the plasma radius. Since A_L hardly changes from its initial value, due to the very moderate changes in liner density then for a compression ratio of ~ 20, Δ increases roughly by 20 from its initial value. Conservatively, we take $\Delta \sim 10\ \Delta_i$. Also, the code CHAMISA indicates that the deceleration occurs over a distance, s, comparable to the final radius. Thus, taking s=(2.5 cm)/20=0.125 cm, $(\nu_M \tau)$ of Eq. (III-113) becomes

$\nu_M \tau$ =	0.47	for	ε = .06
	1.00		.006
	2.16		.0006

It therefore appears that the Rayleigh-Taylor instability on the inside surface is not necessarily detrimental. For a reactor with s=(10 cm)/30=0.33 cm, $\nu_M \tau$ is larger by a factor of 1.8. The viscosity coefficient, ε, of course is still not known.

Thus the Rayleigh-Taylor instability of the inner liner surface may not be a serious problem. In closing this discussion we refer again to the experiments of Alikhanov and of Fowler. In the former work no incursion of impurities into the plasma load was observed. In the experiments of Fowler et al., the load was a magnetic field (no plasma), but the high compression, indicated by the high magnetic fields that were reached, implies that instability at the inner surface did not spoil the implosion. In fact the field measurements show a decreasing magnetic field for about 2 μs after peak compression before the signal ended by probe destruction. Thus the probe survived through the peak compression, which would have been unlikely if there had been a serious growth of instabilities on

the inner surface.

3. Other Effects. Irregularities of liner thickness from point to point will amplify upon collapse even without any instability whatsoever. This is purely the result of convergent hydrodynamic flow which causes the liner to thicken as it collapses. This phenomenon simply establishes a relationship between the compression desired and the necessary liner tolerances. The greater the compression, the more nearly uniform must be the liner.

Implosions can also be spoiled by jetting of liner material and by spalling of the inner surface. The great uniformity of magnetic pressure over the liner surface, in contrast with what can occur with an explosive drive, will preclude jetting provided the liner is seamless. Spalling is the result of reflection of a shock wave by a free surface. As our drive is shockless, spalling of the inner surface cannot be a problem at any time during the compression phase. On the rebound, tension will probably occur in the metal and, if sufficiently severe, may break up the liner, but we are prepared to live with this.

4. Note on Viscosity. Viscosity of metals at high pressures is a field about which our knowledge is quite meager. At present there are no equation-of-state calculations of which the authors are aware which make any attempt to compute viscosity, in the liquid or in the plastic state. It is possible to make a relatively crude theory, which does contain sensible physics, but from which it is very hard to extract reliable numbers. It predicts viscosity to be a linear function of the pressure, but with a complicated dependence on the temperature.

Experimentally the case is not hopeless, but it is far from satisfactory. Mineev and Savinov[45] have measured the viscosity of aluminum, lead, and sodium chloride by perturbing a stable shock wave and observing the decay of the perturbations. Swanson and Mader[38] have made one-dimensional shock calculations with a code which includes elastic-plastic transitions, strain-hardening and strain-rate effects in aluminum. By adjusting parameters of the calculation to fit experimental shock wave data they deduce a value for the viscosity. All in all, 12 shots are matched. White[60] has found that he can fit the Rayleigh-Taylor growth rate data of Barnes et al.[40] by a purely hydrodynamical calculation using a semitheoretical value of 1.4 kP. And finally, Perry and Mix[61] have deduced a

viscosity from an observed instability in a shocked aluminum plate. In this last experiment, the reflection of the shock from the back of the plate accelerates the surface outward. Subsequently, on rebound, the back surface accelerates inward. During this inward acceleration an instability develops which is interpreted as Rayleigh-Taylor. From its wavelength η = 1.7 kP is deduced.

In Fig. III-8 we have plotted all of the above results for aluminum as best we could, and have drawn in the straight line fit

$$\eta = 0.06\ p, \tag{III-114}$$

η in poise and p in bars. This extrapolates to 6 cP at one bar which is quite reasonable for a liquid metal (mercury, for example, is 2 cP). The surprising agreement of this extrapolation necessitates a few words of caution. The data of

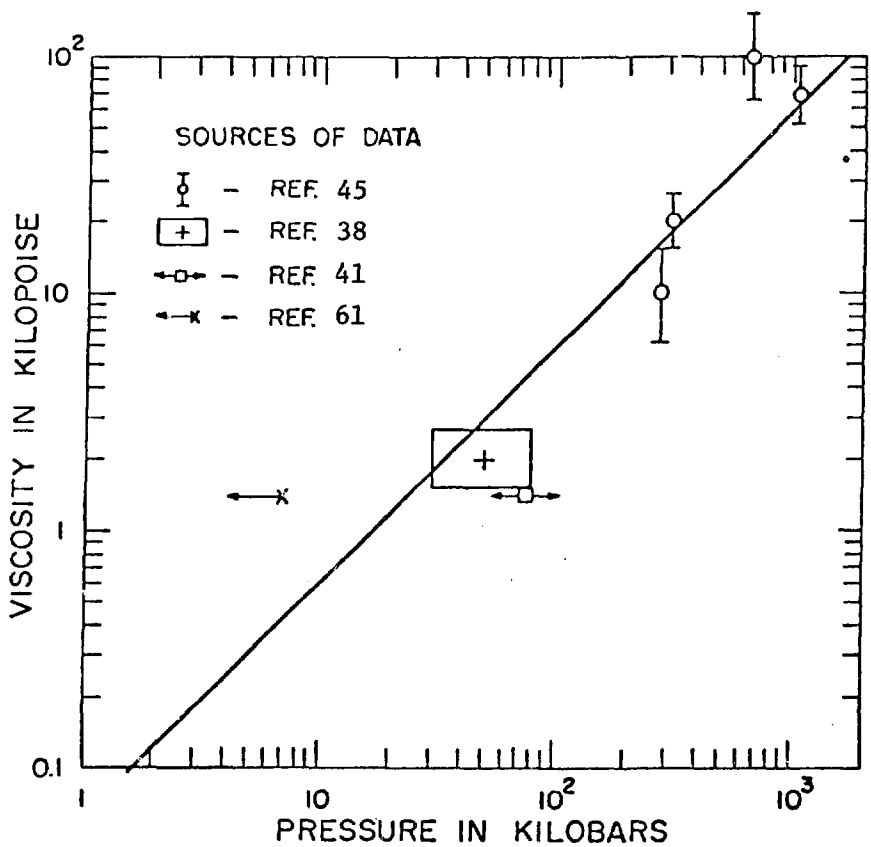

Fig. III-8.
Viscosity of aluminum as a function of pressure. In most cases the pressure was produced by an explosive driven shock wave.

Mineev and Savinov include shocks of temperatures ranging from 630 to 3500 K, and viscosity is known to depend on temperature. Swanson and Mader give shock pressure for each shot but no temperature. They find that over the range 25 to 90 kbar the value $n = 2$ kP fits better than do 1 or 3 kP. We have therefore plotted their results as a rectangle covering this range. Furthermore, the quality of their calculated fits to data depends on other parameters in addition to the viscosity. The data of Barnes et al. gives only peak driving pressure, thus the actual pressure during the Rayleigh-Taylor growth is only approximately known, and the temperature is not given. Finally Perry and Mix state only the shock pressure whereas the instability actually develops in the rarefaction following shock reflection, so the material is actually under tension. We have plotted their point at a pressure corresponding to their shock pressure; this questionable choice has been compensated by completely ignoring their point in fitting the straight line, Eq. (III-114). The data we have plotted are all for aluminum. Mineev and Savinov[45] also give similar data for lead with viscosities very similar to those of aluminum; they conclude that the viscosity is not a sensitive function of the metal.

It is clear from the above discussion that Eq. (III-114) is not an established natural law. On the other hand, there is reason to hope that Eq. (III-114) is order of magnitude correct for temperatures which are not too high.

IV. PRELIMINARY POWER REACTOR CONSIDERATIONS FOR INERTIALLY CONFINED PLASMA SCHEMES BASED UPON IMPLODING LINERS

A. Introduction

In an imploding-liner fusion reactor the very dense plasma is heated and confined inertially by the imploding liner. A continuous spectrum of operating modes can be envisaged, varying from the ~ 10^5-m/s implosions associated with pellet fusion to the ~ 10^2-m/s slow compressions proposed by the NRL group.[62] Very simple scaling laws[9,28] show that the ratio Q of thermonuclear yield to initial liner energy increases nonlinearly with both invested liner energy and the inverse of the liner aspect ratio (ratio of initial inner radius to initial thickness). Since low aspect ratio (i.e., massive) liners are typically slow, this very simple scaling points to the desirability of slow implosions, as in the NRL approach. Consideration of the shortcomings of this very simple scaling, however, points to problems for the slow liner approach. For instance, the constraints of particle/energy end loss (cylindrical geometries are being considered), liner compressibility, and/or hydrodynamic (Rayleigh-Taylor) stability of the inner liner surface generate optimum Q-values at higher and higher liner aspect ratios (thinner and faster liners). The penalty incurred for the nonideal behavior of both liner and plasma is the increase in liner kinetic energy required to achieve a given system Q. The following sections give a preliminary analytic rationale for considering intermediate-to-fast (i.e., high aspect ratio) imploding-liner fusion systems.

The preliminary nature of these "reactor" studies cannot be overemphasized. The absence of in-depth systems studies and experimental results makes comprehensive and self-consistent evaluation of the reactor potential[63] in terms of "reactor desirability" (e.g., reactor size, duty cycle, cycle time, stored and recirculating energy, plant factor, planned outages, siting/environmental problems, and development costs), "confidence in physics assumptions" (e.g., equilibrium/stability, particle/heat transport, heating, impurity effects, and refueling) and "reactor technologies" (e.g., first-wall/blanket/shielding, energy storage/transfer, fueling and impurity control, vacuum, system control, and energy conversion/recovery) ill-advised at this time. Nevertheless, the material contained herein gives a preliminary indication of the reactor advantages and disadvantages portended by a fast-liner inertially confined reactor (FLICR).

Specifically, the FLICR approach heats and confines the plasma on its own timescale, thereby obviating or alleviating major problems associated with slow-pulsed or quasi-steady-state confinement schemes. The major penalty incurred is the requirement of large fast-pulsed energy release and transfer. Given an acceptable physics operating point for FLICR, the technological task is clear: how to efficiently, economically, and repeatedly transfer large amounts of energy to a destructible liner/electrical-lead system while simultaneously minimizing damage to the more expensive, permanent structure surrounding the implosion/explosion region. A very preliminary and sketchy scenario is given which addresses this problem.

The desire and need for compact high-overall--power-density (> 10 MW/m^3) fusion systems will require very fast burns simply because of the nature of the plasma medium. The attributes of compactness and a virtual decoupling of system efficiency from significant size scaling, should also result in considerably reduced development costs for a FLICR device. The aforementioned problems and unknowns associated primarily with "reactor technologies" are acknowledged but are not significantly understood at present. "Confidence in physics assumptions" is also poorly resolved (few relevant experiments have been made), although the potential advantages portended by the FLICR approach may be truly significant. The "reactor desirability" of FLICR should be high from the viewpoint of size (costs, degree of modularity, maintainability, etc.), power density, and first-wall considerations.

B. Dynamic, Incompressible Liner Model

The results of preliminary studies of rotationally stabilized imploding liner fusion systems are discussed. An idealized model of an incompressible cylindrical liner is developed, based on earlier work by Turchi,[64] Shearer,[65] and Robson.[9] An energy principle is used to determine the liner and thermonuclear burn dynamics in the presence of axial particle loss. A simple energy balance is used to relate liner characteristics to the required liner efficiency (i.e., reversibility) for a given recirculating power fraction.

Aside from the assumption of incompressibility, this model is intended to be more general than would be required for the experimental approach of this proposal or for the reactor concept that follows (Sec. IV. C). In this spirit, the effects of the energy balance of a rotating liquid liner are included in this

model. By considering the nonrotating case within the model, the results apply equally well for a solid nonrotating liner.

1. Calculational Model. Referring to Fig. IV-1, a unit length ℓ of cylindrical liner is described by inner and outer radii r_1 and r_2, respectively, at time t after the implosion has commenced. Subscript "o" refers to the initial (t = 0) condition, and subscript "f" designates conditions at maximum compression. The plasma radius is r_p, and for all cases considered here the plasma is assumed to be wall-confined ($r_p = r_1$). Axial particle loss is described by a simple sonic flow model. An energy principle based upon the initial and final states of the liner-plasma system is used to derive the liner dynamical equation. The liner material is assumed to be an incompressible liquid, and the plasma is assumed to behave as an ideal gas. All energies (Fig. IV-1) are expressed per unit liner length, and, except for the plasma temperature T(keV), mks units are used.

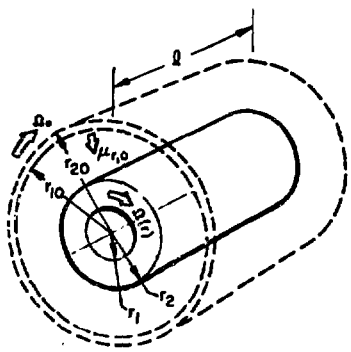

VOLUME COMPRESSION RATIO	$\kappa = (r_{10}/r_1)^2$
RADIAL KINETIC ENERGY	$W_{KR}\ell$
ROTATIONAL KINETIC ENERGY	$W_{K\theta}\ell$
PLASMA ENERGY	$W_P\ell$
COMPRESSIONAL ENERGY	$W_{PV}\ell$
END-LOSS ENERGY	$W_{EL}\ell$
THERMONUCLEAR ENERGY	$W_N\ell$

$$W_{PO} + W_{KRO} + W_{K\theta O} = W_P + W_{KR} + W_{K\theta} + W_{PV} + W_{EL}$$

$$Q \equiv W_N/(W_{KRO} + W_{K\theta O} + W_{PO})$$

Fig. IV-1.

Illustration of liner geometric model and list of key notation used in reactor analyses.

a. Pressure-Volume Work on Plasma. If $\kappa = V_o/V = (r_{po}/r_p)^2$ is defined as the volumetric plasma compression, the adiabatic relationship for a plasma with a particle line density $N(m^{-1})$ that is depleted from an initial inventory N_o by end loss is given by[31]

$$(T/T_o) = \kappa^{\gamma-1}(N/N_o)^{\delta} \quad , \tag{IV-1}$$

where $\gamma = (2 + f)/f$, f is the degree of freedom, $\delta = 2\langle E\rangle/f(kT) - 1$, and $\langle E\rangle$ is the mean energy of end-loss plasma. The work W_{pv} expended by the liner in compressing the plasma from $r_{po} = r_{10}$ to $r_p = r_1$ is equal to

$$W_{pv}/W_{po} = (2/3)\int_1^{\kappa} (N/N_o)^{1+\delta}\, \kappa^{\gamma-2}\, d\kappa \, . \tag{IV-2}$$

For the case of no end loss ($N/N_o = 1$) Eq. (IV-2) reduces to

$$W^o_{pv}/W_{po} = (2/3)(\kappa^{\gamma-1} - 1)/(\gamma-1) \quad , \tag{IV-3}$$

where $W_{po} = 3N_o(kT_o)$ is the initial plasma energy.

b. End-Loss Energy. The rate of particle end loss is assumed to be given by

$$dN/dt = - N/\tau_{EL} \tag{IV-4A}$$

$$\tau_{EL} = \ell^*/2v_s \tag{IV-4B}$$

$$v_s = (\gamma kT/m_i)^{1/2} \, . \tag{IV-4C}$$

The parameter ℓ^* equals the device length only when end loss is not inhibited by a buffer magnetic field. The end-loss energy is given by

$$W_{EL} = \int_o^t (N/\tau_{EL})\, \langle E\rangle dt' \quad , \tag{IV-5}$$

where $\langle E\rangle$ is the average energy carried away by an end-loss particle. Typically,

<E> is assumed equal to 3(kT).

c. Liner Radial Kinetic Energy. Designating u_r as the radial liner velocity at position r, the radial kinetic energy is given by

$$W_{KR} = (1/2)\int_{r_1}^{r_2} 2\pi r\rho u_r^2 dr \qquad \text{(IV-6A)}$$

$$= \pi\rho(r_1 u_{r_1})^2 \ln(r_2/r_1)$$

$$W_{KRO} = (\pi\rho/2)(r_{10}u_{r_{10}})^2 \ln\alpha \qquad \text{(IV-6B)}$$

$$W_{KRf} = 0 \text{ (maximum compression)} \quad . \qquad \text{(IV-6C)}$$

For an incompressible liner the product ru_r is a constant of radius and $\alpha = (r_{20}/r_{10})^2$.

d. Liner Rotational Kinetic Energy. The liquid liner is given an initial, uniform angular frequency Ω_o to stabilize Rayleigh-Taylor instabilities at the inner liner surface when $u_{r_1} \to 0$ (maximum compression). Designating $u_\theta = r\Omega(r)$ as the rotational velocity at position r and time t, the rotational kinetic energy is given by

$$W_{K\theta} = (1/2)\int_{r_1}^{r_2} 2\pi r\rho u^2_\theta dr \qquad \text{(IV-7A)}$$

$$= \pi\rho \int_{r_1}^{r_2} r^3\Omega^2(r)\, dr \quad . \qquad \text{(IV-7B)}$$

On the basis of mass conservation for an incompressible liner an element of liner material positioned at r(o) at t = 0 will be located at $r(t) = [r(o)^2 + r_1^2 - r_{10}^2]^{1/2}$ at time t. Conservation of angular momentum for each liner element requires

$$r^2\Omega(r) = r(o)^2\Omega_o = \Omega_o(r^2 - r_1^2 + r_{10}^2) \quad . \qquad \text{(IV-8)}$$

Substituting Eq. (IV-8) into Eq. (IV-7) leads to

$$W_{K\theta 0} = (\pi\rho/4)\,\Omega_o^2 r_{10}^2(\alpha^2-1) \qquad \text{(IV-9A)}$$

$$W_{K\theta} = [W_{K\theta 0}/\kappa^2(\alpha^2-1)]\,\{1 + \kappa(\alpha-1)^2 - 1$$

$$+ (\kappa-1)\{4\kappa(\alpha-1) + 2(\kappa-1)\,\ell n[1 + \kappa(\alpha-1)]\}\} \; . \qquad \text{(IV-9B)}$$

In the limit of high compressions with $\kappa(\alpha-1) >> 1$ Eq. (IV-9B) approaches the limit $W_{K\theta}/W_{K\theta 0} \rightarrow 4\kappa/(\alpha+1)$; the considerable increase in rotational energy at high compressions must be supplied by the initial radial energy W_{KRO}.

e. Rayleigh-Taylor Condition. Equating $d(W_{KR} + W_{K\theta})/dt$ to dW_{pv}/dt [Eq. (IV-2)], solving for du_{r_1}/dt at maximum compression ($u_{r_1} = 0$), and equating the radial de-acceleration to the centripetal acceleration $r\Omega^2(r)$ evaluated at the inner radius gives the following relationship for Ω_o^2,

$$\Omega_o^2\,[(\alpha-1)\left(1 + \frac{(\hat{\kappa}-1)^2}{1+\hat{\kappa}(\alpha-1)}\right) + (\hat{\kappa}+2(1-1/\hat{\kappa}))\ell n(1+\hat{\kappa}(\alpha-1))]$$

$$= (4/3\pi\rho)\hat{\kappa}^{\gamma}(N/N_o)^{1+\delta}\, W_{po}/r_{10}^4 \; , \qquad \text{(IV-10)}$$

where $\hat{\kappa}$ designates the maximum compression $(r_{10}/r_{1f})^2$. This expression is used to determine the initially uniform rotational frequency Ω_o required to satisfy the Rayleigh-Taylor condition at the inner surface r_1 under conditions of maximum compression ($u_{r_1} = 0$, $du_{r_1}/dt = -r_1\Omega^2(r_1)$, $\kappa = \hat{\kappa}$).

f. Liner Dynamics. The major energy quantities that describe the liner have been derived. The following energy balance is used to define the liner dynamical equation for the incompressible case being considered.

$$W_{KRO} + W_{K\theta 0} + W_{po} = W_{KR} + W_{K\theta} + W_p + W_{EL} \; , \qquad \text{(IV-11)}$$

where $W_p = 3N(kT)$ is the plasma energy at time $t > 0$. Defining $\tau = tu_{r_{10}}/r_{10}$ and substituting the previously derived energy quantities into Eq. (IV-11) leads to

$$(d\kappa/d\tau)^2 \ln(1 + \kappa(\alpha-1)) = 4\kappa^4 \ln\alpha - 2(\Omega_o r_{10}\kappa/u_{r_{10}})^2$$

$$\times ([1 + \kappa(\alpha-1)]^2 - 1 - \kappa^2(\alpha^2-1)$$

$$+ (\kappa-1)\{4\kappa(\alpha-1) + 2(\kappa-1)\ln[1 + \kappa(\alpha-1)]\})$$

$$- [16W_{po}/(3\pi r_{10}^2 \rho u_{r_{10}}^2)]\, \kappa^4 \int_1^{\kappa} (N/N_o)^{1+\delta}\, \kappa^{\gamma-2} d\kappa \quad . \qquad \text{(IV-12)}$$

Equation (IV-12) is evaluated at the point of maximum compression ($d\kappa/d\tau = 0$) to determine the initial radial velocity $u_{r_{10}}$ in terms of the maximum compression $\hat{\kappa}$. Equation (IV-10) is used to determine Ω_o, and, once a final desired temperature is specified, Eq. (IV-1) is used to determine $\hat{\kappa}$. Obviously, an iterative numerical procedure must be used when end loss ($N/N_o \neq 1$) occurs, integration of (Eq. IV-4A) giving (N/N_o) versus t.

g. Liner Energy Balance. As a measure of liner efficiency the following ratio is defined,

$$Q = W_N/(W_{KRO} + W_{K\theta O} + W_{po}) \quad , \qquad \text{(IV-13)}$$

where W_N is the thermonuclear yield

$$W_N = (E_N/4\pi r_{10}^2)\int_o^t \kappa N^2 \langle\sigma v\rangle\, dt \qquad \text{(IV-14A)}$$

$$\langle\sigma v\rangle = (5 \times 10^{-18}/T^{2/3})\, e^{-19.94/T^{1/3}} \ (m^3/s) \quad . \qquad \text{(IV-14B)}$$

A highly idealized energy flow diagram for a liner fusion power plant is illustrated in Fig. IV-2. An indication of the degree of liner reversibility needed for a given circulating power fraction ε is η, defined as the fraction of the total liner energy ($W_{KRO} + W_{K\theta O}$) that is recovered reversibly each cycle. Given the re-circulating or make-up energy $W_c = (1-\eta)(W_{KRO} + W_{K\theta O}) + W_{po} + W_{EL}$, the electrical energy $W_E = \eta_{th}\,[W_N + W_{po} + (1-\eta)(W_{KRO} + W_{K\theta O}) + W_{EL})]$, and $\varepsilon = W_c/W_E$, the required liner efficiency becomes

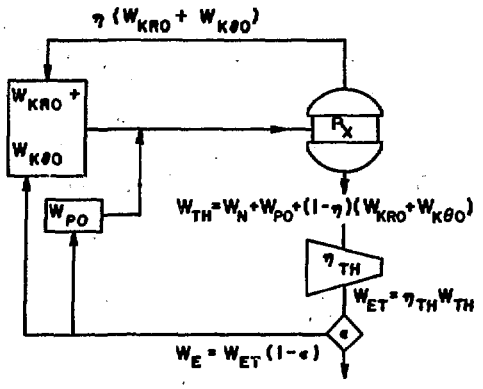

Fig. IV-2.

Schematic diagram of simple energy balance used to evaluate the dependence of liner reversibility η required for a given recirculating power fraction ε and thermal conversion efficiency η_{th}.

$$\eta = \{1-Q[\varepsilon\eta_{th}/(1-\varepsilon\eta_{th}) - (W_{EL}/W_N)]\}/[1-Q(W_{po}/W_N)] \ . \qquad \text{(IV-15)}$$

Equation (IV-13) gives Q, and η_{th} represents the thermal-to-electric conversion efficiency. The quantity $\varepsilon(\eta=0)$ designates the recirculating power fraction of a "throwaway" liner reactor.

2. Results of Dynamical, Liner Reactor Calculations. The foregoing definitions of Q, ε, and η are used to give a preliminary estimate of the reactor potential of an imploding-liner fusion system. It is emphasized that detailed design and systems studies must follow on the basis of these preliminary results; the intent here is to give general indications and not to present a firm operating point in either the physics or engineering sense. The significant influence of liner compressibility effects are not included in these results, but are treated in Section III.

a. Results from Incompressible Liner Model. The dependence of Q on the initial liner inverse aspect ratio Δ_o/r_{10} for $r_{10} = 0.1$ m is depicted in Fig. IV-3 for the values of r_{10}, n_o, T_o, and Ω_o indicated. The effects of end loss for the case of no Rayleigh-Taylor stabilization ($\Omega_o = 0$) is shown in Fig. IV-4 as a function of the effective length ℓ^* [Eq. (IV-4B)], which describes the line-density exponentiation time τ_{EL} as a function of sonic velocity v_s. Hence,

ℓ^* is not the true device length when poloidal field end loss inhibition is used, but is used here only as a measure of end-loss reduction required relative to the free streaming case. The optimum shown in the Q *vs* Δ_o/r_{10} dependence results from the increased implosion time and integrated end loss as Δ_o is increased; without end loss Q increases monotonically with Δ_o.

Shown also on Fig.IV-4 is the case where Rayleigh-Taylor stabilization is imposed [Ω_o given by Eq. (IV-10)] for r_{10} = 0.10 m but without end loss ($\ell^* = \infty$). An optimum Q is shown at $\Delta_o/r_{10} = 0.32$. For thin liners the effective thermonuclear burn time $\tau_B = W_N/P_N(\max)$ is small, and, consequently, Q is diminished. Thickening the liner increases Q at the expense of increased radial energy needed to supply the increased rotational energy at maximum compression, $\mathcal{R}$. For very thick liners, $\Delta_o/r_{10} \geq 1.0$, the rotational energy requirement becomes appreciable, eventually dominating W_N and decreasing Q. This latter effect is easily shown by the ratio $\eta_{pv} = W_{PV}/(W_{KRO} + W_{K\theta O})$ of pressure-volume

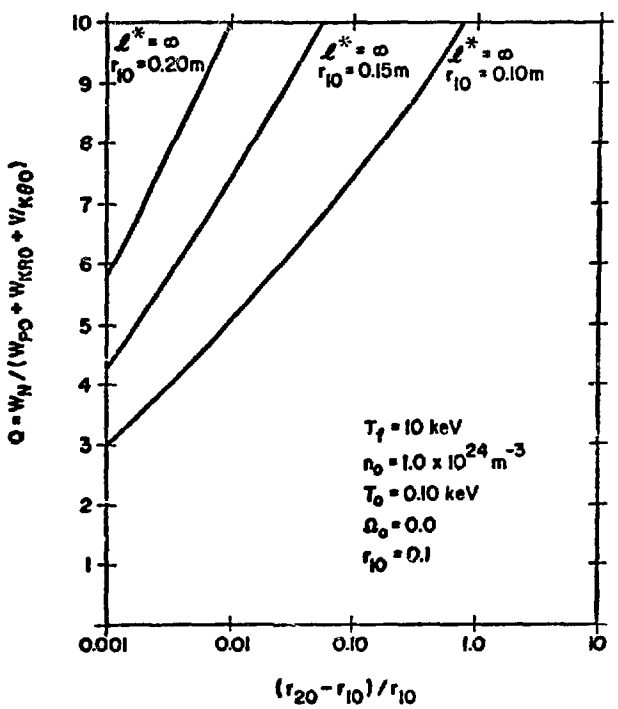

Fig. IV-3.
Dependence of Q on liner aspect ratio Δ_o/r_{10} for an incompressible liner (ρ = 9.4 x 10^3 kg/m^3), without end loss ($\ell^* = \infty$) and without rotation (Ω_o = 0).

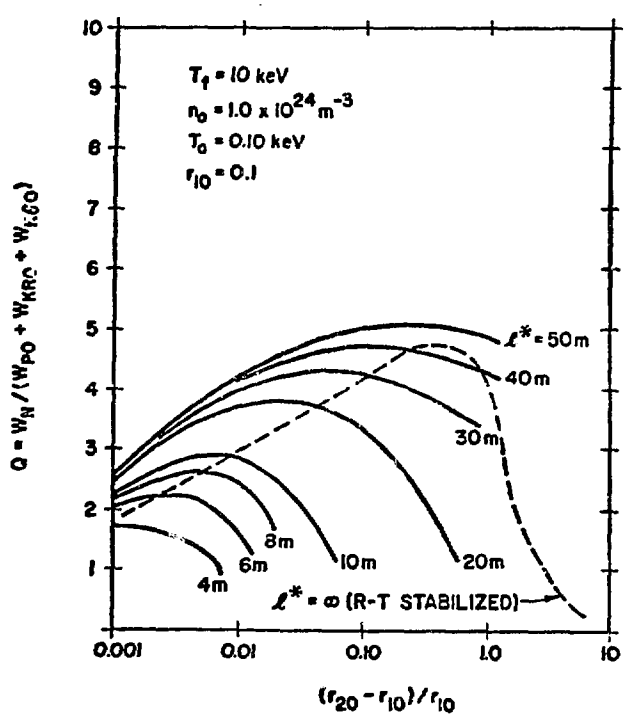

Fig. IV-4.
Dependence of Q on liner aspect ratio Δ_o/r_{10} for an incompressible liner, including end loss, but without rotation. Also shown is a curve for no end loss, but with rotation.

work and the total initial liner energy. From Eqs. (IV-6B), (IV-9B), and (IV-10) in the limit $\kappa >> 1$, it follows that,

$$(1/\eta_{pv}-1) = \frac{(\gamma-1)}{2} \frac{\kappa\{(\alpha-1)^2 + 4(\alpha-1) + 2\,\ell n[\kappa(\alpha-1) + 1]\}}{(\alpha-1) + \kappa\{1+\ell n[\kappa(\alpha-1)]\}} \quad . \qquad \text{(IV-16)}$$

Depending on the relative values of $\alpha = (r_{20}/r_{10})^2$ and κ, Eq. (IV-16) exhibits two limits. If α is ~ 1 to 2, Eq. (IV-16) predicts that $\eta_{pv} = 1/\gamma = 3/5$ for large κ. On the other hand, for $\alpha \geq 4$ to 5, the quantity $(1/\eta_{pv} - 1)$ approaches $[(\gamma-1)/2][\alpha-1]^2/\ell n[\kappa(\alpha-1)]$, which diverges (i.e., $\eta_{pv} \to 0$) for very thick liners and any realistic value of κ.

b. Preliminary Indications of Liner Compressibility on Energy Balance. For the example case considered here ($n_o = 10^{24} m^{-3}$, $T_o = 0.1$ keV, $\kappa = 1000$, $T_f = 10$ keV), the plasma pressure exerted on the liner at maximum compression will be tremendous (32 MB). Clearly, liner compressibility effects will be significant. Although these effects are considered in Section III, it will be instructive at this point to examine the effects of compressibility on the foregoing reactor predictions. The inner radius trajectory and instantaneous fusion power (20 MeV/n) as calculated from the present code are shown in Fig. IV-5 as a function of time for a $r_{10} = 0.1$ m, $\Delta_o/r_{10} = 0.01$ liner which is initially filled with an $n_o = 10^{24} m^{-3}$, $T_o = 0.1$ keV plasma and compressed to 10 keV ($\kappa = 1000$). Similar results obtained from the code CHAMISA (see Section III.B) are also shown on Fig. IV-5, and Table IV-I gives a numerical comparison between these cases. Two compressible calculations are illustrated: a) the initial liner kinetic energy W_{KRO} is identical to that of the incompressible case (only 68% of the initial liner energy is converted to plasma energy), and b) the initial liner energy is sufficient to insure that the compressed plasma conditions ($\kappa = 1000$, $T_f = 10$ keV) are identical to those specified in the incompressible calculation. Table IV-I and Fig. IV-5 show that for the same initial liner energy the compressibility reduces the overall system performance, as measured by $Q = W_N/(W_{KRO} + W_{po})$, by 55%, from the incompressible case. An increase in the initial liner energy by a factor of 1.87 is required to achieve the same compressed plasma conditions, and the efficiency of liner energy transfer to the plasma decreases, but the increased fusion yield W_N renders a Q

TABLE IV-I.

COMPARISON OF LINER COMPRESSIBILITY EFFECTS FOR SAMPLE CASE[a]

	Incompressible Reference Case	Compressible[b] Calculation with Same Initial Liner Energy	Compressible[b] Calculation with Same Final Compression
Initial radial kinetic energy W_{KRO}(MJ/m)	150.	150.	281.
Maximum compression $\hat{\kappa} = (r_{10}/r_{1f})^2$	1000.	567.	1000.
Initial radial velocity $u_{r_{10}}$ (m/s)	7.3×10^3	7.3×10^3	1.0×10^4
Maximum plasma temperature T_f(keV)	10.0	6.8	10.0
Radial kinetic energy at maximum compression W_{KRf}(MJ/m)	0.0	4.0	27.0
Compressional energy in liner, W_{PVL}(MJ/m)	0.0	44.	100.
$(W_{PVL} + W_{KRf})/W_{KRO}$	0.0	0.32	0.45
Turn-around time $\tau_{1/2}$ (μs)	13.3	13.3	9.7
Peak fusion power P_N(W/m) x 10^{-15}	2.69	0.53	2.69
Total fusion energy W_N(MJ/m)	771.	424.	1400.
$Q = W_N/(W_{KRO} + W_{PO})$	5.1	2.8	5.0
$\tau_B = W_N/P_N$ (μs)	0.29	0.80	0.52
$\varepsilon(r=0)$	0.41	0.66	0.42
$\langle nT\rangle \times 10^{20}$ (s/m^3)	2.90	4.54	5.20

(a) $r_{10} = 0.1$ m, $\Delta_0/r_{10} = 0.01$, $n_0 = 1 \times 10^{24}$ m^{-3}, $T_0 = 0.1$ keV, $\rho = 9.4 \times 10^3$ kg/m^3, $\Omega_0 = 0.0$.

(b) Nickel equation of state used, $\rho = 8.90 \times 10^3$ kg/m^3.

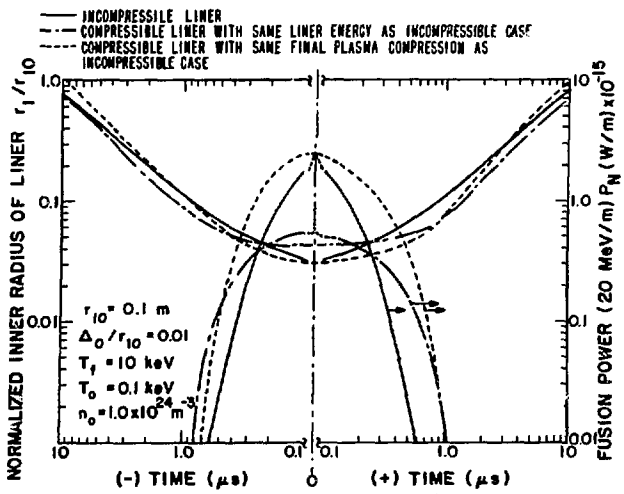

Fig. IV- 5.
Time dependence of the liner radius r_1 (relative to the initial radius r_{10}) and fusion power P_N (20 MeV/n) for both compressible and incompressible liners ($\rho = 9.4 \times 10^3$ kg/m^3). The incompressible case is calculated from the present model and the compressible case is from the code CHAMISA.

value which equals that predicted by the incompressible calculation. As seen from Fig. IV-5, the increased reaction yield is a consequence of the longer time spent at higher compressions, which is a peculiarity of compressional effects when the same final state is achieved. The penalty extracted for this situation is the considerable increase in initial liner energy W_{KRO} and initial liner velocity $u_{r_{10}}$.

In view of the limits imposed by liner compressibility, the $r_{10} = 0.1$ m, $\Delta_o/r_{10} = 0.01$ case selected here for numerical examination represents a "break-even"-to-marginal reactor operating point. That is, according to Eq. (IV-15) with $W_{EL} = 0$ and no direct recovery of liner energy [$\eta = 0$] such a system would at best have an $\varepsilon = 0.66$ recirculating power fraction.

As discussed in Section III the influence of liner compressibility on reactor efficiency gives an optimum initial plasma density for a given n_oT_o product. For the cases considered in Fig. IV-5 and Table IV-I ($n_oT_o = 1.0 \times 10^{23}$ keV/m^3), these optimum Q-values are ($n_o = 0.33 \times 10^{24}$ m^{-3}, $T_o = 0.30$ keV) 4.50 and ($n_o = 0.50 \times 10^{24}$ m^{-3}, $T_o = 0.2$ keV) 5.87, respectively. Other concerns and uncertainties are: a) mechanism and efficiency of energy transfer to the liner from either an inductive or capacitive store, b) mechanical/hydrodynamic/thermal response of structure surrounding the liner, c) degree of energy-transfer in both the liner and associated electrical lines that is possible and/or necessary to assure a good recirculating power fraction, and d) efficiency of initial plasma formation.

C. Preliminary Reactor Design Considerations

From the results presented in Table IV-I and the discussions given in Section IV.B.2.b, interesting design points for a fast-liner inertially confined reactor (FLICR) may exist for $n_o \sim 0.5\text{-}1.0 \times 10^{24}$ m^{-3}, $T_o \sim 0.1\text{-}0.2$ keV, $r_{10} \sim 0.1$ m and $\Delta_o/r_{10} \sim 0.01$ ($Q \sim 4\text{-}6$, $\varepsilon(\eta{=}0) \sim 0.3\text{-}.5$) under the assumption of effective radial and axial plasma confinement by poloidal fields and the neglect of energy transfer inefficiencies. The liner radial kinetic energy W_{KRO} will be in the range 150-300 MJ/m. Hence, if the liner length ℓ can be held below 1 m, mechanical energy releases will be in the range 300-600 MJ/m (including alpha-particle and plasma kinetic energies); clearly, the liner *per se* and a portion of the power leads and pre-plasma injector will be destroyed (1 MJ = 0.24 kg TNT equivalent). This mechanical energy will be deposited

ultimately as sensible heat to a high-temperature coolant and, therefore, will be recoverable by the thermodynamic cycle. No attempt is made to recover the liner energy directly (i.e., $\eta = 0$), as is proposed by NRL.[62] The numerical values given above in no way should be construed collectively as an optimized operating point for a FLICR, but are used only to give an estimate of reactor size and operating mode. Since the ~ 1000 MJ/m fusion energy release corresponds to ~ 100 kWeh/m (1 kWeh = 9.0 MJ (thermal) at $\eta_{TH} = 0.4$), the cost of materials and re-fabrication of demolished components must fit within the constraint of ~ 10-20 \$/m of total energy release each pulse. Finally, a 100-MWe power station will require ~ 5-10 s between power pulses, although a multi-liner system would allow longer dwell times per liner (with added capital costs, \$/kWe). Although the physics, technological, and economic constraints summarized in Section IV.B.2.b have yet to be quantitavely integrated into a consistent picture of the FLICR, the following qualitative description does reflect the essential elements of a fusion reactor as well as the major questions which eventually must be resolved.

1. Description of Possible Reactor Embodiment. Figure IV-6 schematically illustrates a reactor concept based upon the fast liner implosion. A precast liner (solid $Li_{0.1}Pb_{0.9}$ is used here, but a different material having higher electrical conductivity would be required) (A) encased in an electrically insulating cylindrical shell (e.g., glass) (B) is affixed to an insulating tube (C) and plunged into a liquid-metal bath ($Li_{0.1}$ $Pb_{0.9}$) (D). The insertion of the liner is rapidly followed by insertion of a long support tube (E) to form the coaxial arrangement shown. Filling the support tube, coaxial insulating tube and associated flat-plate insulation with liquid metal (e.g., $Li_{0.1}$ $Pb_{0.9}$) forms a current conductor for the Z-pinch plasma formation and the Z-pinch liner drive. To the liner end of the support tube is fixed a small ampule of D-T fuel (F), which upon emersion into hot liquid metal heats and ejects DT gas/liquid through an orifice downward to the grounded end of the liner [refer to detail drawing on Fig. (IV-6)]. Voltage is applied across the D-T fuel ampule by means of the coaxial support tube (E), and the resulting discharge forms both the initial plasma and poloidal insulating field onto which the liner eventually implodes. Obvious stability questions arise with respect to the Z-pinch plasma discharge, in that the liner requires ~ 10 μs to reach maximum compression. Radial current

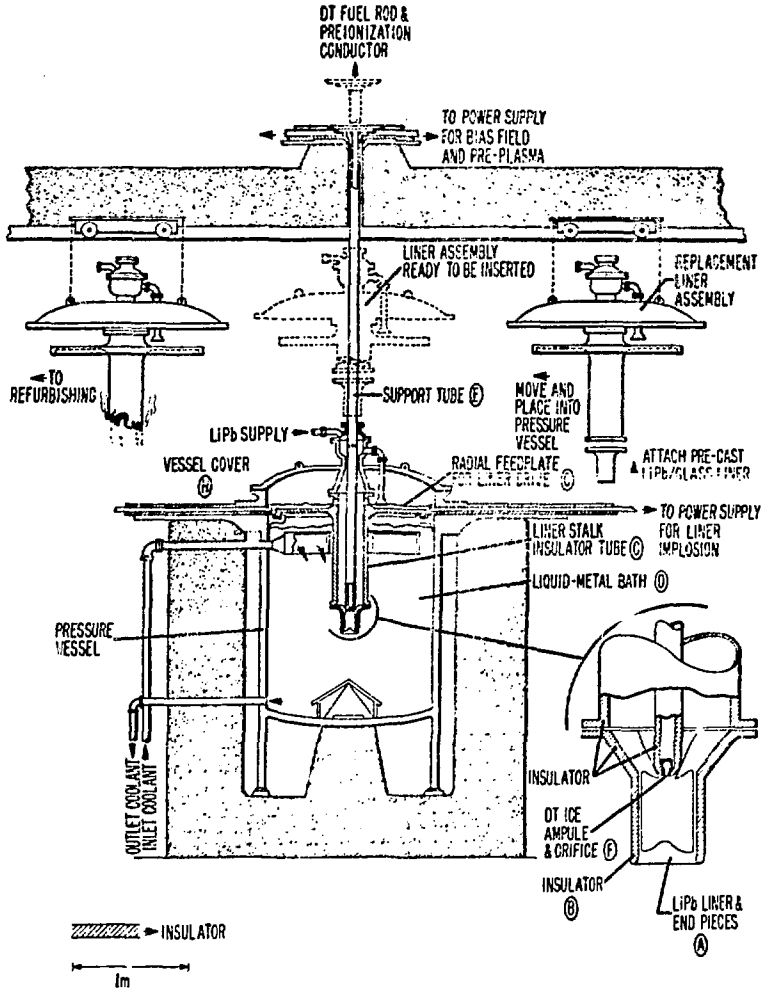

Fig. IV-6.

Schematic diagram of a fast-liner inertially confined reactor (FLICR). Refer to text for description of operation.

feedplates (G) of liquid metal are used to minimize parasitic inductance, the question of overall energy transfer being addressed in the following section. The degree of demolition and damage to the supporting insulator structure is an open question at present, but is amenable to calculation if and when more detailed studies are required. It is postulated here that the liner and < 1 m of support insulator are destroyed each shot, but the more complex feedplate insulator and feedthroughs can be recycled for many implosions. Given the validity of this assumption, the tubular insulator of ~ 0.1- to 0.3-m diam and < 1-m length (~ 1-mm wall thickness) will be destroyed and enter the primary $Li_{0.1}\ Pb_{0.9}$ coolant as a slag and debris. Figure IV-6 shows the liner and

associated apparatus (coaxial support tube (E) and D-T fuel ampule (F), flat plate insulator (G), vessel cover (H), plumbing for injection of liquid-metal conductors, etc.) in before, during, and after locations. A conveyor-belt operation is proposed to insert, remove, and refurbish these liner assemblies (J). Hence, the insulator represents the only materials-related cost, and since this insulator has virtually no structural, thermal, or radiation-damage requirement, this cost should be small, but not negligible. Glass tubing of this size and shape costs ~ 2.00 \$/kg, and ~ 1.4 kg/m (r_{10} = 0.1 m, 1-mm thickness) of the material would be destroyed each shot. The major expense will probably be related to capital and operating cost associated with repair and refurbishment of the recovered liner stalk (e.g., liner casting, cutting and grinding of damaged liner stalk, bonding of new liner/insulator and D-T ampule/insulator to the liner stalk and support tube, fabrication of replacement liner, etc.).

Clearly, numerous physics, technological, and economic unknowns can be found with the above described FLICR concept. For example: a) What is the MHD stability of a wall-confined, dense Z-pinch? b) To what degree can the postimplosion explosion be directed away from sensitive regions and be dissipated as heat into the (multiphase, perhaps) liquid-metal coolant? c) Can a mechanical design for the proposed liner insertion and recovery be realized which has some chance for fast (seconds, but probably not minutes) and reliable operation? d) Can liquid-metal conductors be flowed and reformed in a fashion indicated? e) Can this system operate at a total cost of at most a few dollars per liner and associated destroyed apparatus?

2. Liner Driving Circuit and Energy Transfer/Storage (ETS) Efficiency.

The rapid (10-20 μs) energy transfer times envisaged for the FLICR eliminates from consideration all but capacitive and inductive (slow homopolar motor/generator to charge a transfer inductor, which is rapidly switched into the liner inductance) energy transfer and storage (ETS) systems. Examples of both capacitive and inductive ETS were considered for driving the FLICR. Electrical aspects of the liner assembly schematically depicted in Fig. IV-6 were idealized according to Fig. IV-7. Shown also on Fig. IV-7 are the characteristic dimensions and liner parameters used in the single, unoptimized calculational example. The results of the incompressible calculation summarized on Table IV-I (W_{KRO} = 150 MJ/m) were used for an ℓ = 0.30-m-long liner.

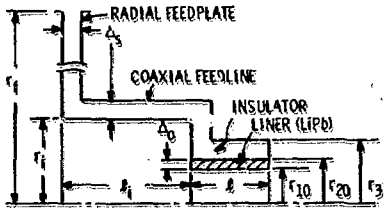

LINER		
r_{10}	INITAL INNER RADIUS	0.10 m
Δ_0	$r_{20} - r_{10}$ INITIAL LINER THICKNESS	0.001 m
Δ_s	INSULATOR THICKNESS	0.005 m
ℓ	LINER LENGTH	0.3 m
ρ	LINER DENSITY (LIPD)	9.4×10^3 kg/m^3
η	LINER RESISTIVITY	2.2×10^{-7} Ω-m
LEADS		
r_i	RADIUS OF COAXIAL FEEDLINE	0.2 m
r_f	RADIUS OF RADIAL FEEDPLATE	5.0 m
Δ_s	INSULATOR THICKNESS	0.005 m
ℓ_i	LENGTH OF COAXIAL FEEDLINE	1.0 m
η	RESISTANCE OF LEADS (Cu)	1.7×10^{-8} Ω-m

Fig. IV-7.
Idealized model of liner, coaxial feedline, and radial feedplate used to perform circuit analysis of the reactor concept depicted in Fig. IV-6.

For the dimensions given on Fig. IV-7, the transfer line inductance is L_t = 12 nh and the liner inductance per se is given by

$$L_\ell(nh) = 60\ \ell n(r_{20}/r_2) = 60\ \ell n[\alpha^2\kappa/(\kappa(\alpha^2-1)-1)] \quad , \qquad (IV-17)$$

where $\kappa = (r_{10}/r_1)^2$ and $\alpha = (r_{20}/r_{10})^2$ (See Sec. IV.B.1). The results of a solution to the dynamic (capacitive ETS) circuit equations show that the implosion time is ~ 19 μs (compared to the ideal value of 13.3 μs given in Table IV-I). For this case the skin depth of $Li_{0.1}Pb_{0.9}$ alloy is 1.4 mm. Since this skin depth is greater than the initial liner thickness Δ_0 = 1.0 mm chosen for this calculation, all of the liner is assumed to contribute to resistive heating. During the compression the liner thickness exceeds the 1.4-mm skin depth, but at this point the peak current will be frozen into the moving liner and little skin effect will be seen. Hence, the liner resistance is fixed at 2.1×10^{-4} Ω. The coaxial feedline and the radial feed-plate, which for these computations are assumed to have the resistivity of copper, sustained a joule loss equivalent to one skin depth (0.4 mm).

a. Capacitive ETS Example. The electrical circuit used to model the capacitive ETS system is depicted on Fig. IV-8. The means by which the capacitor is charged was not examined, nor were the resistances and inductances of the capacitor bank and switches. The circuit equation is given by,

$$V(t) = q/C = I(R_t+R_\ell+\dot{L}_\ell) + (L_t+L_\ell)\dot{I} \quad , \tag{IV-18}$$

where $I = -\dot{q}$ and $\dot{L}_\ell(nh/s) = (60/r_2)\dot{r}_2$. The kinetic energy of the liner [Eq. (IV-6)] is rewritten as,

$$W_{KR} = \rho(\dot{r}_2 r_2)^2 \ell n(r_2/r_1) \quad , \tag{IV-19}$$

where within the thin-liner approximation,

$$(r_2/r_1) = (1 - 2r_{20}\Delta_o/r_2^2)^{1/2} \quad . \tag{IV-20}$$

Finally, the force balance on the liner can be approximated as,

$$F_\ell(Nt) = (I^2/2)(dL_\ell/dr_2) = -(3.0 \times 10^{-8}/r_2)I^2 \quad . \tag{IV-21}$$

The circuit and liner-dynamics equations were numerically solved under this thin-liner approximation in the same manner as in Section II (see e.g., Fig. II-3). Table IV-II summarizes the calculational results. The liner radius, driving current, voltage, and kinetic energy are shown as a function of time on Fig. IV-9. Of the 68 MJ (227 MJ/m) initially stored in the capacitor bank 66% is transferred to the liner, 18% is lost as resistive heating (mostly recovered as sensible heat, see Fig. IV-5), and 5% remains in the capacitor bank. The remaining 11% is stored inductively in the leads and liner and may be recovered in part, depending on circuit dynamics after the liner inductance is disruptively removed from the circuit (i.e., on how much of and the mode in which the circuit survives the implosion).

It must be emphasized that the foregoing example is unoptimized, is based on a very simple circuit analogy, evokes a thin-liner approximation, and uses the unoptimized liner parameters summarized in Table IV-I. More complete impedance matching between the capacitor, transfer lines and liner, and increased ETS

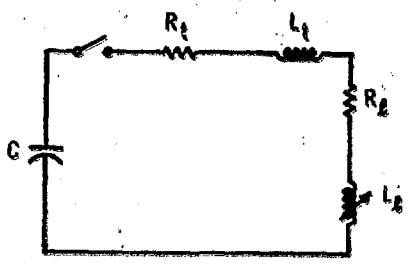

C EFFECTIVE ETS CAPACITANCE
R_t RESISTANCE OF TRANSFER LINES
L_t INDUCTANCE OF TRANSFER LINES
R_ℓ RESISTANCE OF LINER
L_ℓ INDUCTANCE OF LINER

Fig. IV-8.
Circuit diagram used to analyze the capacitive ETS option for the liner reactor.

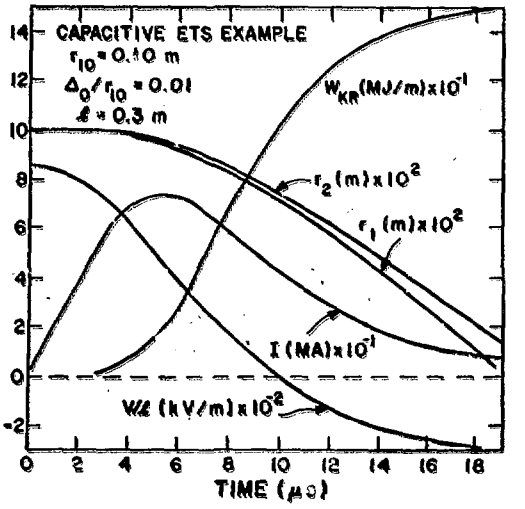

Fig. IV-9.
Time dependence of feedplate voltage V(kV), liner current I(MA), inner and outer liner radii r_1(m) and r_2(m), and liner kinetic energy W_{KR}(MJ/m) for the capacitive ETS example.

TABLE IV-II

SUMMARY OF CAPACITIVE ETS PARAMETERS USED TO DRIVE THE INCOMPRESSIBLE $Li_{0.1}Pb_{0.9}$ LINER CASE GIVEN IN TABLE IV-1

r_{10}	Initial liner inner radius	0.10 m
Δ_0	Initial liner thickness	0.001 m
ℓ	liner length.	0.3 m
C	ETS capacitor	2 mF
V	Initial ETS capacitor voltage	260 kV
E_{co}	Initial ETS capacitor energy	68 MJ
E_{cf}	Final ETS capacitor energy	3.6 MJ
E_{KRf} (a)	Final liner energy	45 MJ
$E_{\ell f}$	Final inductive energy	7.4 MJ
E_R	Total resistive losses	12 MJ
$E_{R\ell}$	Resistive losses in liner	8 MJ
$\tau_{1/2}$	Implosion time	19 μs

(a) Corresponds to initial liner energy $W_{KRO}\,\ell$ used in the calculations summarized in Table IV-1.

efficiency is undoubtedly possible. Approximately 1/3 of the resistive energy loss occurs in the $Li_{0.1}$ $Pb_{0.9}$ liner *per se*, and changing to a better conductor for the liner material would reduce this loss. The ~ 2.1 x 10^4 MJ/m^3 deposited into this particular liner material is worrisome from another viewpoint; an appreciable portion of the liner would be vaporized by resistive heating alone (3.4 x 10^4 MJ/m^3 required to vaporize this material starting from 300 K).

b. Inductive ETS Example. The use of inductive energy transfer and storage is possibly cheaper than the capacitive ETS described in the previous section. An example of the inductive ETS system is depicted in Fig. IV-10 wherein a long-term energy storage (e.g., a homopolar motor/generator[66]), C_{HP}, is used to transfer energy into a room-temperature storage coil, L_s on a ~ 30-ms timescale. At the point of complete transfer to L_s and for times short compared to the $C_{HP} \rightarrow L_s$ transfer time, the capacitive element C_{HP} (i.e., the homopolar) appears as a short circuit to the current transients. The contactor switch S_3 isolates the load inductance $L_t + L_\ell$ during the slow energy transfer to L_s.

When the current peak occurs in L_s (85 MA in this example), the switch S_2 is closed and S_1 is opened. A small reverse charge on the counterpulse capacitor C_{cp} assures the current through S_1 is zero to permit opening. The current from L_s resonantly transfers to the load inductance $L_t + L_\ell$ by means of the transfer capacitor C_{cp}, which is sized to give the desired voltage and current risetime. The switch S_2 is opened at peak voltage (zero current in the C_{cp} leg of the circuit), the currents in L_s and $L_t + L_\ell$ now being equal. The current and voltage waveforms are subsequently determined by the circuit L/R time constant, which in part is determined by the liner dynamics. The circuit equation

$$\dot{I} = -[(R + \dot{L}_\ell)/(L_s + L_t + L_\ell)]\, I \qquad \text{(IV-22)}$$

is solved in conjunction with a liner dynamics equation [Eq. (IV-21)], the results of which are given on Fig. IV-11. The electrical model of the liner and feedplate system is the same as that used in the capacitive ETS example (Fig. IV-7). Table IV-III summarizes key numerical results. Of the energy used

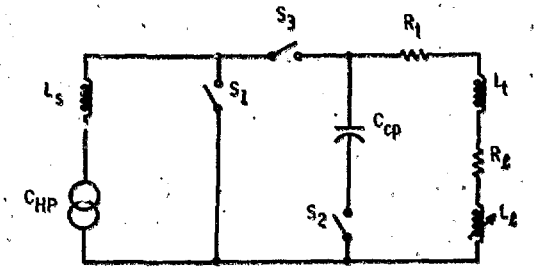

C_{HP} CAPACITANCE OF HOMOPOLAR MOTOR/GENERATOR
C_{cp} COUNTERPULSING AND TRANSFER CAPACITOR
L_s STORAGE INDUCTOR
R_t RESISTANCE OF TRANSFER LINES
L_t INDUCTANCE OF TRANSFER LINES
R_ℓ RESISTANCE OF LINER
L_ℓ INDUCTANCE OF LINER

Fig. IV-10.
Circuit diagram used to analyze the inductive ETS option for the liner reactor.

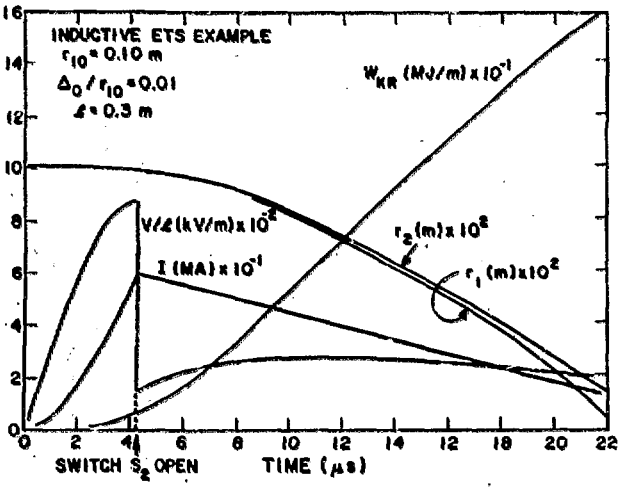

Fig. IV-11.
Time dependence of feedplate voltage V(kV), liner current I(MA), inner and outer liner radii r_1(m) and r_2(m), and liner kinetic energy W_{KR}(MJ/m) for the inductive ETS example.

TABLE IV-III

SUMMARY OF INDUCTIVE ETS PARAMETERS USED TO DRIVE THE INCOMPRESSIBLE $Li_{0.1}Pb_{0.9}$ LINER CASE GIVEN IN TABLE IV-1

r_{10}	initial liner inner radius	0.10 m
Δ_o	initial liner thickness	0.001 m
ℓ	liner length	0.30 m
C_{HP}	homopolar capacitance	20 kF
C_{cp}	transfer capacitance	0.886 mF
V_{HP}	initial homopolar voltage	110 V.
V_{FP}	peak voltage at liner feedplate	260 kV
L_s	storage inductance	27.7 nh
E_{HP}	initial energy in homopolar	130 MJ
E_{so}	energy initially transferred to L_s	100 MJ
E_{sf}	final energy stored in L_s	2.8 MJ
E_{KRf} (a)	energy given to liner	48.3 MJ
$E_{\ell f}$	final energy remaining in $L_t + L_\ell$	8.8 MJ
E_c	final energy stored in C_{cp}	30.0 MJ
E_R	total resistive losses	10.1 MJ
$\tau_{i/2}$	implosion time	32.0 μs
τ_s	time to charge L_s	37.0 ms
τ_ℓ	time to charge $L_c + L_\ell$	4.2 μs

(a) Corresponds to initial liner energy $W_{KRO}\ell$ used in the calculations summarized on Table IV-I.

by the liner system, $E_{so}-E_{o}-E_{sf}$ = 67.2 MJ, 48.3 MJ is actually delivered to the plasma, resulting in a transfer efficiency of 72%. This compares to the 66% efficiency computed for the capacitive ETS example. The energy stored in C_{op} and the final energy stored in L_s are assumed here to be reclaimable at nearly 100% efficiency. Although unoptimized, both the capacitive and inductive ETS systems are expected to have overall transfer efficiencies of ~ 70%.

3. Nuclear Heating of the Liner at Maximum Compression. Although detailed neutronic calculations of the FLICR $Li_{0.1}$ $Pb_{0.9}$ blanket are premature, related calculations have been made in support of the NRL liner reactor concept.[53] Calculations have been made for the FLICR concept by Dudziak in order to estimate the degree of nuclear (gamma/neutron) heating incurred within the fully compressed $Li_{0.1}$ $Pb_{0.9}$ liner. (These are the same calculations that are discussed in Section III.D.3.) Figure IV-12 gives the fraction of the 14.1-MeV (2.25-pJ) neutron energy deposited into compressed liners of varying thicknesses and materials. A vacuum boundary condition is assumed at the outer radius of a liner of given thickness. For the $Li_{0.1}$ $Pb_{0.9}$ case being considered, the liner thickness is 11.3 mm at maximum compression, and Fig. IV-12 indicates ≥ 2% of the 14.1-MeV neutron energy is deposited. For the incompressible case given on Table IV-1 the (20 MeV/n) fusion yield is W_N = 771 MJ/m. Hence, the average energy density within the liner resulting from neutron/gamma heating amounts to 1.72×10^4 MJ/m^3. Figure IV-13 shows the computed spatial distribution of nuclear heating within fully compressed liners of various thicknesses. The peak-to-average energy density is 3-4, so local heating near the inner surface will be more severe than that given by the average value. Hence, nuclear heating of the liner material is comparable to that predicted for joule heating in Section IV.C.2.a, both being sufficiently high to vaporize a significant portion of the liner. The spatial and temporal behavior of both joule and nuclear heating, the related evaporation rates, and the effects of these processes on liner dynamics and thermonuclear yield represents a complex problem which has yet to be calculationally explored. These preliminary estimates show, however, that liner heating and mass transport may be quite important, and more detailed analyses are certainly warranted.

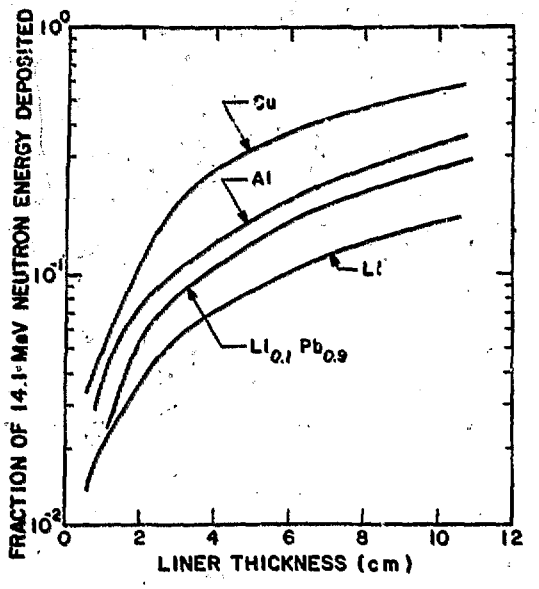

Fig. IV-12.
Dependence of the fraction of the 14.1-MeV neutron energy deposited into an imploded liner of varying thickness for various materials. (Neutronic calculation used normal densities and cylindrical geometry.)

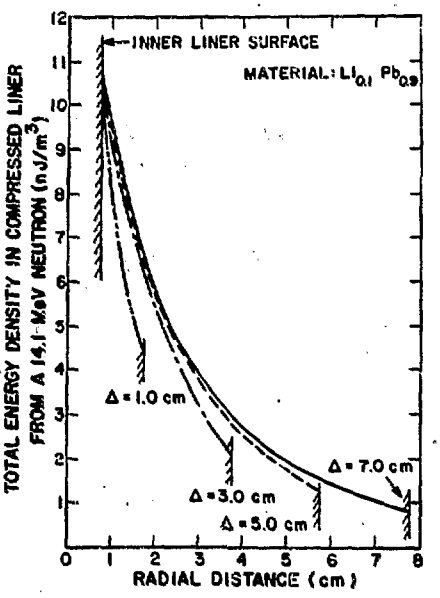

Fig. IV-13.
Total (neutron plus gamma) energy density deposited per 14.1-MeV incident neutron as a function of distance into an imploded liner $Li_{0.1}Pb_{0.9}$ liner for four thicknesses, Δ. (Neutronic calculation used normal density and cylindrical geometry.)

D. Summary and Conclusions

Although simple scaling assumptions point to relatively thick, slow liners, accounting for the real and serious problems of hydrodynamic stability (of the liner), liner compressibility, and plasma particle/energy end loss present convincing arguments for very fast implosions ($\lesssim$ 10-20 μs liner transit times, $\lesssim$ 1-μs burn time). Physical containment of the mechanical energy release and the need for fast, high-voltage energy transfer represent serious disadvantages for this concept, although the direct recovery of the postimplosion liner energy is not necessary for operation as an economic power reactor. The compact, high-power density characteristics of this system offer strong advantages. Numerous problems and/or uncertainties with respect to "reactor desirability," physics requirements, and technological demands have been identified throughout the text. Many of these problems and/or uncertainties undoubtedly can be resolved or at least put into a more quantitative perspective by detailed study and systems optimization, the results presented here being based entirely on unoptimized

scoping studies. The absence of a firm experimental basis upon which to extrapolate into and to evaluate the reactor regime, however, represents a major limitation to the required parametric systems studies. In this context the fast liner experiment is proposed to provide data and operating experience with which to substantiate or to disprove the cautiously optimistic reactor projections made herein. A parallel systems studies effort should also be maintained which will analytically probe into these numerous uncertainties as well as incorporating into the systems analyses new experimental findings.

Acknowledging, therefore, the need for more profound systems studies and physics analysis, these scoping studies indicate that investments ~ 150 MJ/m into a r_{10} = 0.10-m radius, Δ_0/r_{10} = 0.01 inverse aspect ratio liner will yield a FLICR with a recirculation power fraction $\varepsilon \sim 0.40$, if none of the liner energy is recovered and no plasma energy loss occurs. Radial and axial diffusion have not been incorporated into this reactor analysis. The effects of liner compression will require a factor of 1.87 increase in liner energy, whereas the transfer efficiency of either a capacitive or inductive ETS system will be on the order of 70%; both inefficiencies will require ~ 400 MJ/m to be transferred to the liner reactor to yield 1400 MJ/m (20 MeV/n) of thermal energy. This example is based upon the injection of 0.1-keV precompression plasma at a density of $1.0 \times 10^{24} m^{-3}$. In addition to liner compressibility, liner heating by both return currents and fusion neutrons may significantly affect plasma compression if a less resistive/absorptive liner cannot be found; increasing the liner thickness will ameliorate the joule heating, while exacerbating nuclear heating.

More realistic modeling of essential physics into the reactor analysis (e.g., alpha-particle heating and confinement, axial and radial plasma confinement, compression of buffer/insulating fields, liner heating and evaporation, plasma injection, etc.) will undoubtedly influence significantly the reactor concept depicted in Fig. IV-6. Aside from these aforementioned modelistic shortcomings, however, the problem of efficient blast confinement in a way to minimize damage to expensive reactor components represents an engineering challenge with deep economic implications for the FLICR concept. The compactness, high-power density, and relatively inexpensive development cost associated with the FLICR, however, definitely warrant more serious consideration of the concept on both a physics and engineering (i.e., systems studies) level.

V. ESTIMATED MANPOWER, COST, AND MILESTONES

It is proposed that this experiment carry over directly from the Implosion Heating Experiment. The starting date would depend somewhat on the final measurements being made on the IHX, but it could probably be started near the beginning of FY 78. The level of effort proposed here for FY 78 represents orderly continuation of the IHX program and is regarded as the lower limit of a viable liner program.

The cost of the plasma preparation experiments would be covered by the operations budget. The liner drive bank will use about 800 14.6-μF 20-kV capacitors that were recently removed from the Zeus capacitor bank. The cables are available from a supply of failed cables from the Scyllac and Scylla IV-P systems. The bank will be switched by homemade solid dielectric switches. A major procurement of $50 k will be required for collector plates, a blast chamber, and some trigger components. The bank will be constructed by the group technicians, perhaps with help from summer students who are hired from a special budget.

Table V-I shows the manpower requirements for the first three fiscal years and Table V-II gives estimated costs by fiscal year. The major procurement for the second fiscal year is mostly for the replacement of liner components destroyed on each shot. In the third fiscal year the jump in major procurement represents a start towards development and acquiring parts for expanding the liner drive bank.

TABLE V-I

MANPOWER REQUIREMENTS

FY 78	4.5	Scientific Staff
	5.5	Other Technical
FY 79	5.5	Scientific Staff
	7.0	Other Technical
FY 80	5.5	Scientific Staff
	1.0	Engineer
	9.0	Other Technical

TABLE V-II

COST ESTIMATES

	FY 78	FY 79	FY 80
Total man years	10.54	12.78	15.78
Manpower cost	$560 k	$740 k	$1017 k
Major procurement	50 k	60 k	200 k
	$610 k	$800 k	$1217 k

Preliminary estimates for the time required for various activities after the end of the IHX experiment (month 0) are (in months):

Plasma preparation experiments	0 on
Bank construction and testing	0 to 12
Liner implosions without plasma	12 to 24
Liner implosions on plasma	24 on.

REFERENCES

1. V. M. Alipchenkov, V. I. Vasilyev, I. K. Konkashbayev, I. S. Landman, L. B. Nikandrov, Yu.V. Skvortsov, F. R. Ulinich, S. S. Tserevitinov, "A Theta Pinch with External Plasma Injection," (translated by W. B. Riesenfeld), preprint, Kurchatov Institute (Moscow, 1976).

2. I. I. Rudakov, "A Review of Investigations on Pulsed Thermonuclear Reactors," ERDA Report ERDA-tr-176 (1976).

3. J. G. Linhart, "Plasma and Megagauss Fields," in Proceedings of the Conference on Megagauss Magnetic Field Generation by Explosives and Related Experiments, H. Knoepfel and F. Herlach, Eds., Frascati, Italy, Sept. 21-23, 1965, (Euratom, Brussels, 1966, Rept. EUR 2750.e), pp. 387-396.

4. S. G. Alikhanov, G. I. Budker, A. V. Komin, V. A. Polykov, and B. S. Estrin, Proc. 7th Intern. Conf. on Phenomena in Ionized Gases, Belgrad, 1966.

5. G. I. Budker, "Thermonuclear Fusion in Installations with a Dense Plasma," Proceedings 6th European Conference on CTR, Moscow, 1973.

6. S.G. Alikhanov, V.P. Bakhtin, Wm.M. Brusnikin, I.S. Glushkov, R.Kh. Kurtmullaev, A.L. Lunin, A.D. Muzychenko, V.P. Novikov, V.V. Pichugin, V.N. Semenov, G.E. Smolkin, E.G. Utyugov, and I.Ya. Shipuk, "Study of Models of Liner Thermonuclear Systems," (translated by D. L. Book), Proc. 6th Int. Conf. on Plasma Physics and Controlled Nuclear Fusion Research Berchtesgaden, FGR, October 1976, (IAEA, Vienna, to be published), Paper No. E-19-2.

7. S. G. Alikhanov and I. S. Glushkov, "Stationary Cooling Wave in a Magnetized Plasma," Sov. Phys. Dokl. 21, 37 (1976).

8. C. Rioux, C. Jablon, "Losses of a Thermonuclear Plasma Imploded by a High-Velocity Wall," Nucl. Fus. 15, 425 (1975).

9. A. E. Robson, "Plasma Confinement by Megagauss Magnetic Fields," Ann. New York Acad. Sci. 251, 649 (1975).

10. P. J. Turchi and A. E. Robson, "Conceptual Design of Imploding Liner Fusion Reactors," Sixth Symposium on Engineering Problems in Fusion Research, San Diego, Nov. 1975.

11. D. L. Book, A. L. Copper, R. Ford, D. Hammer, D. J. Jenkins, A. E. Robson, P. J. Turchi, "Stabilized Imploding Liner Fusion Systems," Proc. 6th Int. Conf. on Plasma Physics and Controlled Nuclear Fusion Research, Berchtesgaden, FGR, Oct. 1976 (IAEA, Vienna, to be published).

12. E.P. Velikhov, A.A. Vedenov, A.D. Bogdanets, V.s. Golubev, E.G. Kasharskii, A.A.Kiselev, F.G.Rutberg, and V.V. Chernukha, "Generation of Megagauss Magnetic Fields using a Liner Compressed by High Pressure Gas," Sov. Phys. Tech. Phys. 18, 274 (1973).

13. R. M. Patrick, "High-Speed Shock Waves in a Magnetic Annular Shock Tube," Phys. Fluids 2, 589 (1959).

14. R. A. Gross, Y. G. Chen, E. Halmoy, and P. Moriette, "Strong Shock Waves," Phys. Rev. Lett. 25, 575 (1970).

15. H. Knoepfel, Pulsed High Magnetic Fields, (North-Holland Publishing Co., Amsterdam, 1970), p. 17.

16. H. Knoepfel, Pulsed High Magnetic Fields, (North-Holland Publishing Co., Amsterdam, 1970), p. 118.

17. P. J. Turchi, "Rotating Liquid Liner Implosion Experiment," NRL Progress Report, June 1-Dec. 31, 1975.

18. L. Spitzer, Jr., Physics of Fully Ionized Gases, 2nd Rev. Ed. (Interscience Publishers, New York, 1967).

19. B. Feinberg and R. A. Gross, "A Study of Hot Plasma in Contact with a Cold Wall," J. Nucl. Mater. 53, 111 (1974).

20. J. Marshall and I. Henins, "Fast Plasma from a Coaxial Gun," Plasma Physics and Controlled Nuclear Fusion (IAEA, Vienna, 1966), Vol. II, p. 449.

21. Dah Yu Cheng and Peter Wang, "The Properties of a Coaxial Deflagration Plasma Gun," Proc. of the Second Int. Conf. on Pulsed High Beta Plasmas, Garching, Germany, July 1972, pp. 257-260.

22. A.M. Zhitlukhin, V.N. Lyashenko, S.A. Pavichev, Yu.V. Skvortsov, V.M. Strunnikov, and S.S. Tserevitinov, "Transport of Plasma Blobs with Energy ~ 100 KJ," (translated by W.B. Riesenfeld), preprint, Kurchatov Institute (Moscow, 1976).

23. A. M. Zhitlukhin, I. V. Ilyushin, B.Ya. Lyubimov, Yu.V. Skvortsov, and V. G. Solovyeva, "Passage of Plasma Along a Magnetic Field," (translated by W. Riesenfeld), preprint, Kurchatov Institute (Moscow, 1976).

24. B. Dunne and B. P. Benham, "Xenon Plasma from a Focused Coaxial Gun," General Atomic Report GA-6779 (1965).

25. T. R. Jarboe and W. R. Baker, "Apparatus for Producing Laser Targets of 50 Micron Deuterium Pellets," Rev. Sci. Instrum. 45, 431 (1974).

26. E. Halmoy, "Production and Investigation of Very Strong Ionizing Shock Waves," Phys. Fluids 14, 2134 (1971).

27. P. Moriette, "Experimental Study of Strong Transverse Ionizing Shock Waves," Phys. Fluids 15, 51 (1972).

28. James W. Shearer and William C. Condit, "Magnetically Driven Metal Liners for Plasma Compression," in Energy Storage, Compression, and Switching, W.H. Bostick, V. Nardi, and O.S.F. Zucker, Eds. (Plenum Publishing Corp., New York, 1976).

29. Ya. B. Zeldovich and Yu. P. Razier, Physics of Shock Waves and igh Temperature Hydrodynamic Phenomena, (Academic Press, New York, 1966), Vol. 2, Chap. XI, pp. 685-784.

30. C.A. Swenson, "Equation of State of Cubic Solids; Some Generalizations," J. Phys. Chem. Solids 29, 1337 (1968).

31. S. Glasstone and R. H. Lovberg, Controlled Thermonuclear Reactions, (D. Van Nostrand Co., Princeton, New Jersey, 1960).

32. J. L. Tuck, "Thermonuclear Reaction Rates," Nuclear Fusion 1, 201 (1961).

33. In making this comparison, the initial liner kinetic energy of the model, ϕ_L, corresponds to the work done on the liner by the driving pressure in the code, CHAMISA.

34. G.I. Kerley, "Equation of State and Phase Diagram of Dense Hydrogen," Phys. Earth Planet. Interiors 6, 78 (1972).

35. J.F. Barnes, "An Equation of State for Sodium Over an Extended Temperature and Density Range," in Thermodyhamics of Nuclear Materials 1974, (International Atomic Energy Agency, Vienna, 1975), Vol. I, pp. 327-339.

36. J.F. Barnes, "Statistical Atom Theory and the Equation of State of Solids," Phys. Rev. 153, 269 (1967).

37. C.L. Mader and W.R. Gage, "FORTRAN SIN: A One-Dimensional Hydrodynamic Code for Problems which include Chemical Reactions, Elastic-Plastic Flow, Spalling, and Phase Transitions," Los Alamos Scientific Laboratory Report LA-3720 (1967).

38. R.E. Swanson and C.L. Mader, "One-Dimensional Elastic-Plastic Calculations Involving Strain-Hardening and Strain-Rate Effects for Aluminum," Los Alamos Scientific Laboratory Report LA-5831 (1975).

39. P.J. Blewett, "Stress Calculations in MAGEE Difference Form," Los Alamos Scientific Laboratory Report LA-4601-MS (1971).

40. J.F. Barnes, P.J. Blewett, R.G. McQueen, K.A. Meyer, and D. Venable, "Taylor Instability in Solids," J. Appl. Phys. 45, 727 (1974).

41. G.N. White, Los Alamos Scientific Laboratory, personal communication (November 1976).

42. S. I. Braginskii, "Transport Processes in a Plasma," in Reviews of Plasma Physics, M. A. Leontovich, Ed., (Consultants Bureau, New York, 1965), Vol. 1.

43. B. Jensen, "Physics of a Fusion Plasma Boundary Layer," Ph.D. Thesis, Plasma Laboratory Report 67 (Columbia University, New York, 1976).

44. D. V. Sivukhin, "Coulomb Collisions in a Fully Ionized Plasma," in Reviews of Plasma Physics, M. A. Leontovich, Ed., (Consultants Bureau, New York, 1965), Vol. 4; H. Dreicer, Los Alamos Scientific Laboratory, personal communication (June 1975).

45. V. N. Mineev and E. V. Savinov, "Viscosity and Melting Point of Aluminum, Lead, and Sodium Chloride Subjected to Shock Compression," Sov. Phys. JETP 25, 411 (1967).

46. Numerical values are calculated from the SESAME equation-of-state tables used by the hydrodynamic code CHAMISA. The SESAME tables are produced by group T-4 at the Los Alamos Scientific Laboratory; see the discussion and references in section III.B. The numerical values are for nickel, but should be representative for copper as well.

47. Handbook of Chemistry and Physics, 38th Ed. (Chemical Rubber Publishing Co., Cleveland, 1956).

48. E.A. Kraut and G.C. Kennedy, "New Melting Law at High Pressures," Phys. Rev. Lett. 16, 608 (1966).

49. G.C. Kennedy and S.N. Vaidya, "The Effect of Pressure on the Melting Temperature of Solids," J. Geophys. Res. 75, 1019 (1970).

50. L. H. Cohen, W. Klement, G. C. Kennedy, "Melting of Copper, Silver, and Gold at High Pressures," Phys. Rev. 145, 519 (1966); C. L. Mader, Los Alamos Scientific Laboratory, personal communication (December 1976).

51. H. Knoepfel, Pulsed High Magnetic Fields, (North-Holland Publishing Co., Amsterdam, 1970).

52. M. S. Chu, "Hot Plasma in Contact with a Cold Wall," Phys. Fluids 16, 1441 (1973).

53. D. J. Dudziak, Los Alamos Scientific Laboratory, personal communication (November 1976).

54. American Institute of Physics Handbook (McGraw-Hill, New York 1957).

55. M. L. Wilkins and M. W. Guinan, "Impact of Cylinders on a Rigid Boundary," J. Appl. Phys. 44, 1200 (1973).

56. C. M. Fowler, W. B. Garn, and R. S. Caird, "Production of Very High Magnetic Fields by Implosion," J. Appl. Phys. 31, 588 (1960).

57. C. M. Fowler, et. al., in Proceedings of the Conference on Megagauss Magnetic Field Generation by Explosives and Related Experiments, H. Knoepfel and F. Herlach, Eds., Frascati, Italy, September 1965, (Euratom, Brussels, 1966, Rept. EUR 2750.e). There are three papers in these proceedings, namely:

4.1. C. M. Fowler, R. S. Caird, W. B. Garn, and D. B. Thomson, "The Los Alamos Flux Compression Program from its Origin."

4.2. R. S. Caird, W. B. Garn, D. B. Thomson, and C. M. Fowler, "A Cylindrical Explosive Flux-Compression System."

4.3. D. B. Thomson, R. S. Caird, W. B. Garn, and C. M. Fowler, "Plasma Compression by Explosively Produced Magnetic Fields."

58. R. S. Caird, W. B. Garn, D. B. Thomson, and C. M. Fowler, "An Explosive-Driven High-Field System for Physics Applications," J. Appl. Phys. 35, 781 (1964).

59. S. Chandrasekhar, Hydrodynamic and Hydromagnetic Stability (Clarendon Press, Oxford, 1961).

60. G. N. White, Los Alamos Scientific Laboratory, personal communication (November 1976).

61. F. C. Perry and L. P. Mix, "Electron-beam-drive Instability in a Solid," Appl. Phys. Lett. 27, 194 (1975).

62. D.L. Book, A.L. Cooper, R. Ford, D. Hammer, D.J. Jenkins, A.E. Robson, P.J. Turchi, "Stabilized Imploding Liner Fusion Systems," Proc. 6th Int. Conf. on Plasma Physics and Controlled Nuclear Fusion Research, (Berchtesgaden, FGR, October 1976).

63. J.F. Decker, "Evaluation of Exploratory Concepts," USERDA/DMFE, personal communication (October 26, 1976).

64. P.J. Turchi, "Imploding Liner Fusion Systems in Cusp-Ended Theta-Pinch Geometry," NRL Memorandum Rept. 3094, (August 1975).

65. J.W. Shearer, "Magnetically-Driven Liners for Plasma Compression," USERDA Rept UCRL-75915 (September 1974).

66. K.I. Thomassen, "Conceptual Engineering Design of a 1-GJ Fast Discharging Homopolar Machine for the Reference Theta-Pinch Fusion Reactor," EPRI Report ER-249 (August 1976).

☆U.S. GOVERNMENT PRINTING OFFICE: 1977—777-018/108